

Doctoral thesis

Doctoral theses at NTNU, 2022:206

Tongtong Wang

Physics-data Cooperative Modeling for Ship Motion Prediction

NTNU
Norwegian University of Science and Technology
Thesis for the Degree of
Philosophiae Doctor
Faculty of Engineering
Department of Ocean Operations and Civil
Engineering



Norwegian University of
Science and Technology

Tongtong Wang

Physics-data Cooperative Modeling for Ship Motion Prediction

Thesis for the Degree of Philosophiae Doctor

Ålesund, June 2022

Norwegian University of Science and Technology
Faculty of Engineering
Department of Ocean Operations and Civil Engineering



Norwegian University of
Science and Technology

NTNU

Norwegian University of Science and Technology

Thesis for the Degree of Philosophiae Doctor

Faculty of Engineering

Department of Ocean Operations and Civil Engineering

© Tongtong Wang

ISBN 978-82-326-5724-7 (printed ver.)

ISBN 978-82-326-5633-2 (electronic ver.)

ISSN 1503-8181 (printed ver.)

ISSN 2703-8084 (online ver.)

Doctoral theses at NTNU, 2022:206

Printed by NTNU Grafisk senter

Abstract

Increasing development on autonomous vehicles and concern on ship navigation safety put forward a higher requirement for ship motion forecasting technology. The predictions of ship motion in the near future can give the operator (autonomous ship operating system or human) ample time to respond and avoid dangerous operations. Therefore, modeling and predicting the behavior of ships have been pursued extensively to enhance state estimation and motion control. Vessels operating on the surface of the ocean are exposed to an array of uncertainties, such as the external perturbations produced by wind, waves, and sea currents, etc. Creating an advanced model that comprehensively represents the system and its interaction with its immediate environments has always been challenging. Existing ship motion prediction approaches leverage a wide variety of modeling techniques. The dynamic models can propagate the estimated states into the future. Still, due to the nonlinearity, time-varying dynamics, and coupling with also time-varying environments, it is difficult to derive a good state estimator with high accuracy from observing and understanding the complex system. The fast advancement in instrumentation and data analysis techniques offers an alternative solution by constructing end-to-end models based only on data sampled from ships. For the lack of physical interpretability and inspection of internal structure, these data-based models do not always meet the expectations. The new knowledge and technology to bridge the gap are in demand.

The physics-data hybrid concept is an approach of cooperation, differentiation, and maximizing the potential of both models. Either model offers partial solutions for the vessel system. To ensure optimal outcomes, different modeling principles are working in a cooperative way, which requires the capabilities of both segments to operate as efficiently as possible. Leveraging the speed and flexibility advantages of the data-driven technologies and ensuring the robustness and quality of the high-fidelity physics-based model, the cooperative modeling appears to provide fast and accurate predictions for offshore surface vessels.

This dissertation exploits the physics-data cooperative modeling methodology and contextualizes the synthesis in maritime motion prediction. In the hybrid framework, modeling principles and formats of fusion aligned differently at various operation scenarios. Three case studies are conducted to validate the developed physics-data cooperative models for optimization and prediction. The first one relates to physics-based disciplines and enabling applications. The rest deploy two forms of cooperation. Experiments are carried out in both simulator and the vessel R/V Gunnerus operating in the real world. The results confirm the enhanced mode quality and prediction performance observed for the physics-data cooperative models.

Acknowledgment

The research presented in this thesis was conducted at the Norwegian University of Science and Technology in Ålesund within the Department of Ocean Operations and Civil Engineering (IHB). Financial support was provided by the Knowledge-Building Project for Industry “Digital Twins for Vessel Life Cycle Service” from the Research Council of Norway under Project 280703.

My supervisors throughout this Ph.D. project have been Prof. Houxiang Zhang, Prof. Guoyuan Li and Prof. Vilmar Æsøy. The guidance and support I received during the last three years are highly appreciated. In particular, I would like to express my thanks to my main supervisor, Prof. Houxiang Zhang, for motivating and shaping me into an independent researcher. Your advice on both researches as well as on guiding me has been priceless. I would also like to thank Prof. Guoyuan Li for his insightful comments and suggestions when I met difficulties. Thanks to Prof. Vilmar Æsøy for his feedback and comments on my research. I would like to thank the faculty members for their kind help from time to time. All of you have been there to support me when I need help.

I would like to acknowledge all my colleagues at the Intelligent Systems Lab (formerly Mechatronics Lab) at NTNU Ålesund. It has been a pleasure to be a part of the group. Especially, I would like to thank Dr. Robert Skulstad, with whom I have the pleasure of sharing an office and discussing, Dr. Lars Ivar Hatledal for his help on co-simulation, Dr. Pierre Major for his support on the simulator issues.

My sincere thanks go to all of my friends who supported and incited me along this way. Thanks to Peihua Han, Baiheng Wu, and Xinru Wang, your continuous support and encouragement over the past years are appreciated. Thanks to Motoyasu Kanazawa for teaching me to ski. Thanks to Dr. Shuai Yuan, Dr. Luman Zhao, Dr. Ting Liu, and Chunlin Wang, whom I had the pleasure of traveling with.

Finally, immense gratitude goes to my parents for their unconditional love and belief in me.

Contents

Abstract	i
Acknowledgment	iii
List of Publications	ix
List of Abbreviations	xi
Nomenclature	xiii
List of Figures	xv
List of Tables	xvii
1 Introduction	1
1.1 Background and motivation	1
1.1.1 Physics-based modeling	2
1.1.2 Data-driven modeling	3
1.1.3 Physics-data cooperative modeling	3
1.2 Research questions	4
1.3 Scope of work	6
1.3.1 Research objectives	6
1.3.2 Interconnection between the research objectives	7
1.4 Structure of the dissertation	7
2 Physics-data cooperative model for motion predictions	9
2.1 Hybrid modeling methodology	9
2.1.1 Insertion	11
2.1.2 Cascaded	14
2.1.3 Parallel	14
2.2 Fundamentals of the physics-based model	15
2.2.1 Maneuvering model	15
2.2.2 Dynamic positioning model	17
2.3 Principles of the data-driven model	17
2.3.1 Support vector regression	18

2.3.2	Multi-layered perceptron	19
2.3.3	Long short-term memory	20
2.4	Experimental platforms and data collection	20
2.4.1	OSC simulator	21
2.4.2	Co-simulation	21
2.4.3	Research vessel Gunnerus	22
2.4.4	MSS toolbox	24
2.5	Chapter summary	24
3	Case study: Model-based thruster failure detection and retrofit	27
3.1	Thruster failure detection and isolation	27
3.1.1	Methodology	27
3.1.2	Experimental results	29
3.2	Co-simulation based thruster retrofit	33
3.2.1	Co-simulation setup	33
3.2.2	Results analysis	35
3.3	Chapter summary	36
4	Case study: Parameter identification	39
4.1	Methodology	39
4.1.1	Ship regression model	40
4.2	Experimental results	41
4.2.1	Identification without disturbance	41
4.2.2	Identification under disturbance	41
4.3	Chapter summary	43
5	Case study: Knowledge transfer	45
5.1	Incorporating approximate dynamics into data-driven calibrator	45
5.1.1	Methodology	45
5.1.2	Experimental results	46
5.2	Knowledge transferring across ships	48
5.2.1	Methodology	48
5.2.2	Experimental results	51
5.3	Physics and data competition	52
5.3.1	Methodology	52
5.3.2	Experimental results	52
5.4	Chapter summary	54
6	Conclusion and further work	57
6.1	Summary of contributions	57
6.2	Summary of publications	58

6.3 Future work	59
References	61
Appendix	67
A Paper I	69
B Paper II	77
C Paper III	87
D Paper IV	97
E Paper V	113
F Paper VI	123

List of Publications

This thesis is based on research resulting in five journal papers and one conference paper. They are all enclosed in the appendix section. In the following list of publications, the papers are listed chronologically, but in the main body of the text a more thematic presentation order is prioritized over the chronological one.

- I T. Wang, G. Li, R. Skulstad, V. Æsøy, and H. Zhang, “An Effective Model-based Thruster Failure Detection Method for Dynamically Positioned Ships”, *2020 IEEE International Conference on Mechatronics and Automation (ICMA)*, pp. 898–904, August 2020. **Finalist of best paper.**
- II T. Wang, G. Li, B. Wu, V. Æsøy, and H. Zhang, “Parameter Identification of Ship Manoeuvring Model Under Disturbance Using Support Vector Machine Method”, *Ships and Offshore Structures*, vol. 16(sup1), pp. 13–21, 2021.
- III T. Wang, G. Li, L. Hatledal, R. Skulstad, V. Æsøy, and H. Zhang, “Incorporating Approximate Dynamics Into Data-Driven Calibrator: A Representative Model for Ship Maneuvering Prediction”, *IEEE Transactions on Industrial Informatics*, vol. 18, issue 3, pp. 1781–1789, 2021.
- IV T. Wang, L. Hatledal, M. Kanazawa, G. Li, and H. Zhang, “Effect of Ship Propulsion Retrofit on Maneuverability Research Based on Co-simulation”, *Springer Lecture Notes in Computer Science*
- V T. Wang, R. Skulstad, M. Kanazawa, G. Li, and H. Zhang, “Knowledge Transfer Across Ships: Leveraging Trends to Enhance Grey-box Trajectory Prediction”, *IEEE Transactions on Industrial Informatics*, submitted, 2022.
- VI T. Wang, R. Skulstad, M. Kanazawa, G. Li, V. Æsøy, and H. Zhang, “Physics-informed Data-driven Approach for Ship Docking Prediction”, *IEEE International Conference on Real-time Computing and Robotics (RCAR)*, July 2022.

The following papers will not be discussed in this thesis. They may, however, be considered relevant due to co-authorship and similar topics:

- i B. Wu, G. Li, T. Wang, H. Hildre, and H. Zhang, “Sailing status recognition to enhance safety awareness and path routing for a commuter ferry”, in *Ships and Offshore Structures*, vol. 16(sup1), pp. 1–12, 2021.
- ii R. Skulstad, G. Li, T. Fossen, T. Wang, and H. Zhang, “A Co-operative Hybrid Model For Ship Motion Prediction”, in *Modeling, Identification and Control*, vol. 42, issue 1, 2021.
- iii M. Kanazawa, R. Skulstad, T. Wang, G. Li, L. Hatledal, and H. Zhang, “LSTM-SHV: physics-ML hybrid trajectory predictor for an autonomous ship”, in *IEEE Sensors Journal*, submitted, 2022
- iv M. Zhu, T. Wang, H. Zhang, and G. Li, “Ship maneuvering model identification under wind disturbance”, in *IEEE International Conference on Real-time Computing and Robotics (RCAR)*, submitted, 2022.
- v C. Wang, T. Wang, T. Nord, O. Osen, H. Zhang, and G. Li, “Uncertainty and sensitivity analysis for the performance evaluation of ship dynamical model”, in *International Ocean and Polar Engineering Conference*, accepted, 2022.

List of Abbreviations

DT	Digital Twin
DOF	Degree of Freedom
DP	Dynamic Position
MMG	Mathematical Modeling Group
CFD	Computer Fluid Dynamics
PB	Physics-based
DD	Data-driven
ML	Machine Learning
GNSS	Global Navigation Satellite Systems
RPM	Revolution per Minute
RO	Research Objective
SVM	Support Vector Machine
NN	Neural Networks
LSTM	Long Short-Term Memory
GP	Gaussian Process
NED	North-East-Down
SVR	Support Vector Regression
KKT	Karush-Kuhn-Tucker condition
MLP	Multi-Layered Perceptron
ReLU	Rectified Linear Unit
MSE	Mean Square Error
RNN	Recurrent Neural Networks
OSC	Offshore Simulation Centre
FMI	Functional Mock-up Interface

FMU	Functional Mock-up Unit
SSP	System Structure and Parameterization
R/V	Research Vessel
PM	Permanent Magnet
MRU	Motion Reference Unit
MSS	Marine Systems Simulator
GNC	Guidance, Navigation, and Control
FDI	Failure Detection and Isolation
PMM	Planar Motion Mechanism
MAE	Mean Absolute Error

Nomenclature

η	NED position and heading vector
ν	Linear and rotational velocity vector
ψ	Heading angle
R	Rotation matrix
M	Mass matrix
C	Coriolis-centripetal matrix
D	Damping matrix
τ	Force vector
T	Thruster configuration matrix
ρ_a	Density of air
$C_{X/Y/N}$	Wind force coefficient matrices
V_w, V_{rw}	Wind velocity, velocity relative to the ship
β_w	Wind angle
γ_w	Wind angle relative to the ship bow
A_{FW}	Projected longitudinal area of the ship above water
A_{LW}	Projected lateral area of the ship above water
L_{oa}	Overall length of the ship
ϵ, C	Two hyperparameters in the SVR
$k(\cdot, \cdot)$	Kernel function
$a()$	Activation function
w	Weight vector
h_t	Hidden state vector at time t in LSTM
c_t	Cell state vector at time t in LSTM
i_t, f_t, g_t, o_t	The input, forget, cell and output gates at time t in LSTM
σ	Sigmoid function

List of Figures

1.1	An illustration of physics-data cooperation.	3
1.2	Overview of research objectives and interconnection with published paper. The capital roman letters indicate publications on which the thesis is based, and lower roman letters indicate associated publications.	8
2.1	Illustration of physics-data cooperative modeling for decision support. . .	9
2.2	Functional interactions of PB and DD model components.	11
2.3	Categories of physics-data hybrid modeling architectures.	11
2.4	Structure of a general MLP.	19
2.5	Schematic illustration of a LSTM cell.	20
2.6	The selected offshore vessel and its simulation in the OSC simulator. . .	21
2.7	Thruster configuration the vessel simulated in OSC.	22
2.8	Diagram showing the relationship of components in co-simulation of executing zigzag maneuver.	23
2.9	Starboard side-view of the R/V Gunnerus.	23
2.10	The thruster configuration the R/V Gunnerus.	24
2.11	The propulsion arrangement of the R/V Gunnerus before and after retrofit. . .	25
2.12	Interconnection of the PB and DD models as well as data source contained in different chapters.	25
3.1	Thruster failure detection and isolation architecture.	28
3.2	Thruster configuration for the offshore surface vessel.	30
3.3	Mathematical model validation results.	31
3.4	Bow thruster failure detection and isolation.	31
3.5	Main thruster failure detection and isolation.	32
3.6	Residuals of each failure mode in detected faulty period. (a) first anomaly in bow thruster; (b) second anomaly in bow thruster; (c) first anomaly in main thruster; (d) second anomaly in main thruster.	32
3.7	Diagram showing the relationship of the engaged ship components. . . .	33
3.8	10°/10° zigzag at high speed.	35
3.9	20°/20° zigzag at high speed.	35
3.10	10° turning circle properties at higher speed.	36
4.1	Scheme of parameter identification for ship maneuvering model.	39

4.2	The SVM predictions at different disturbance levels compared with model reference of 18° turning circle.	44
5.1	A complete flowchart showing the incorporating of approximate dynamics into the data-driven calibrator.	46
5.2	The predictive performance of hybrid approach in simulation studies. . .	47
5.3	The predictive performance of hybrid approach in real-life experiment. . .	48
5.4	The structure overview of knowledge transfer across ships.	49
5.5	Target ship predictions: (a) Average distance error, (b) Relative surge velocity, and (c) Relative sway velocity.	51
5.6	The predictive trajectories of target ship and the trends leveraged by source ship at test scenarios.	51
5.7	Overview of the three model constructions.	53
5.8	Predicted trajectories of three models.	53
5.9	The predictive average distance errors of three various models.	54

List of Tables

2.1	Pros and cons of model-based and data-driven methods.	10
2.2	Physical parameters of the OSC-simulated vessel.	21
2.3	Physical parameters of the R/V Gunnerus.	24
2.4	Data channels sensed onboard the R/V Gunnerus.	25
3.1	Thruster failure cases of simulation.	31
3.2	The zigzag characteristics for the ship before and after propulsion unit retrofit.	35
3.3	The turning characteristics for the ship before and after propulsion unit retrofit.	36
4.1	Identified non-dimensional hydrodynamic coefficients ($\times 10^{-5}$).	42
4.2	Disturbance/noise level set up.	43
4.3	Experiment case set up.	43
4.4	Maneuvering characteristics comparison between SVM predictions and model reference.	43

The maritime industrial clusters are experiencing a digital revolution. The advances in digital technology are continuously pushing the boundaries of ship technology towards intelligence more in line with the demanding marine operations. It can be seen that the modern marine vessels operate increasingly autonomously through strongly interacting subsystems, which are dedicated to a specific, primary objective of the vessel or may be part of the general essential ship operations. Between subsystems, they exchange data and make coordinated operational decisions, ideally without any user interaction. Designing, operating, and life cycle service supporting such vessels is a complex and intricate engineering task requiring an efficient development approach to consider the mutual interaction between subsystems and the inherent multi-discipline.

Vessels operating on the surface of the ocean are exposed to an array of uncertainties, which may come in terms of environmental disturbances such as winds, waves, and currents, actuator faults resulting from long-term operations, signal loss during maneuvering etc. Ensuring navigation safety and security, technologies of developing an advanced model that comprehensively represents the current states and accurately reveals the likely future conditions of the ship are always in demand. Digital twin, enabling the concurrent combination of the physical world with its digital counterpart, appears as a potential solution for the next generation of advanced marine simulation [1]. As a virtual representation of the physical asset, the digital twin monitors and controls the physical entity, while the physical entity can send data to update its virtual model. In this way, offerings such as real-time prediction, optimization, and improved decision-making are within reach. In order to make digital twin concepts in ship life cycle service a success, its accurate digital representation will be indispensable and must flexibly adapt with its physical counterpart. This dissertation explores the concept of physics-data cooperative modeling methodology and contextualizes it by offering predictive insights and decision support for the modern ship.

1.1 Background and motivation

The increasing availability of live sensor data and digital technologies are accelerating the marine industries towards an intelligent era [2]. High-level automation in ship design and operation is increasingly emphasized by academia and industry to increase competitiveness and enhance efficiency. The digital twin (DT) is introduced as a concept that delivers superior solutions in the area of health management, optimization and decision support, and remote and autonomous operation. In the technology outlook 2030 recently published by DNV GL¹, digital twins are emerging as a quantum leap from earlier efforts

¹Bringing it all together: Digital twins, <https://www.dnv.com/to2030/technology/bringing-it-all-together-digital-twins.html>, Data accessed 25-February-2022

at modeling complex systems. Kongsberg AS proposed the Kognitwin Energy concept to support a higher degree of automation of decisions². Even more complex systems and greater interactions between the physical and virtual spaces in digital twins require the twinship model to best describe and flexibly adapt the time-varying vessel status.

1.1.1 Physics-based modeling

Naturally, the ship dynamic simulation initiates from the understanding of the marine system. The traditional approach has been utilized in a way to postulate a deterministic model structure and treat its parameters as being imperfectly known. It is expected to be a precise description of a ship's dynamics (position, velocity, etc.) and its surrounding environment (wind, wave spectrum, etc.). To capture the ship's hydrodynamic effects, many models have been proposed by pioneers, such as the 1 degree of freedom (DOF) Nomoto model for autopilot heading control [3], 3 DOF maneuvering model of Abkowitz [4], the nonlinear or linearized dynamic positioning (DP) model, and the mathematical modeling group (MMG) model [5], etc. They are carefully used to provide a tractable and inexpensive approximation of the actual ship behaviors in many routine engineering and design activities, e.g., domain exploration, sensitivity analysis, development of empirical models, and optimization. The models as mentioned above are developed according to physical and hydrodynamics knowledge, as well as naval architecture principles [6]. It has been widely accepted that the modeling process is a compromise between simplicity to use and fidelity in the representation of reality. Deciding which phenomena and assumptions should be incorporated into the model is not easy, which relies intensely on sufficient observations, expert domain knowledge, as well as sound judgment in establishing hypotheses that support the validity of the model. When it comes to ship dynamics, usually complex ordinary differential equations are derived theoretically to define how the vessel performs over time. Although the approximate simulation model is acceptable if at least the most relevant characteristics are reflected, its fidelity still suffers from the disturbance of unpredictable environments and process noise due to approximation errors or unmodelled inputs [7].

Despite increased efforts paid to optimize the model structure, it still has circumstances deriving adequate models associated with parameter uncertainty. The parameter error is mainly produced from uncertainties related to defining the practical values of the hydrodynamic parameters [8]. The efforts and time needed to develop parameters should not be underestimated. The most reliable manner is thought to be experimentally determined. But this way could also be the most time-consuming and expensive. Only a limited number of hull ships have had any coefficients determined experimentally. While the use of a modern simulation environment, for instance, computer fluid dynamics (CFD), could facilitate the task [9]. If the system identification techniques are applied, the data quantity and quality for model tuning is always the main concern [10]. Ill-prepared data may give rise to deterioration. Given the accuracy deficiencies as well as the considerable efforts that went into the modeling process, the physics-based (PB) models are not always prioritized in demanding operations.

²This is Kognitwin energy, <https://www.kongsberg.com/digital/solutions/kognitwin-energy/this-is-kognitwin-energy>, Data accessed 25-February-2022

1.1.2 Data-driven modeling

The development of the information industry and advanced measuring instruments boost the data-driven (DD) modeling approaches and open up new possibilities for optimization and decision support. Onboard sensors can capture physical effects such as deformation or vibration under real-life conditions that cannot always be easily described by numerical models. By diving only into the data monitored, a data-based model could be established without explicit knowledge of the physical behavior of the system [11]. As an end-to-end technique, the DD approaches implicitly simulate the dependencies between the system's input and output variables and yield a sophisticated black-box model with plenty of parameters appropriately tuned. During the last decade, the number of researchers active in this area has considerably increased. The well-known machine learning (ML) domain is being increasingly used as a forecasting and analyzing tool to support effective decisions in operations in the marine context. Within certain data-intensive areas, like behavior learning and image recognition, the technology can deliver state-of-the-art performance [12].

While the flip side of this advantage is that large quantities of process data are required before the DD approaches are helpful. Once the data is ill-prepared, like the data volume is limited or the distribution is unbalanced, the performance of DD models could be far away from expectations. Moreover, the DD approaches are often criticized for the inherent 'black box' nature so that pure DD models are failing to gain full acceptance within fields rooted in engineering with zero risk tolerance [13].

1.1.3 Physics-data cooperative modeling

The physics-based and data-driven modeling can build into the context of the situation they are engaged in. From a broader perspective, the physics-data hybrid philosophy is one of cooperation, differentiation, and maximizing the potential of both participants in the modeling community. In the hybrid concept deployed as Fig. 1.1, modeling principles and styles of synthery have aligned differently in different operation scenarios. Briefly, the methodology and mission must be compatible to ensure optimal outcomes. By identifying the pros and cons of the physics and data modeling, conclusions are drawn that this hybrid concept is motivated by requisites from technical and practical aspects:

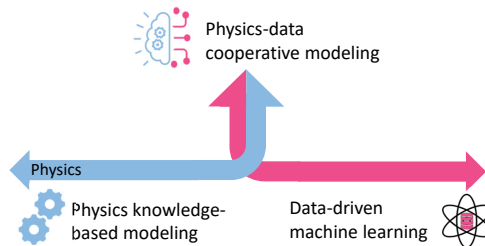


Figure 1.1: An illustration of physics-data cooperation.

- Technical advance: the hybrid model potentially integrates the advantages of both participants.

- Practical necessity: the hybrid model aims at situations where partial but not complete details (physics or data) are known about a system.

The core of this idea is that different modeling principles work in a cooperative way, which requires the capabilities of all the segmentation to operate as efficiently as possible to lower the modeling threshold and costs while enhancing the reliability, stability, and flexibility of the system. As a result, the yielded solutions are expected to provide fast and accurate predictions for optimization and autonomous control for offshore surface vessels. The terms cooperative, collaborative, and hybrid will be interchangeably used in the same context. Leveraging the speed and flexibility advantages of the data-driven technologies and ensuring the robustness and quality of the high-fidelity physics-based model, the cooperative modeling appears promising.

1.2 Research questions

The focus of this dissertation is concerned with physics-data cooperative modeling for ship motion prediction. It prompts the first question of this dissertation:

- **Can existing data-driven or physics-based modeling methods provide predictions as desired?**

In order to answer this question, it is necessary to investigate the state-of-the-art technologies in maritime modeling and prediction context and how they are being applied for different operational scenarios. Reviewing and summarizing the related work will lead to the next research question:

- **What are the challenges with applying physics-based and data-driven methods to predict ship motion?**

There are always assumptions involved in the physics deterministic model and ML models. To figure out what they can and cannot do, one has to dive into the basic principles behind each approach. For the classic numerical models in naval architecture, the governing equations are derived from Newton-Euler or Lagrange laws and fluid mechanisms. The analytical models render the inherently nonlinear characteristics of ship systems and are able to simulate ships, high-speed craft, underwater vehicles, and floating structures within a valid scope [14]. In contrast, the ML is learning from experience, which requires the test data to be sampled independently and identically from the same distribution as the training data [15]. However, the marine vehicles are operating in a highly nonlinear and dynamic environment, so the assumptions cannot be met everywhere. Thus the following research question appears:

- **When and where should either physics-based or data-driven approaches be used?**

The most suitable solution could be accessed from two aspects—principle and phenomenon. Pursuing interpretability and robustness or matching as much of reality as possible is a decision to be made before stepping into the modeling process. Except for

the subject customization, the decision is also constrained by the available object conditions. If the process data of the system or a specific scenario is not qualified to construct a data-driven predictive model, then the physics-based model is the only solution. In seeking the balance between two choices, the following research question is raised:

- **Why should a physics-data hybrid model be implemented? And where could it be applied for?**

The physics-data hybrid modeling concept is proposed from several considerations. 1), the state-of-art modeling approaches are not qualified to meet the stringent requirements on the interaction of digital twin model construction. 2), the hybrid modeling methodology aims to leverage both strengths and bridge the gap between two disciplines: learn from the knowledge and learn from experience. 3), in many real cases in the maritime domain, there exists some but not complete knowledge of the system. Meanwhile, some but insufficient data are available about the modeled process. These limitations lead to neither purely physics-based models nor solely data-driven models. In other words, when one model type suffers from inadequacies and cannot be applied independently, we expect that they can cooperate and complement each other.

- **How can data-driven approach be combined with ship physics knowledge?**

As mentioned above, the physics-data cooperative modeling appears promising in constructing a digital-twin ship. The exploration of the possible hybrid modeling methods will be the primary challenge. According to different requirements and scenarios, the hybrid modeling form will vary. Therefore, determining the architecture is the first to be paid attention to when performing hybrid modeling. Furthermore, the model structure optimization problems should be stressed.

- **How to evaluate the physics-data hybrid model?**

Ships often operate in complex environments with significant uncertainties, and the data comes from different sensory equipment. Ship speed, orientation, and positions are sampled from sensors such as Global Navigation Satellite Systems (GNSS), gyroscopes, accelerometers, etc. And the propulsion systems are monitored by the signal of power consumption, Revolution per Minute (RPM), torque, propeller or rudder angles, etc. Ideally, uncertainty analysis and sensitivity analysis, as integral assessments of the modeling process, could be used to inform the confidence of the results. While until now, there is no existing standard for hybrid modeling evaluation, and how to access the hybrid model is still an open question. Although the global "best model" is still pending, we can at least decide which model best suits the current local scenario. Upon this consideration, the following research question arises:

- **How can the physics-data hybrid model benefit a digital twin?**

Ship motion prediction is an enabling tool for operations involving ships and their immediate environment. It is widely applied to support the decision-making process, enhance

situational awareness, and detect collisions by revealing the likely future states of a ship. To achieve prediction, the physics-data cooperative model works in two ways. One is to improve data-driven models by simulating data for a wide range of operating conditions. The other is to improve the physics model to better match reality by integrating data-driven components. Either way will provide an enhanced representative model for the twinship. In this dissertation, the application scenarios involve situational awareness, such as component's status and system identification, and forecasting on what will happen if a specific action is taken, also referred to as what-if analysis.

1.3 Scope of work

1.3.1 Research objectives

In seeking to answer the above research questions, this dissertation seeks to obtain the following research objectives (ROs):

- ✓ **RO1: Exploring the physics-data cooperation architecture. The main target is to leverage the physics-data cooperative modeling technology and provide predictive insights into the facilities, enabling solid decision-support onboard.**

The main objective of this thesis is to develop a physics-data hybrid modeling approach that enhances motion prediction for marine vessels, which will be highlighted in all publications. Hybrid could take several forms, stemming from particular situations. While to support the development of hybrid methods, the single physics-based models are needed to be investigated as the enabling technology, which is covered in paper I and IV. Stepping further into the hybrid modeling domain, methodologies are proposed and explained in paper II, III, V, and VI.

- ✓ **RO2: Assessing the status the components of the ship and identifying their exterior effects using physics-based modeling method.**

The continuous monitoring of the internal components' status is a crucial enabler to provide higher reliability and safety. Inspecting the propulsion components' healthy conditions and resulting effects on the ship's maneuverability is required to be fast and efficiently implemented because of the detrimental effects of a breakdown. While since the vessel is not allowed to work continuously under faulty conditions, the high-quality labeled data scarcity is always an obstacle to data-driven fault diagnosis. Thereby, physics-based modeling is the best available solution to detect and isolate failures. The development of fault detection and isolation model for thruster is covered in paper I, and the propulsion unit retrofit effect research is conducted in paper IV.

- ✓ **RO3: Identifying the maneuvering model of the ship in realistic disturbance by estimating the unknown parameters.**

Apart from being aware of the status of the components, the integral ship dynamic properties are of particular concern when developing predictive control strategies. As discussed before, the environmental effects on the ship are difficult to accurately model,

but their results are not to be ignored. Identifying the ship dynamics in disturbed environments is thus practically important for real-time forecasting. With the ship maneuvering model plant known, the uncertain parameters could be estimated and tuned using experimental data and advanced data-driven techniques. Paper II presents a complete study on this topic. At the same time, it is noticed that the model plant is clarified in this context, and partial information on parameters is missing. If even less prior knowledge is known about a system, how could we construct an extensive model upon that? That answer leads to the following research objective.

✓ **RO4: Deriving representative models of a ship by incorporating and adapting other domains' knowledge properly.**

Benefiting from the physical knowledge from a well-developed domain, for example, a benchmark ship, the modeling process of the target research vessel is expected to be noticeably enhanced. The goal is to investigate the feasibility and strategies of identifying, incorporating, and adapting the specific domain knowledge to facilitate the target ship modeling.

1.3.2 Interconnection between the research objectives

The interconnection between the research objectives and publications is shown in Fig. 1.2. To fulfill RO2, two case studies are presented: one is regarding thruster failure detection and isolation, and the other concerns the thruster retrofit process.

For RO3, one case study of identifying the hydrodynamic derivatives in the ship maneuvering model is presented. It discusses the estimation performance in the existence of environmental disturbances, and this work is covered in Paper II. Moreover, several related works on model uncertainty analysis and sailing status recognition are taken in to achieve RO3.

The last objective RO4 delivers three case studies validating the knowledge transfer concept by physics-data combination. The representative model derived in paper III is based on a best available numerical model from a shorter version of the research vessel. While in paper V, the surrogate model of the target ship adapts the knowledge transferred from a benchmark source ship. For the vessels whose rough simulation model is available, we propose a cascaded hybrid model in paper VI. The validation cases involve various operational scenarios, including standard zigzag/circle maneuvers, docking operations, as well as drifting when shutting down the active dynamic positioning control. In paper VI, we also compare the capacities of physics-based, data-driven, and physics-data cooperative models and try to present a discussion on the assortment of modeling principles.

1.4 Structure of the dissertation

This introductory chapter presented the background for the dissertation research, clarifying its main objectives and defining the scope of work. The rest of this dissertation unfolds as follows. Chapter 2 introduces the proposed physics-data cooperative modeling framework and methodology. The foundations of the physics-based and data-driven model are also explained in detail. Chapters 3, 4 and 5 present case studies that show the use of developed hybrid approaches for ship motion prediction and system awareness.

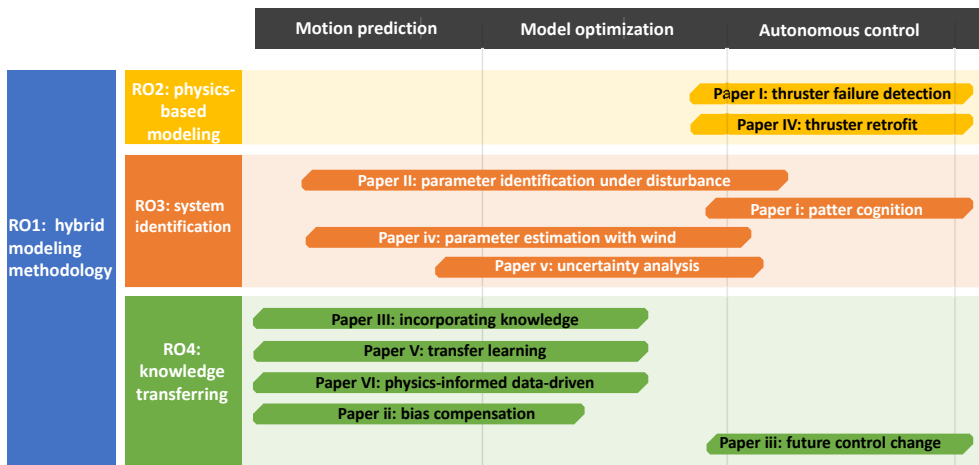


Figure 1.2: Overview of research objectives and interconnection with published paper. The capital roman letters indicate publications on which the thesis is based, and lower roman letters indicate associated publications.

Chapter 6 concludes the dissertation, summarizes the contributions and indicates the directions for future works. The first-author publications listed on page ix are shown in the appendices.

Physics-data cooperative model for motion predictions

This chapter explores the physics-data cooperative modeling technology and how it could be applied in maritime context to provide predictive insights. Fig. 2.1 presents an illustration of the physics-data collaborative approach to support demanding ocean applications. In the physics space, when clarifying the parameter sets in the simulation model through model tests or full-scale sea trials, the physics-based model of a ship sailing on the water is constructed. There is no doubt that this modeling process relies on domain expertise and thorough investigation. At the same time, the real-world ship in service is monitored and lots of operational data are accumulated to a database, from which the data-driven models are trained and validated. Communicating and bridging the two separate models will provide solid support to ship motion predictions, model optimizations, as well as autonomous control, etc. Section 2.1 proposes the physics and data integration methods. The fundamental principles of physics-based and data-driven modeling are explained in Section 2.2 and 2.3, respectively. Finally, Section 2.4 introduces the experimental platforms from which the analysed data are obtained.

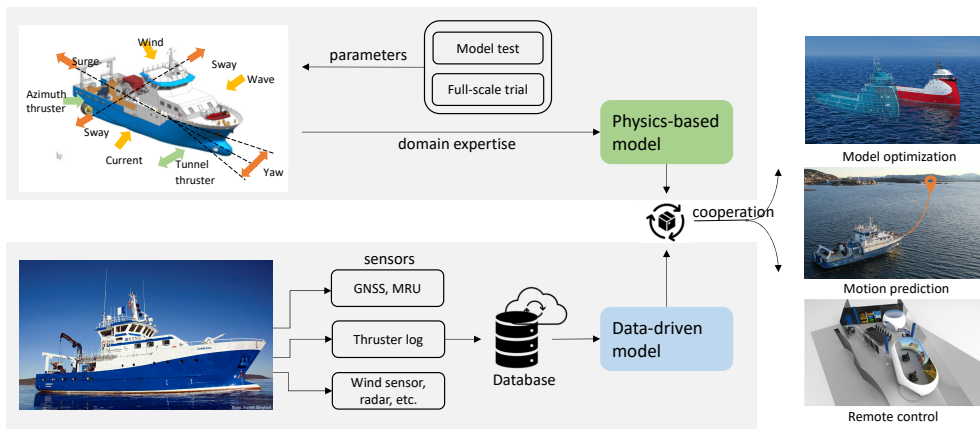


Figure 2.1: Illustration of physics-data cooperative modeling for decision support.

2.1 Hybrid modeling methodology

Both the model-based and data-driven approaches can be used for marine system modeling, and each has its advantages and drawbacks as summarized in Table. 2.1. The PB models have a deep understanding of the system dynamics, and they do not need data

to model the system. Still, they may need data for calibrating their effectiveness. In contrast, DD models rely on data solely without considering the dynamics of the plants, which empowers the DD models to apply to vast types of systems. However, data can never be complete to capture all complex patterns of the considered system and ensure stable out-of-sample performance [16]. Therefore, hybrid modeling bridging the gap between knowledge models and data-driven models is proposed. The core idea of hybrid modeling is that different modeling principles are working in a coordinated way, where the capabilities of both segments operate as efficiently as possible to lower the modeling threshold while enhancing the reliability and flexibility of the system.

Table 2.1: Pros and cons of model-based and data-driven methods.

Approach	Advantages	Limitations
Physics-based	<ul style="list-style-type: none"> • derived on fundamental theoretical principles. • has universal validity in range of conditions for which the model's assumptions hold. 	<ul style="list-style-type: none"> • requires simplifying assumptions. • mathematical solutions are complex. • needs extensive domain knowledge. • hard to accommodate with noise and uncertainties. • lengthy trials and efforts are needed to go into the modeling process.
Data-driven	<ul style="list-style-type: none"> • ensures better match with the reality. • requires little domain knowledge. • enables accommodate uncertainties. 	<ul style="list-style-type: none"> • requires a large amount of high-quality data. • yields uninterpretable black-box model • restricts to range of scenarios experienced in training data set.

From the functionality point of view, the PB and DD models could work together in three modes: *completeness*, *cooperation* and *competition*, as shown in Fig. 2.2. As the definition suggests, when one model reflects the majority of the system but with some details missing, the other model comes to work for the completeness. While if the two models both capture certain properties, which are much likely to be discriminative, they are trying to work out a resolution in a coordinated way so that everybody is accommodated, and both participants come out benefiting. If the two candidates are both proven to be qualified representing the system, they will be competing with each

other. Characterizing different features, they will rank differently depending on the mission requirements.

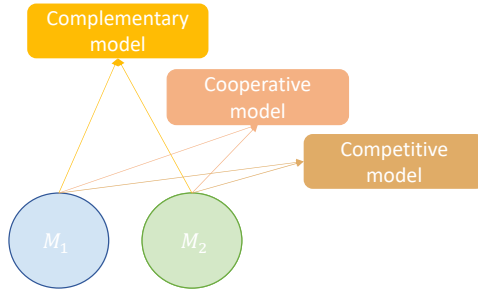


Figure 2.2: Functional interactions of PB and DD model components.

From the methodology perspective, hybrid modeling could be implemented in multiple ways. According to the structural interaction between the PB models and DD models, we categorize it as Fig. 2.3 shows. M_1 and M_2 are two model participants constructed on different disciplines. Specifically speaking, if M_1 is assigned as the physics-based model, then M_2 turns out data-driven, and controversially, if M_1 is data-driven one, and M_2 will be the physics induced one. It is seen in this figure that the synthesis of two separate domain models takes three forms:

- (1) **Insertion**: where a global model M_1 is adopted, the other model M_2 functions interpolated to M_1 .
- (2) **Cascaded**: where the two models work in a sequential way, with the information cascading from M_1 to M_2 .
- (3) **Parallel**: where the two models work in a parallel way, the outcome of each model is summed up to the ultimate result.

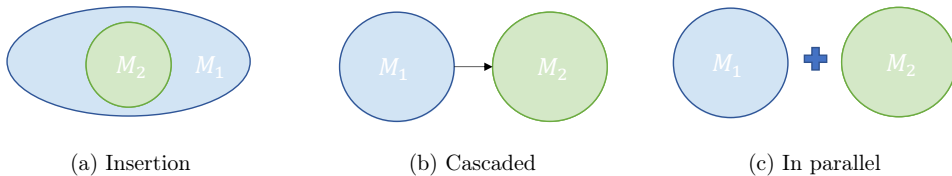


Figure 2.3: Categories of physics-data hybrid modeling architectures.

2.1.1 Insertion

As Fig. 2.3a indicates, insertion can take place in two directions depending on the definition of M_1 : One is data-optimized physics-based model and the other one is physics-informed data-driven.

Data-optimized physics-based model

It is applied when the model structure is available from deep understanding of the underlying process, still some parameters need to be estimated from the observed data [17]. The optimized physics model is getting improved in terms of accuracy and reliability. The ship dynamics is usually modeled as (2.1) reflecting the knowledge of the ship hull's geometry, mass distribution, propeller characteristics, main engine consumption, etc.

$$\begin{aligned}\dot{x}(t) &= f(x, u, \theta) \\ y(t) &= Cx(t)\end{aligned}\tag{2.1}$$

where the $x \in \mathbb{R}^n$ is the state vector of the vessel system, $u \in \mathbb{R}^m$ is the control signal, $y \in \mathbb{R}^p$ is the output vector and f is the nonlinear function of ship dynamics.

Fitting a model within a given structure is the most cases a lesser problem which is often established by an optimization method as (2.2) shows.

$$\begin{aligned}\hat{y}_i &= f(x_i, \theta) \\ \theta^* &: \min_{\theta} \sum_{i=1}^n \|\hat{y}_i - y_i\| \\ y^* &= f(x, \theta^*)\end{aligned}\tag{2.2}$$

where y and \hat{y} are the observations of target variable measurements and estimates respectively.

The optimizations applied to estimate specific parameters for a model structure built on physical grounds are widely recognized as a case of grey-box modeling [18]. In this situation, it is often assumed that the parameters of such models can be assigned physical meaning. For interpretation of model parameters to be justified, the results of the parameter estimation process must show a low degree of dispersion [19], e.g., be independent of the initial guess parameter vector for the estimation algorithms. By uniquely determining the model parameters from the process data, the resulting model is expected to reproduce and generalize the ship motions. Lots of intelligent algorithms are proposed in this subject, such as the genetic algorithms [20, 21], Support Vector Machine (SVM) approach [22, 23], etc.

In marine systems, the nonlinear maneuvering model identification is made, in practice, by conducting maneuvers with the ship using rudder and thrusters/propellers for excitation. However, with limits to the possible excitation, all parameters are rarely identifiable [8]. On the one hand, not all parameters in the maneuvering model can be obtained using system identification, no matter what input-output samples are given and which optimization scheme is adopted. On the other hand, parameter drift happens to some hydrodynamic coefficients, which means the obtained coefficients deviate from their valid values. Various solutions have been put forward to improve the identification process, such as constrain the parameter relations to achieve convergence [24], intentionally design the excitation signals to cover the maximum dynamic information [25], reconstruct the model [26][27], preprocess the training data [28], and so on.

Physics-informed data-driven model

As opposed to the previous kind of interpolation, physics knowledge is employed to improve the data-driven segment on the interpretability of the underlying system in this approach.

The general data-driven modeling process is completed in two phases: (i) training phase, a set of data is used to induce a model that best fits them, according to specific criteria; (ii) the trained model is employed for prediction and control purposes of the marine system. Targeting a regression problem when representing a continuous system aims to find the best-approximating function $h(x)$, where $h : \mathbb{R}^n \rightarrow \mathbb{R}$. During the training phase, the quality of the regressor $h(x)$ is measured according to a loss function $\ell(h(x), y)$, which calculates the discrepancy between the true and the estimated output. The empirical error representing the average discrepancy is reported by a model over the entire training dataset \mathcal{D}_n (n is the sample length):

$$\mathcal{L}_n(h) = \frac{1}{n} \sum_{i=1}^n \ell(h(x_i), y_i) \quad (2.3)$$

Except for minimizing the empirical error $\mathcal{L}_n(h)$ (empirical risk) as much as possible, the model complexity $\mathcal{R}(h)$ (structural risk) also has to be taken into account. The overall criterium for selecting the best-approximating model consists of these two metrics:

$$h^* : \min_h \mathcal{L}_n(h) + \lambda \mathcal{R}(h) \quad (2.4)$$

where λ is a hyperparameter that regulates the trade-off between the overfitting tendency, related to the minimisation of the empirical error, and the underfitting tendency, related to the minimisation of structural error. The optimal value for λ is problem-dependent, and tuning this hyperparameter is a non-trivial task.

Looking into the DD process, several possible ways of knowledge fusion are indicated to enhance the DD model.

- **Feature selection:** Selecting appropriate features that are derived from physical understanding of the process is an effective way to encode the priori knowledge in DD models [29]. Moreover, employing physics-based features in DD models potentially reduces the number of independent model features and reduces the risk of model overfitting.
- **Custom loss function:** Incorporating the physical understanding into the training loss functions, the ML models may provide a physically consistent, good approximate solution to the system [30, 31]. The knowledge could be preserved in the form of initial conditions, boundaries, residual errors, etc. In general, the customized loss function can be defined as $h^* : \min_h \mathcal{L}_n(h) + \lambda \mathcal{R}(h) + \lambda_p f_p$, where the physics-based equations f_p are used as an additional regularization term in the loss function of the networks.
- **Insert knowledge layer:** Extending the network topology by inserting a physics-related layer could be an alternative [32, 33]. This way the first principle physics-based information is decomposed, memorized, and integrated into the DD model.

2.1.2 Cascaded

This hybrid structure is also referred to as the serial approach, as shown in Fig. 2.3b. This form of the hybrid is approached by carrying the information leveraged by one model forward into the other model and providing a strongly correlated insights. It could be evolved in two directions: 1) leveraging physics knowledge to data models or 2) passing data mining information to the physics-based model.

For the first manner, the domain expertise of the underlying system is processed and carried forward into the DD component in the form of inputs, so that the non-parametric component of the DD model is strongly linked to the physics. It is opposed to relying on the universal approximation property of any purely DD method. Such a relationship is expressed as (2.5).

$$\begin{aligned}\dot{x} &= f(x, u, \theta) \\ y^* &= g(x, u, \dot{x})\end{aligned}\tag{2.5}$$

where x is the state of the vessel system. u and y^* are registered as system control and output, respectively. f represents the physical-based model, and the production of the reference model is integrated as an additional input to the the nonlinear DD model g . It could be a neural network (NN) that represents a transfer function from the base physical model to the representative model of the target system.

For the second situation, data-driven techniques are utilized to facilitate and optimize the physics understanding. For instance, when the sensitivity analysis is implemented for the hydrodynamic coefficients in the mathematical model, the numerical model could be simplified by omitting the less related components [34]. Another significant benefit of data analysis before stepping into the modeling phase is the enabling of locally modeling on a specific context. Thus, in addition to the global general model which preserves the majority of the underlying process characteristics, the introduction of multiple local models covering discriminative features allows unlocking more potential properties. The ensemble of multi-local models or the integration of global-local models would both advance the physical understanding.

2.1.3 Parallel

The parallel manner refers to those methods which consist of a DD learner that compensates the process model in the sense of correcting the error, as shown in Fig. 2.3c. It has been widely accepted that modeling errors are unavoidable but influenceable aspects of identification practice. Moreover, it is not reasonable to model the behavior of a process entirely through deterministic relations. The PB model derived from fundamental theoretical principles is assumed to be noise-free and capture specific dynamic characteristics. And the DD model is utilized in parallel to accommodate the bias issues and deliver accurate results by accounting for uncertainties and nonlinearities that cannot be easily modeled in the PB and correcting noise.

Usually, the practice of using a DD learner to model the residuals from a model is referred to as "bias correction", acknowledging that there is likely to be some error in the complex mathematical representation of the system [35]. The summation of PB predictions and DD compensation takes the following form.

$$\begin{aligned}
 y_p^* &= f(x, u, \theta) \\
 y_d^* &= g(x) \\
 y^* &= y_p^* + y_d^*
 \end{aligned} \tag{2.6}$$

The DD predictions y_d^* are usually generated through supervised learning algorithms. For instance, in [36], a long-short term memory (LSTM) neural network was integrated into the ship dynamic model to compensate for the unmodeled behavior and inaccuracies. Similarly, in [37], a Gaussian process (GP) regressor was trained to correct the physics-based model's systematic errors.

From the review above, the main principles of the physics-data cooperation are introduced and categorized according to the structural characteristics of interaction. Among them, the first two hybrid ways are mainly investigated in this thesis. Although the third way is not fully developed in this thesis, it is studied in cooperation with team members, and covered in the co-authored publications. The present thesis aims to be detailed in definitions and applications of specific categories while providing a broad perspective of the hybrid philosophy.

2.2 Fundamentals of the physics-based model

The physics-based models describing ship dynamics could be formulated in the frequency-domain or the time-domain. When the model structure is determined, proper parameters need to be tuned within physically reasonable ranges to reflect the specific properties as close to reality. In this section, the simulation model of the ship motion will be elaborated. This thesis deals with ocean scenarios including standard maneuvers (Kempf's zigzag and turning circle), ship docking, and dynamic positioning, with the forward speed varying from high-speed to low-speed. Depending on the cruising speed and motion of directions, the nonlinear maneuvering model as well as the linearized DP model describing the horizontal motions (surge, sway, and yaw) are employed for simulation and prediction.

2.2.1 Maneuvering model

The 3 DOF horizontal plane maneuvering model describes relations between actuators, external environmental disturbances, and the hull [14]. The ship model based on the rigid-body kinetics is expressed as (2.7):

$$\begin{aligned}
 \dot{\eta} &= R(\psi)\nu \\
 M_{RB}\dot{\nu} + C_{RB}(\nu)\nu + M_A\dot{\nu}_r + C_A(\nu_r)\nu_r + D(\nu_r) + D_n(\nu_r)\nu_r &= \tau_c + \tau_{wind} + \tau_{wave}
 \end{aligned} \tag{2.7}$$

where $\eta = [x, y, \psi]^T$ is the ship position vector containing the north, east positions and yaw angle in the Earth-tangential North-East-Down (NED) frame. $\nu = [u, v, r]^T$ is the ship velocity vector in surge (longitudinal axis), sway (lateral axis), and yaw (rotation about the up-down axis) directions in the ship's coordinate, respectively. $R(\psi)$ is the horizontal plane rotation matrix which is given as (2.8):

$$R(\psi) = \begin{bmatrix} \cos(\psi) & -\sin(\psi) & 0 \\ \sin(\psi) & \cos(\psi) & 0 \\ 0 & 0 & 1 \end{bmatrix} \quad (2.8)$$

In the ship's coordinate frame, the model reflects the ship response due to the forces including wind, waves, thrusters, hull friction, and inertia. Here, $\nu_r = \nu - \nu_c$ is the relative velocity vector through water, $\nu_c = [u_c, v_c, 0]^T$ is the generalized ocean current velocity of an irrotational fluid. $M_{RB} \in \mathbb{R}^{3 \times 3}$ is the vessel's rigid-body mass matrix, and M_A is the added mass matrix. $C_{RB}(\nu) \in \mathbb{R}^{3 \times 3}$ and $C_A(\nu_r) \in \mathbb{R}^{3 \times 3}$ are the skew-symmetric Coriolis and centripetal matrices of the rigid body and the added mass. $D(\nu_r) \in \mathbb{R}^{3 \times 3}$ and $D_n(\nu_r) \in \mathbb{R}^{3 \times 3}$ are the linear, and nonlinear damping matrices, which are functions of the relative velocity ν_r between the vessel and the current.

External force components generally come from three sources (the ocean current-induced force has been accounted by the relative velocity ν_r):

- $\tau_c \in \mathbb{R}^3$ — the control vector consisting of forces and moments produced by the thruster system;
- $\tau_{wind} \in \mathbb{R}^3$ — force induced by wind acting at a certain angle relative to the ship;
- $\tau_{wave} \in \mathbb{R}^3$ — force induced by waves. This force is not directly measurable and the drift component is generally observed as nonzero slowly varying process.

The generalized control force τ_c is obtained by translating the individual thruster forces, that act at specific locations on the ship hull, to the ship's body frame, as shown in (2.9).

$$\tau_c = T(\delta)F_T \quad (2.9)$$

where δ is the thruster orientation angle, and $T(\delta)$ is the thrust configuration matrix, which describes the geometrical locations of the thrusters. $\tau_c = [\tau_x, \tau_y, \tau_n]^T$ refers to the control force vector acting on the vessel. F_T consists of forces produced by tunnel thruster, main propellers, or azimuth thrusters, respectively.

The individual propeller thrust T and torque Q are generally formulated as a function of shaft speed n in revolution-per-minute, time-varying states \mathbf{x}_p , and fixed thruster parameters θ_p [38]. The thruster models (2.10) are generic models parameterized to fit the research vessel.

$$\begin{aligned} T &= f_T(n, \mathbf{x}_p, \theta_p) \\ Q &= f_Q(n, \mathbf{x}_p, \theta_p) \end{aligned} \quad (2.10)$$

The wind force is the only environmental disturbance that can be estimated based on the wind speed and velocity measured on board. The deterministic model to estimate wind forces is given in (2.11).

$$\tau_w = \frac{1}{2} \rho_a V_{rw}^2 \begin{bmatrix} C_X(\gamma_{rw}) A_{FW} \\ C_Y(\gamma_{rw}) A_{LW} \\ C_N(\gamma_{rw}) A_{LW} L_{oa} \end{bmatrix} \quad (2.11)$$

The relative wind speed is defined as $V_{rw} = \sqrt{u_{rw}^2 + v_{rw}^2}$ and attack angle $\gamma_{rw} = -\text{atan2}(v_{rw}, u_{rw})$, where $u_{rw} = u - V_w \cos(\beta_w - \psi)$, and $v_{rw} = v - V_w \sin(\beta_w - \psi)$. V_w and β_w represent the wind speed and its direction, respectively. C_X, C_Y , and C_N are wind coefficients specific for the hull or superstructure shape. A_{FW} and A_{LW} are frontal and lateral projected areas and L_{oa} is the overall length of the ship.

Except for the feedforward estimation method of environmental loads like (2.11), they could also be modeled as a stochastic process [14]. Such a process can represent the slowly varying environmental forces and moments due to wind loads, second-order wave drift forces, and current forces. The overall effects of environmental factors as well as unmodeled nonlinear dynamics are lumped into a bias term $b \in \mathbb{R}^3$. The resulting model becomes

$$\begin{aligned} \dot{\eta} &= R(\psi)\nu \\ \dot{b} &= w_1 \\ M\dot{\nu} + C\nu + D\nu &= R^T(\psi)b + \tau_c + w_2 \end{aligned} \quad (2.12)$$

Alternatively, the bias could be modeled as first-order Markov process (2.13).

$$\dot{b} = -T^{-1}b + w_1 \quad (2.13)$$

In (2.12), the variables $w_i (i = 1, 2)$ are zero-mean Gaussian noise vectors representing model uncertainty.

2.2.2 Dynamic positioning model

The DP models are valid for station-keeping and low-speed maneuvering up to approximate 2m/s where the linear assumption is a good solution for simplification. For horizontal motion of a fully actuated offshore surface vessel exposed to wind disturbances, considering the surge, sway and yaw motion components, the linearized mathematical model of ship in DP maneuvering is expressed as [14]:

$$\begin{aligned} \dot{\eta} &= R(\psi)\nu \\ M\dot{\nu} + D\nu &= \tau_c + \tau_{wind} \end{aligned} \quad (2.14)$$

where, $\eta = [x, y, \psi]^T$ is the ship position vector in the NED frame. $\nu = [u, v, r]^T$ is the ship velocity vector in the body-fixed frame. The rotation matrix is specified by (2.8). $M = M_{RB} + M_A$ is the ship's inertia matrix including added mass. D is the linear damping matrix. τ_c is the generalized control forces which are distributed among the thrusters as indicated in (2.9). The thruster configuration matrix depends on the location and orientation of thrusters. The wind force τ_{wind} acting on the vessel moving at a forward speed are estimated as (2.11).

2.3 Principles of the data-driven model

Data-driven method is the general term for constructing models based on analysing data. The term machine learning is often used interchangeably, which refers to the computational methods that learn through experience. Problem learning indicates the process of improving a certain performance of a certain task through a certain type of training experience. The experience is expressed in the format of data and therefore the methods are called data-driven.

Depending on whether labels (or corresponding target values) are provided to train and evaluate a model, the process can be divided into two paradigms: supervised learning and unsupervised learning. Both learning strategies can be used for solving the classification, regression, and ranking tasks. For the motion prediction applications, the supervised learning methods which usually focus on function approximation are chosen to perform the regression problems. Generally, given the training data set in the form of a collection of (x, y) pairs, the task is to find a function f so that a prediction $y^* = f(x^*)$ can be made to a query x^* based on the training data. The input x could be a vector or other complex objects, like images. The function f may take many forms depending on the learning algorithms. For example, f could be explicitly expressed as a parameterized function and the parameters are determined by the training data through an optimization process, or f as well as its parameters are implicitly determined simultaneously by a search process with tunable hyperparameters.

Recent years have seen plenty of machine learning algorithms developed to cover different data and tasks. As clarified before, only the supervised machine learning models are focused to tackle the regression problems in this thesis. The following are some of the algorithms that have been used as modeling tools in this dissertation.

2.3.1 Support vector regression

Support vector regression (SVR) is an effective method for modeling and interpolating nonlinear functions. It was formally proposed in the 1990s [39] and is widely used for regression analysis for its global optimal solution. Given the training data sets $S = \{s_k | s_k = (x_k, y_k), x_k \in \mathbb{R}^n, y_i \in \mathbb{R}\}_{k=1}^m$ where x and y represent the input and corresponding target values respectively, m is the sample length, the basic idea of SVR is to fit a function $f(x) = \langle w, x \rangle + b$ onto a training data set. The weights vector w, b can be obtained by solving the optimization problem:

$$\begin{aligned} \min_{w,b} \quad & \frac{1}{2} \|w\|^2 + C \sum_{i=1}^n (\xi_i - \xi_i^*) \\ \text{s.t.} \quad & -\epsilon - \xi_i^* \leq \langle w, x_i \rangle + b - y_i \leq \epsilon + \xi_i \\ & \xi_i, \xi_i^* \geq 0 \end{aligned} \tag{2.15}$$

where ξ and ξ^* are slack variables representing the deviation from a predefined gap with hyperparameter ϵ . The hyperparameter C denotes the strength of the regularization which is inversely proportional to C . The minimization solution is offered by the Lagrangian multiplier technique, which by itself leads to a dual optimization problem:

$$\begin{aligned} \min_{\alpha, \beta} \quad & \frac{1}{2} \sum_{i,j=1}^m (\alpha_i - \beta_i)(\alpha_j - \beta_j) k(x_i, x_j) \\ & + \epsilon \sum_{i=1}^m (\alpha_i + \beta_i) - \sum_{i=1}^m y_i (\alpha_i + \beta_i) \\ \text{s.t.} \quad & 0 \leq \alpha_i, \beta_i \leq C \end{aligned} \tag{2.16}$$

where α, β are the Lagrangian multipliers, $k(x_i, x_j)$ is a kernel function which is used

to account for nonlinearities. The conditions for optimality is based on Karush-Kuhn-Tucker conditions (KKT). The resulting solution of the function f is given as:

$$f(x) = \sum_{i=1}^m (\alpha_i - \beta_i) k(x_i, x_j) + b \quad (2.17)$$

The kernel functions have several choices, such as the linear, polynomial, radial basis function, etc. To implement the parameter identification application, the linear kernel function which is expressed as $k(x_i, x_j) = x_i^T x_j$ is adopted.

2.3.2 Multi-layered perceptron

The multi-layered perceptrons (MLPs) are neural network models that work as universal approximators. An MLP is specified with an input layer, one or multiple hidden layer, and an output layer. Fig. 2.4 depicts a general structure of such a network. Each neuron in the hidden layer applies an activation function to the sum of the inputs from the previous layer. The input features are passed on to an input function u , which computes the weighted sum of the input features:

$$u(x) = \sum_{i=1}^n w_{ik} x_i + b_k \quad (2.18)$$

where w is the weight vector, and b is the bias vector. x is the input features. The resulting sum is then passed onto an activation function a , which produces the output of the neuron:

$$o_k = a(u(x)) \quad (2.19)$$

In relation to Fig. 2.4, the output of node k is calculated according to (2.19). The frequently used activation functions for the hidden layer nodes are the sigmoid, hyperbolic tangent, Rectified Linear Unit (ReLU), etc. Learning in MLPs relates to adjusting its perceptrons' weights so as to provide low error on the training data. This process is traditionally done using the backpropagating algorithm, which attempts to minimize the loss function, typically mean square error (MSE).

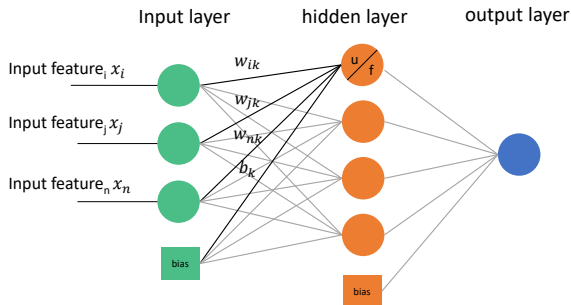


Figure 2.4: Structure of a general MLP.

2.3.3 Long short-term memory

Different from the feedforward MLP, Long short-term memory (LSTM) is a type of recurrent neural networks (RNN). As opposed to traditional RNN, the LSTM introduces a memory cell that regulates the information flow in and out of the cell. As shown in Fig. 2.5, the memory cell consists of three non-linear gating units that protect and regulate the cell state. The introduction of these gating units enables selectively remembering and forgetting the input data. When the input x_i passes through the memory cell, it selectively stores the information and allows it to affect the output. Thus, the LSTM is capable of learning the long-term dependencies in the data and is often used in applications dealing with time sequences. For each element in the input sequence, the LSTM computes the following function:

$$\begin{aligned}
 i_t &= \sigma(W_{ii}x_t + b_{ii} + W_{hi}h_{t-1} + b_{hi}) \\
 f_t &= \sigma(W_{if}x_t + b_{if} + W_{hf}h_{t-1} + b_{hf}) \\
 g_t &= \tanh(W_{ig}x_t + b_{ig} + W_{hg}h_{t-1} + b_{hg}) \\
 o_t &= \sigma(W_{io}x_t + b_{io} + W_{ho}h_{t-1} + b_{ho}) \\
 c_t &= f_t \odot c_{t-1} + i_t \odot g_t \\
 h_t &= o_t \odot \tanh(c_t)
 \end{aligned} \tag{2.20}$$

Where f, i, o and c represent the input gate, the forgetting gate, the output gate and the cell state, respectively. h_{t-1} and c_{t-1} are hidden state and cell state of the LSTM structure at the $t-1$ time step. h_t, c_t , and x_t are the hidden state, cell state at time t , x_t is the input vector at time t . W and b are the weights and bias in the LSTM cell. σ refers the activation function sigmoid $\sigma(x) = 1/(1 + e^{-x})$, \tanh is the hyperbolic tangent function, and \odot is the Hadamard product.

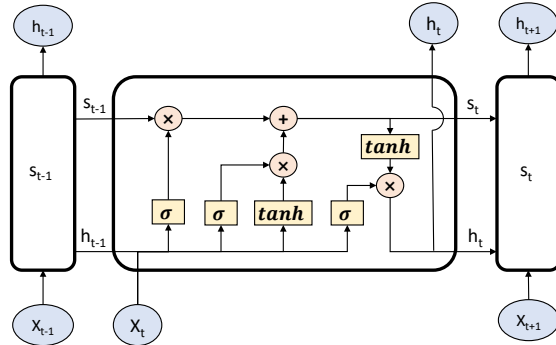


Figure 2.5: Schematic illustration of a LSTM cell.

2.4 Experimental platforms and data collection

For the duration of the Ph.D project, three main experimental platforms have been used extensively to develop and validate the modeling approaches proposed in this thesis.

Three high-fidelity simulators and one NTNU-owned real-world vessel are engaged to sample ship operation data.

2.4.1 OSC simulator

The Offshore Simulation Centre¹(OSC) specializes in providing realistic and integrated simulator solutions for a variety of applications, including training in best practice for critical operations and virtual prototyping. The simulator features a simulated environment in which a user may manipulate the wind, waves, and ocean current to mimic environmental conditions. A multi-purpose offshore vessel is selected for the tests performed in the OSC simulator. Fig. 2.6 depicts the real-life vessel and its simulation solution. The numerical models of the vessel, the simulated environmental disturbances and thrust-producing devices were used in the project. Its main dimensions are given in Table. 2.2. This offshore vessel is equipped with two main propellers, one retractable thruster forward, two side tunnel thrusters forward, and two aft [40], as shown in Fig. 2.7. The simulated vessel solutions of DP and zigzag maneuvers were applied for paper I and V.

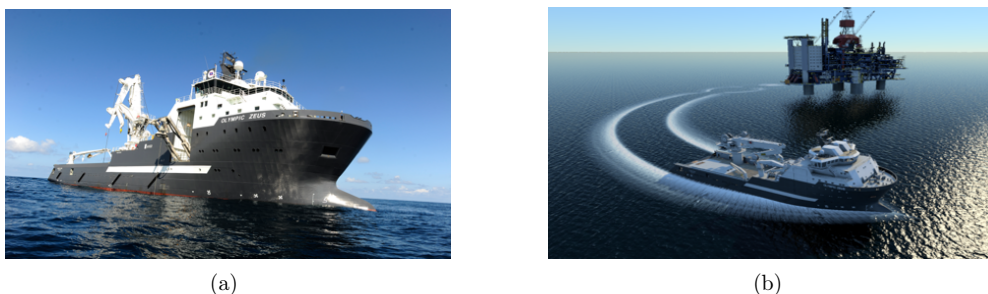


Figure 2.6: The selected offshore vessel and its simulation in the OSC simulator.

Table 2.2: Physical parameters of the OSC-simulated vessel.

Description	Parameters	Value
Length over all	$L_{oa}[m]$	93.8
Length between perpendiculars	$L_{pp}[m]$	82.7
Breadth middle	$B[m]$	23.058
Draught	$T[m]$	7.5
Deadweight	$DWT[t]$	4925
Design speed	$U[knot]$	17.5

2.4.2 Co-simulation

Co-simulation refers to an enabling tool, where distributed sub-systems makes up a global simulation. Each sub-system is a simulator which allows to be modeled with its own tool in its domain, and is broadly defined as a black-box capable of exhibiting behavior. In a co-simulation algorithm, the interactions between these sub-simulators

¹The Offshore Simulation Centre, <https://osc.no/>, Data accessed 08-March-2022

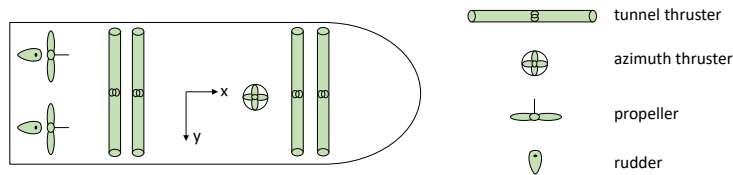


Figure 2.7: Thruster configuration the vessel simulated in OSC.

are synchronized at discrete communication points. Generally, the sub-simulators accept inputs (from other sub-simulators), advance in time with a built-in solver routine up to the next communication point, and finally output some results [41]. The results may in turn be used as inputs to other sub-simulators. The Functional Mock-up Interface (FMI) standard is a commonly used standard for co-simulation, and a model implementing the FMI is known as a Functional Mock-up Unit (FMU). The FMI enables an FMU exported by one tool to interoperate with a variety of host tools and for host tools to orchestrate interactions between FMUs exported by a variety of other tools [42]. A system can then be modelled as a collection of interconnected FMUs.

Vico, developed by our team [43], is a generic co-simulation framework based on the Entity-Component-System software architecture that supports the FMI as well as the System Structure and Parameterization² (SSP) standards. The user may manipulate the wind, waves, and ocean currents to mimic environmental conditions. The experiments implemented by co-simulation cover standard zigzag maneuver and docking operations of a NTNU-owned research vessel *Gunnerus*, and the related works are expanded in paper III and IV.

The co-simulation setup for a zigzag maneuvering experiment is presented in Fig. 2.8, and each block represents an FMI-compatible model. The environmental conditions are specified as initial values for the *VesselModel* which is developed by SINTEF Ocean. The *Zig-zag Controller* is developed by the author in Python, and the *Azimuth* model is supplied by the thrust manufacturer Kongsberg Maritime. The simulation fidelity of the models used in the experiments was verified against the actual ship in terms of ship speed, course, and power consumption [44].

2.4.3 Research vessel *Gunnerus*

The research vessel (R/V) *Gunnerus*³ as seen in Fig. 2.9, which is owned and operated by NTNU, was put into operation in 2006. It is equipped with the latest technology for a variety of research activities within biology, technology, geology, archaeology, oceanography, and fisheries research [45]. In addition to research, the ship is used for educational purposes and is an important platform for marine courses at all levels and disciplines. Table. 2.3 holds the main dimensions of the vessel. The R/V *Gunnerus* was equipped with twin fixed-pitch ducted propellers and rudders and one tunnel thruster from Brunvoll. In 2015, the R/V *Gunnerus* went through a thruster refit, and the original propellers were replaced with Permanent Magnet (PM) rim-drive azimuthing

²Standard for configuring simulations that consist of FMUs, <https://ssp-standard.org/>, Data accessed 08-March-2022

³The R/V *Gunnerus*, <https://www.ntnu.edu/gunnerus>, Data accessed 08-March-2022

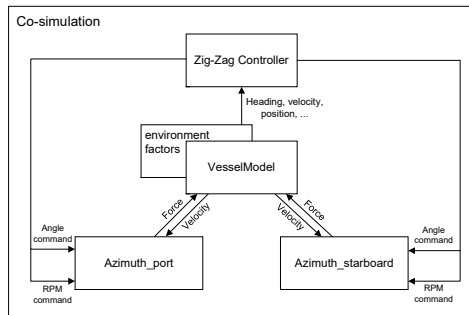


Figure 2.8: Diagram showing the relationship of components in co-simulation of executing zigzag maneuver.

thrusters, and its layout is presented as Fig. 2.10. The original propellers were 5-bladed, high skew type with a diameter of 2.0 meters that rotated in a 19A type duct profile, and the new azimuthing thrusters incorporates a ring propeller in a tailor-made duct with a diameter of 1.9 meter with four blades having a forward skewed shape. Fig. 2.11 shows the propulsion configuration on Gunnerus before and after retrofit, where the left is the origin pitch propeller with ice-fins, and the right is the refitted azimuth thruster provided by Rolls-Royce. The same diesel-electric system supplied the propulsion and maneuvering power before and after the conversion. In 2019, the vessel was elongated to 36.25m from original 31.25m. All other geometrical and propulsion characteristics except the length dimensions remained the same. Because of the elongation, there are two versions of the vessel, which are both used in this project.



Figure 2.9: Starboard side-view of the R/V Gunnerus.

As a research vessel, there are many data acquisition systems installed onboard the Gunnerus, like thrusters, power generators, navigational sensors, and motion control systems, etc. The number of measurable sensor channels is high, and for the motion prediction purpose, we are interested in the data originating from GPS receiver, a motion reference unit (MRU), compasses, a wind sensor, and sensors reflecting orientation and rotational speed of thrusters. The sensor channels related to motion prediction are listed in Table. 2.4. For all measurements in the data set, a sampling rate of 1 Hz was observed.

Table 2.3: Physical parameters of the R/V Gunnerus.

Description	Parameters	Short version	Elongated version
Length over all	$L_{oa}[m]$	31.25	36.25
Length between perpendiculars	$L_{pp}[m]$	28.9	33.9
Breadth middle	$B[m]$	9.6	9.6
Draught	$T[m]$	2.7	2.7
Design speed	$U[knot]$	9.6	9.6

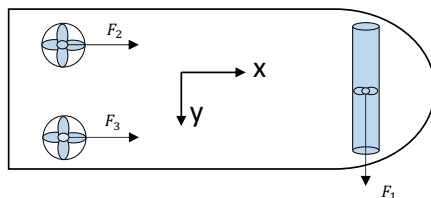


Figure 2.10: The thruster configuration the R/V Gunnerus.

2.4.4 MSS toolbox

The Marine Systems Simulator⁴ (MSS) is a Matlab and Simulink library for marine systems. It includes models for ships, underwater vehicles, unmanned surface vehicles, and floating structures. The library also contains guidance, navigation, and control (GNC) blocks for real-time simulation [46]. Being widely used in marine simulation, the toolbox provides resources for the implementation of mathematical models of benchmark ships, such as the Mariner class vessel [47], the container vessel, and so on. Thus the toolbox is usually used as a verification platform in marine research. In this thesis, the experiments implemented in paper II are conducted in this simulator.

2.5 Chapter summary

This chapter clarifies the physics-data cooperative modeling methodology and possible manners in the maritime domain. The fundamentals of physics-based and data-driven modeling disciplines are introduced. In addition, the experimental platforms and data acquisition that are utilized in this dissertation are presented. Fig. 2.12 displays how these models and media are engaged in the following chapters. According to the outlined research objectives, chapters 3-5 each cover one objective validated by relevant case studies. Chapter 3 presents the applications of physics-based modeling for facilitating a ship's dynamic model as well as its components, and its experiments are performed on OSC and co-simulation. Chapter 4 discusses ship dynamic optimization issues by identifying the hydrodynamic derivatives, categorized as a physics-data collaborative way. The MSS toolbox is taken to generate ship maneuvering data. And in chapter 5, knowledge transfer is conceptualized by integrating the physics-based maneuvering model and data-driven model based on both real-life and simulation data. The three case studies constitute the main objectives of this dissertation, which are to exploit the physics-data cooperative modeling disciplines for ship motion prediction.

⁴Marine Systems Simulator (MSS), <https://github.com/cybergalactic/MSS>, Data accessed 08-March-2022



Figure 2.11: The propulsion arrangement of the R/V Gunnerus before and after retrofit.

Table 2.4: Data channels sensed onboard the R/V Gunnerus.

Signal	Channels	Unit
GPS	Latitude	ddmm.mmmm
	Longitude	ddmm.mmmm
	Surge velocity	knots
	Sway velocity	knots
	Course angle	deg
	Speed over ground	knots
MRU	Heading angle	deg
	Heading rate	deg/s
	Roll angle	deg
	Pitch angle	deg
	Heave displacement	m
	Roll rate	deg/s
	Pitch rate	deg/s
Wind sensor	Heave rate	m/s
	Wind direction	deg
Thruster	Wind speed	knots
	Port thruster rotational speed	%
	Port thruster angle	deg
	Starboard thruster rotational speed	%
	Starboard thruster angle	deg
	Tunnel thruster rotational speed	%

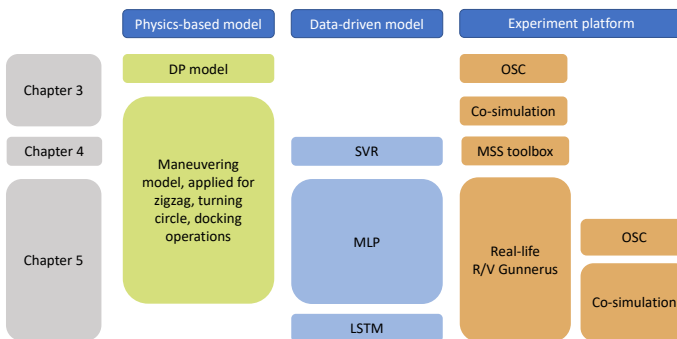


Figure 2.12: Interconnection of the PB and DD models as well as data source contained in different chapters.

Case study: Model-based thruster failure detection and retrofit

This chapter presents research results related to the physics-based model, covering the contents of paper I and IV. During the service life of a vessel, continuously monitoring, diagnosis, and prognostics of components are essential for ship health management and leverage alert for maintenance or conversions. Thrusters, as the main propulsion units used to position a modern vessel, will inevitably undergo faults due to long-time operation in the complex ocean environment. To avoid miserable damage to safety and the economy, timely diagnosis and isolating failed thruster are of great significance. Once faults are detected, decisions of maintenance or conversions can be made. It is reported that by replacing expired components or updating the outdated technology to the latest operational standards, the service life could be significantly prolonged, and the capability will be enhanced meanwhile [48]. Yet, since modern ships are becoming more complex and integrated, retrofitting them is a complex and intricate engineering task. A co-simulation-based thruster retrofit study is conducted to optimize the refit process and speed up the simulation. This chapter proposes a model-based approach for thruster failure detection and isolation (FDI) of a dynamically positioned offshore vessel. And the vessel conversion study is performed based on the research vessel *Gunnerus*.

3.1 Thruster failure detection and isolation

3.1.1 Methodology

An effective failure detection and isolation scheme is proposed for detecting thruster failure in dynamically positioning offshore surface vessels, as shown in Fig. 3.1. When one thruster fails to work normally, the ship's DP performance will diverge from the fault-free status. Thus ship position and orientation in the earth-fixed frame are selected as monitoring states. Failure detection and failure isolation are both included in the proposed framework. This figure specifies three modules in the schema, including ship measurements, mathematical modeling, and failure diagnosis.

In the real ship experiment or simulator, the DP operation is performed through a DP controller. For a fully actuated offshore surface vessel, the horizontal motions—surge, sway, and yaw movements are of great interest. The control force generated from the controller will be further allocated by an allocation algorithm to corresponding thrusters. And then, the vessel can be maneuvered towards the reference point by these thrusters. The simulation process is marked with a red dash line in Fig. 3.1. The mathematical model for ship maneuvering in the framework can be derived from Newton-Euler or Lagrange methods. The interaction between ship hull, propulsion force, and hydrodynamic effect is represented by a set of complex differential equations. At

present, there are several variants for ship maneuvering, such as the Nomoto model and nonlinear maneuvering model [49]. The residual signal, which reflects the variation between model-predicted state and sensor data, flows into the fault diagnosis module in the framework. The fault diagnosis module includes two components. The first one is used for detecting the existence of failures; the other one is to isolate the sources of failures. In a predefined detection time window, by applying the thruster command from the controller to the established mathematical model, an estimated ship state will be obtained. A ship behavior-based residual generator in the detection time window is introduced. It is designed to keep a low level in the fault-free phase and increase to exceed a threshold when a thruster failure occurs. In the isolation phase, residuals are further analyzed to configure the location of the failure by means of probability analysis. It ends up with a probabilistic model, from which better knowledge about the confidence of failure location, as well as more meaningful information to the end-user, can be gained.

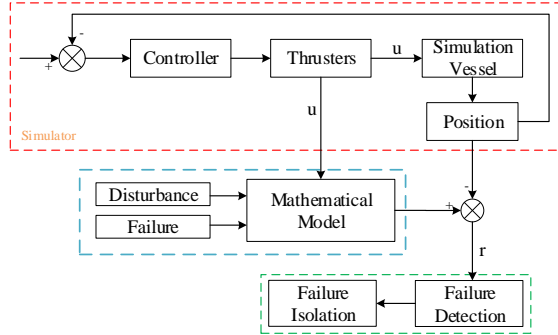


Figure 3.1: Thruster failure detection and isolation architecture.

Fault diagnosis

In the DP operation scenario, the vessel is supposed to keep steady at one fixed position (x_0, y_0) with orientation ψ_0 in the earth-fixed frame. The control force is distributed into each thruster, and then the vessel will be propelled towards the fixed point by the corresponding thrust.

In the failure detection module, a detection time window is adopted to evaluate the residuals between model reference sequences and measurement data. The states of the dynamic model under the command thrust can be estimated by solving the model differential equations. In the window $[t_0, t_T]$, the residuals are defined as:

$$r(t) = \sqrt{e_x^2 + e_y^2} \exp(e_\psi) \quad (3.1)$$

where $e_x = \hat{x} - x$, $e_y = \hat{y} - y$, $e_\psi = \hat{\psi} - \psi$, $[\hat{x}, \hat{y}, \hat{\psi}]$ are model estimated ship position and heading, $[x, y, \psi]$ represents real ship position and heading. After the residuals are generated, the detection of failure can be performed through the following rules, where

δ refers to the threshold obtained through several simulation experiments.

$$\begin{cases} r(t) \leq \delta & \text{normal} \\ r(t) > \delta & \text{failure} \end{cases} \quad (3.2)$$

Define the initial state of model as $X_0 = [\eta(t_0), \nu(t_0)]^T$, with the residual signal $r(t_0) = 0$. If there is no residual in the period $[t_0, t_0 + \Delta t]$ exceeds the threshold, the detected period is judged normal. Then the window slides to the next period $[t_0 + \Delta t, t_0 + 2\Delta t]$. This process will continue until an abnormal alarm happens. The value of the threshold is determined on the basis of a large number of experiments. In this paper, the threshold value is defined as:

$$\delta = \mu + k\sigma \quad (3.3)$$

where μ and σ are the mean and standard deviation of residuals in faulty-free status. The selection of k value is critical, which represents a trade-off between a low false-alarm rate and a high sensitivity to failures.

Once a fault is detected, the next problem to be solved is distinguishing the failure mode. According to the mathematical expression of DP maneuvering, the ship model reference sequences in healthy and different failure conditions can be built, respectively. At the time t_d when fault detection residual surpasses a given threshold, failure isolation can be accomplished by probability analysis between the actual successor sequence and the predicted state sequences based on an analytical model. In the detected faulty period $[t_d, t_e]$, a corresponding residual sequence is generated for each failure mode. The mean integral of residual is considered to obtain a quantitative comparison between the results of different failure mode simulations. The mean integral of the residual index, normalized with respect to the time length of the faulty period, is expressed as

$$s_i = \frac{1}{T} \int_{t_d}^{t_e} r(t) dt, i = 1, 2, \dots, N \quad (3.4)$$

where N represents the number of failure mode. The probability of each failure mode is calculated according to

$$P_i = 1 - \frac{s_i}{\sum_{i=1}^6 s_i} \quad (3.5)$$

The highest probability indicates that the relevant failure mode has the most similar features to the detected abnormal.

3.1.2 Experimental results

To validate the effectiveness of the proposed thruster failure detection and isolation method, simulation experiments of DP maneuvering under different failure scenarios are conducted. The selected simulation vessel is equipped with two main thrusters, two tunnel thrusters at the bow and two tunnel thrusters at the stern, as shown in Fig. 3.2.

The thruster configuration matrix has the form:

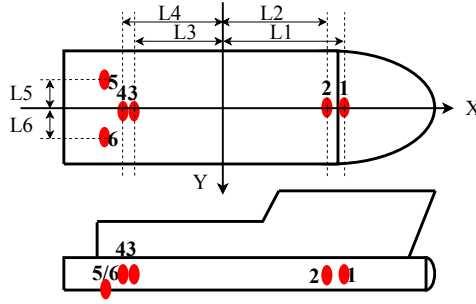


Figure 3.2: Thruster configuration for the offshore surface vessel.

$$\mathbf{T} = \begin{bmatrix} 0 & 0 & 0 & 0 & 1 & 1 \\ 1 & 1 & 1 & 1 & 0 & 0 \\ L_1 & L_2 & -L_3 & -L_4 & -L_5 & L_6 \end{bmatrix} \quad (3.6)$$

where $L_i (i = 1, \dots, 6)$ are the moment arms in yaw. The allocation of the six thrusters is symmetrical with respect to the longitudinal axis of the vessel. The two main thrusters, two bow tunnel thrusters, and two stern tunnel thrusters are considered three pairs of thrusters, and the same force demand is applied to both thrusters in each pair when they are running in fault-free status. It is worth noting that in the selected vessel, the bow tunnel thrusters and stern tunnel thrusters are located near, where the distances $d_b = L_1 - L_2$ and $d_s = L_4 - L_3$ are pretty small, almost 1/40 of the vessel length.

Model validation

The mathematical model is constructed with the known mass, damping terms, and unknown wind coefficients. Thus, the coefficients C_X, C_Y, C_N in the estimation expression need to be identified first. The normal DP simulation data $\{(t_i, X_i), i = 1, 2, \dots, n\}$ from the OSC simulator is divided into two sets, the first set is used to identify the unknown wind coefficients in the mathematical model by applying the least square method and the second set is selected to test the effectiveness and accuracy of the mathematical model.

The results are displayed in Fig. 3.3. It can be seen that the ship trajectory generated by the mathematical model fits well with the simulation data. This fact illustrates the applicability of the proposed failure detection method, which lies in the residuals between the model reference sequence and ship data.

Detection and isolation results

To verify the effectiveness of the proposed method, simulation experiments under different thruster failure modes are carried out. Single thruster failure cases are designed as Table 3.1 shows, where '0' refers to 100% thruster invalid, and '1' represents normal status.

Fig. 3.4a shows the residual results of two bow tunnel thrusters' failure. This failure is characterized by an abrupt invalid of a thruster, whose actual speed freezes at 0 while

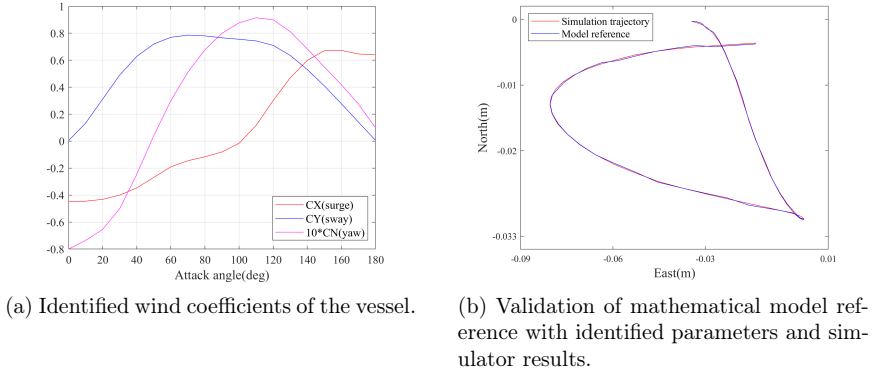


Figure 3.3: Mathematical model validation results.

Table 3.1: Thruster failure cases of simulation.

Case	th1	th2	th3	th4	th5	th6
011111	0	1	1	1	1	1
101111	1	0	1	1	1	1
110111	1	1	0	1	1	1
111011	1	1	1	0	1	1
111101	1	1	1	1	0	1
111110	1	1	1	1	1	0

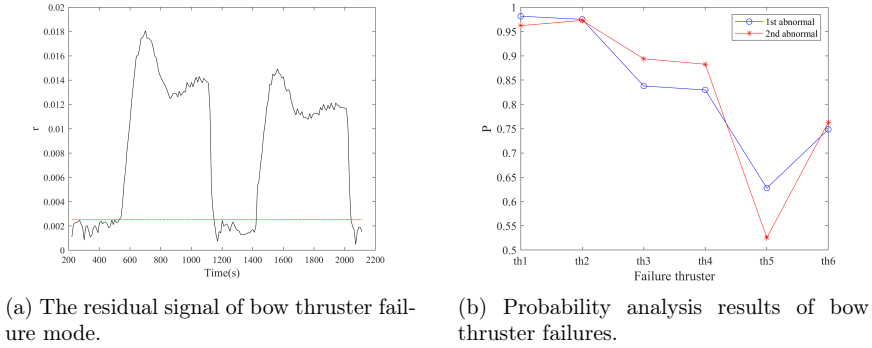


Figure 3.4: Bow thruster failure detection and isolation.

command speed is as usual. It can be seen that the fluctuations of the residual signal at $t = 531.4s$ and $t = 1421.4s$ are strong, implying failure happens. If the residual value is greater than the threshold, it can be judged as a failure. For a low false alarm rate, the threshold (red dash line) should be set no less than $k = 1$ for bow tunnel thruster detection. The probability of each failure mode is analyzed according to the rule (3.5), and the results are presented in Fig. 3.4b. For the two detected faulty periods, to determine the location of the failed thruster, the residual sequence of each failure mode

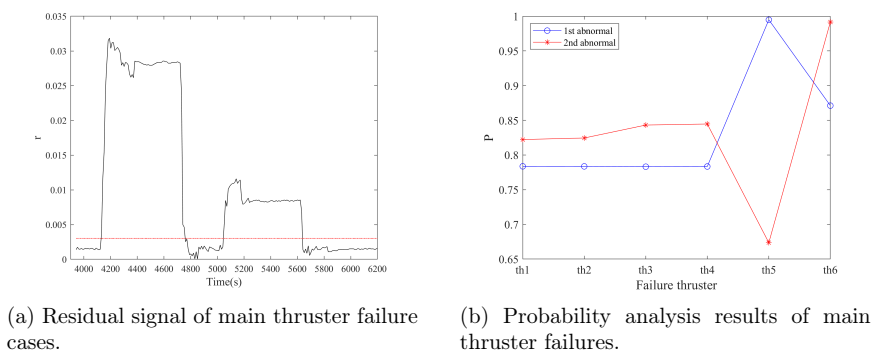


Figure 3.5: Main thruster failure detection and isolation.

is generated, as shown in Fig. 3.6(a)-(b). It shows that in the first abnormal period, the performance of the ship to 011111 failure mode, and in the second period, 101111. It is worth mentioning that in these two faulty cases, 011111 and 101111 failure modes have a pretty high similarity, manifested in little difference in diagnosis probability. The reason is that these two bow thrusters are located quite close to each other.

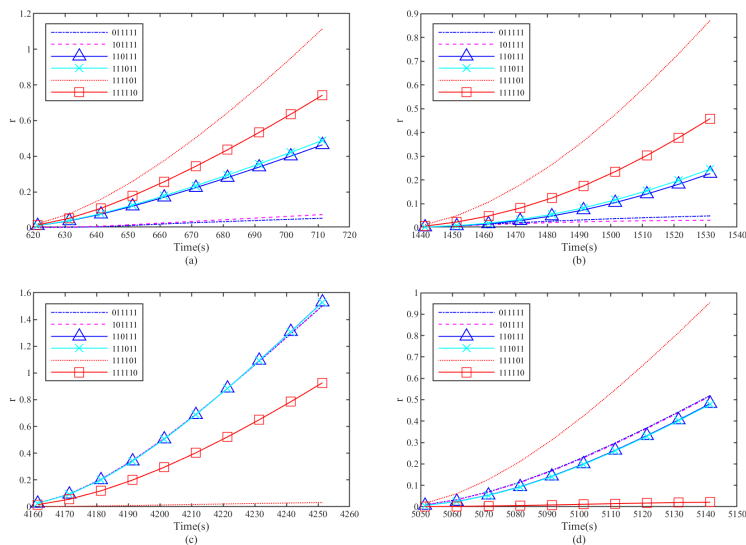


Figure 3.6: Residuals of each failure mode in detected faulty period. (a) first anomaly in bow thruster; (b) second anomaly in bow thruster; (c) first anomaly in main thruster; (d) second anomaly in main thruster.

The residuals caused by each primary thruster failure characterize different peak values in Fig. 3.5a. This is caused by the position difference of the two main thrusters to the wind direction. Here the threshold for failure detection is also set at $k = 1$. The failure mode residual comparison results are presented in Fig. 3.6c-d. It can be seen that the main thruster failure has rather different features compared with tunnel thruster failure because main thrusters and tunnel thrusters provide disparate force to maintain the ship's position under wind disturbances. According to Fig. 3.5b, one can get that the first detected anomaly is caused by port main thruster failure and the second starboard main thruster.

3.2 Co-simulation based thruster retrofit

This study presents the propulsion retrofit process using the co-simulation technique, and the dynamic properties of the retrofitted devices are analyzed and discussed. Co-simulation, as an enabling tool, lessens the modeling pressure and promotes efficiency benefiting from the re-usability of different elements. The research vessel Gunnerus went through a thruster refit in 2015. The origin twin fixed-pitch ducted propellers and rudders were replaced with the Permanent Magnet rim-drive azimuthing thrusters. The ship maneuvering capabilities are simulated to document the effect of the change in the propulsion system.

3.2.1 Co-simulation setup

The ship maneuvering simulation is set up as Fig. 3.7 shows. Each block represents an FMU of which the input and output variables are declared. The experiment is performed in Vico [43].

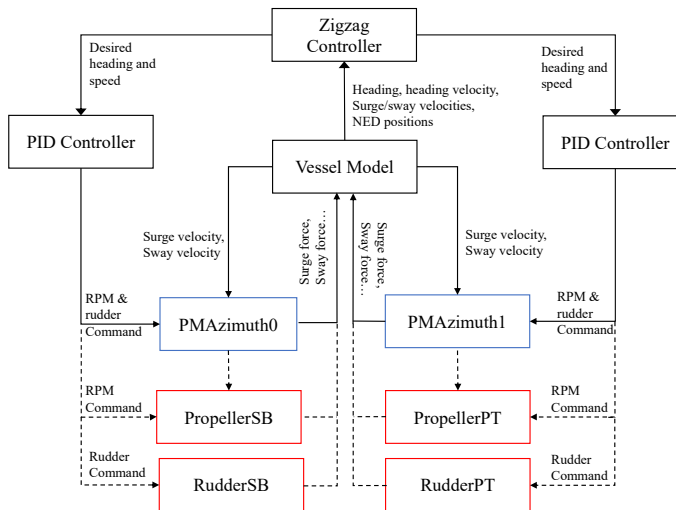


Figure 3.7: Diagram showing the relationship of the engaged ship components.

An overview of FMUs applied in the maneuvering simulation is presented. All the FMUs, except the *VesselModel* and *PMAzimuth*, are developed by the authors using

PythonFMU [50].

1. **VesselModel**

The vessel model reflects the vessel’s hydrodynamic properties, such as the mass, resistance, and cross-flow drag, as well as restoring forces. It is a 6DOF time-domain simulation model developed by MARINTEK’s vessel simulator VeSim [51]. Summing all the external forces acting on the ship, the dynamic equations of vessel motions are then solved.

2. **PID controller**

The PID controller is created to generate shaft speed and rudder angle commands according to Eq. 3.7. In the control law, the $k_{\{\cdot\}}$ is the parameter enabling tuning, and the predefined approach speed u_d as well as the ship heading ψ_d are issued by the *ZigzagController*.

$$\begin{aligned} RPM &= k_{pu}(u - u_d) + k_{iu} \int_0^t (u - u_d)dt + k_{du} \frac{d}{dt}(u - u_d) \\ \delta &= k_{ppsi}(\psi - \psi_d) + k_{ipsi} \int_0^t (\psi - \psi_d)dt + k_{dpsi} \frac{d}{dt}(\psi - \psi_d) \end{aligned} \tag{3.7}$$

3. **Zigzag controller**

It is a logistic solver without numerical computation. Given the current ship speed and heading, it can tell to which side the rudder should turn and deliver the command saturation to the connected *PID controller*.

4. **PMazimuth**

It is a hydrodynamic model of the azimuth thruster without actuator, implemented by the manufacturer Kongsberg Maritime using VeSim. Feeding a specific RPM and angle command, vessel speed, as well as the loss factor into the model, it produces a 3DOF force in heave, surge, and sway directions.

5. **Propeller**

Both the propeller and rudder are generic models parametrized to R/V Gunnerus. The surge force related to the propeller is calculated with:

$$\tau_p = f(n, u) \tag{3.8}$$

where n is the propeller shaft speed (r/min), and u is the vessel’s surge velocity. Note that the sway force and yaw moment due to propeller are neglected as they have smaller magnitudes compared to those of hull and rudder components.

6. **Rudder**

The rudder is modelled according to [52]. It can be expressed as:

$$\tau_r = g(u, v, r, n, \delta, \theta) \tag{3.9}$$

where u, v, r are the velocities in surge, sway, and yaw directions respectively. And δ is the rudder angle. θ refers to the hull-rudder interaction coefficients.

3.2.2 Results analysis

Ship maneuvering experiments with a different set of propulsion units are implemented. It is also worth noticing that the ship maneuverability could be affected by water depth, environmental forces, ship speed, and hydrodynamic derivatives. To ensure the results comparable, identical settings except only the propulsion units are employed. The ship is assuming cruising on calm and deep water without external environmental disturbances.

Zigzag Maneuver

Zigzag trajectories for the ship using both the pitch propellers and azimuth thrusters are simulated. Two test scenarios are presented and compared in Fig. 3.8-3.9. Differences in turning velocities are observed in these figures. A more noticeable yaw velocity distinction between the pitch propeller and azimuth arises during 10° turn command. The statistical results are summarized in Table. 3.2. It could be observed that the measured key time parameters in the azimuth group are effectively decreased. This conclusion reveals that the ship with azimuth installed reaches the desired course in a shorter time and responds more quickly to the given command.

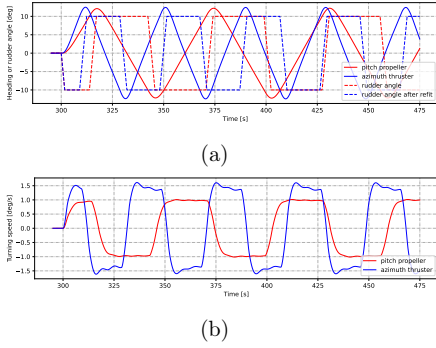


Figure 3.8: $10^\circ/10^\circ$ zigzag at high speed.

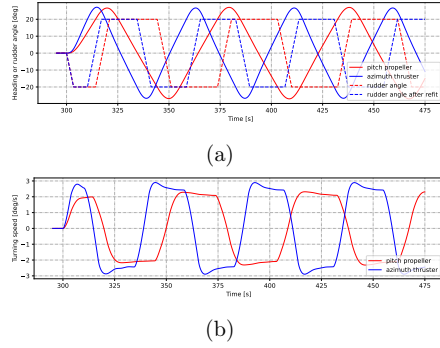


Figure 3.9: $20^\circ/20^\circ$ zigzag at high speed.

Table 3.2: The zigzag characteristics for the ship before and after propulsion unit retrofit.

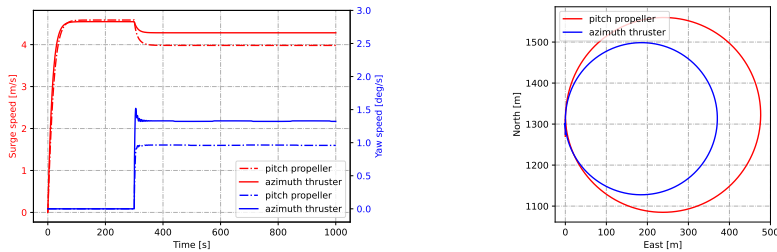
Characteristics		$10^\circ/10^\circ$			$10^\circ/10^\circ$			$20^\circ/20^\circ$			$20^\circ/20^\circ$		
		pr	azi	gain[%]	pr	azi	gain[%]	pr	azi	gain[%]	pr	azi	gain[%]
Approach speed	[m/s]	4.7	4.78	-	2.4	2.5	-	4.7	4.73	-	2.45	2.47	-
t_a	[s]	13.7	8.9	35	24.25	15.6	35.7	8.95	6.45	27.9	14.9	10.4	30.2
t_s	[s]	3.6	2.9	19.4	5	3.6	28	10.8	8.25	23.6	16.3	12.2	25.2
t_A	[s]	31.9	21.3	33.2	54.4	35.25	35.2	34.5	26.25	23.9	55.6	40.7	26.8
t_T	[s]	60.3	40.75	32.4	103.2	67	35.1	64.15	50.3	21.6	103.8	78.75	24.1
First overshoot angle	[°]	2.17	2.37	-9.2	1.57	1.6	-1.9	6.64	6.7	-0.9	4.6	4.7	-2.1
Second overshoot angle	[°]	2.2	2.42	-10	1.58	1.61	-1.9	6.87	6.68	2.8	4.8	4.36	9.2
Average overshoot angle	[°]	2.2	2.42	-10	1.576	1.6	-1.5	7.01	6.7	4.4	4.92	4.35	11.6

Turning Circle

The turning circle maneuver experiments are conducted under the resembling co-simulation structure but replacing the *Zigzag controller* with *Turning controller*. The execution an-

gle and speed are distinguished into two categories: 10° and 20° with higher and lower approach speeds, respectively.

The statistical maneuver results are presented in Table. 3.3. One test case is visualized, as shown in Fig. 3.10. The ship equipped with either the conventional pitch propellers and rudders is approaching at similar speeds before execution. From Fig. 3.10a, a drop in surge speed is observed when the rudder is instantiated, and the reduction in pitch propeller is more apparent compared to that of the azimuth. Meanwhile, a more significant turning velocity is offered by the azimuth. The out-performance in response velocities is expected to lead to a narrower turning radius verified in Fig. 3.10b. Moreover, the statistical results show that the angle command affects the propulsion performance more than the approach speed.



(a) The ship's surge and yaw speed when circling at 10° with a fast speed.

(b) Comparison of propeller and azimuth actuated ship trajectories.

Figure 3.10: 10° turning circle properties at higher speed.

Table 3.3: The turning characteristics for the ship before and after propulsion unit retrofit.

Characteristics		10°			10°			20°			20°		
		pr	azi	gain [%]	pr	azi	gain [%]	pr	azi	gain [%]	pr	azi	gain [%]
Approach speed	[m/s]	4.7	4.8	-	2.4	2.5	-	4.7	4.7	-	2.4	2.5	-
Steady turning radius	[m]	237.5	185.5	21.9	237.8	186.3	21.6	90.4	91.3	-1	93.2	92.9	0.32
Maximum transfer	[m]	476.2	370.6	22.2	476.4	371.9	21.9	190.7	184.8	3.1	195.1	187.7	3.8
Maximum advance	[m]	266.7	200.5	24.8	265.5	200.3	24.5	127.8	108.9	14.8	128.3	109.6	14.6
Transfer	[m]	227.5	173.7	23.6	227.2	173.9	23.4	88.1	82.2	6.7	88.8	82.5	7.1
Advance	[m]	266.4	200.1	24.9	265.2	199.9	24.6	127	108.1	14.9	127.4	108.7	14.7
Tactical diameter	[m]	475.9	370.2	22.2	476.1	371.5	22.0	189.96	184.1	3.1	194.2	186.9	3.8

3.3 Chapter summary

This chapter aims to present the enabling technology related to the physics-based model. A linearized DP model is used to detect and isolate the thruster failures during maneuvering, and a co-simulation-based simulation is conducted to support ship conversions. From the two studies, one can see that the physics-based model qualifies to work effectively on qualitative predictions rather than drawing quantitative conclusions. It has to approve that even if numerous efforts and time are devoted to pursuing a high-fidelity physical model, the model's accuracy might still be unable to match the reality as much as the data-driven derived one. However, if attention is turned from accuracy to the tendency, the not-so-accurate simulation model works well to offer constructive solutions.

In short, when it is somewhat capable of representing reality, even if the errors still exist, the simulation model is proven competent by revealing the potential movement trends. Findings inspire the following work on physics-data cooperative modeling technology.

Case study: Parameter identification

This chapter presents research results from paper II. Pursuing high-fidelity models that reflect the ship's dynamics as well as its interaction with environments is always being prompted by both academics and industries. At the same time, the complex ocean environments add difficulty since the ship dynamics can vary with the sailing status, such as the trim or loading conditions. Therefore, a general hydrodynamic-based model is always far from expectations. However, the continuous measurements data permit the model optimization, which significantly promotes the model reliability and broads the model-related applications. This chapter uses the SVM approach—a data-driven algorithm to identify the ship's hydrodynamic derivatives when the vessel is subject to stochastic environments.

4.1 Methodology

The parameter identification of the ship maneuvering model is complex due to the respective hydrodynamic effects. Normally, the ship dynamics are described by a group of derivative equations associated with linear and nonlinear terms. Specifically, the identification process is described in Fig. 4.1. The regression model, derived from the ship maneuvering model, determines the input and output features of the SVM. After preparing the data containing ship motion and propulsion commands, the SVM is extensively trained, generating optimal coefficients. The estimated model is obtained and could be further examined by substituting the identified results back into the ship maneuvering model. Particularly, the generalization capability of the identified model should be stressed properly.

The training datasets include the vessel's multiple different maneuvers. Note that the ship motion data should be taken extra cleaning treatment to eliminate the measurement noise if it is collected from the onboard sensors.

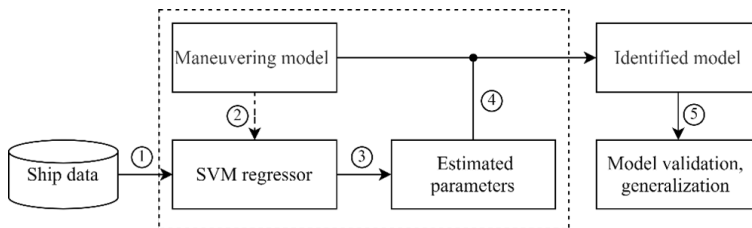


Figure 4.1: Scheme of parameter identification for ship maneuvering model.

4.1.1 Ship regression model

The non-dimensional forms of hydrodynamic forces/moments in the 3DOF Abkowitz model of an offshore surface vessel are expressed as Eq. (4.1).

$$\begin{aligned}
 X' &= X'_u u' + X'_{uu} u'^2 + X'_{uuu} u'^3 + X'_{vv} v'^2 + X'_{rr} r'^2 + X'_{rv} r' v' + X'_{\delta\delta} \delta'^2 + X'_{u\delta\delta} u' \delta'^2 + X'_{v\delta} v' \delta' \\
 &\quad + X'_{u\delta} u' \delta' + X'_{uvv} u' v'^2 + X'_{urr} u' r'^2 + X'_{uvr} u' v' r' + X'_{r\delta} r' \delta' + X'_{ur\delta} u' r' \delta' + X'_0 \\
 Y' &= Y'_v v' + Y'_r r' + Y'_{vvv} v'^3 + Y'_{vvr} v'^2 r' + Y'_{rrr} r'^3 + Y'_{vrr} v' r'^2 + Y'_{vuu} v' u'^2 + Y'_{ruu} r' u'^2 \\
 &\quad + Y'_{vu} v' u' + Y'_{ru} r' u' + Y'_\delta \delta' + Y'_{\delta\delta\delta} \delta'^3 + Y'_{u\delta} u' \delta' + Y'_{uu\delta} u'^2 \delta' + Y'_{v\delta\delta} v' \delta'^2 + Y'_{v\delta} v'^2 \delta' \\
 &\quad + Y'_{r\delta\delta} r' \delta'^2 + Y'_{rr\delta} r'^2 \delta' + Y'_{rv\delta} r' v' \delta' + Y'_0 + Y'_{0u} u' + Y'_{0uu} u'^2 \\
 N' &= N'_v v' + N'_r r' + N'_{vvv} v'^3 + N'_{vvr} v'^2 r' + N'_{rrr} r'^3 + N'_{vrr} v' r'^2 + N'_{vuu} v' u'^2 + N'_{vu} v' u' \\
 &\quad + N'_{ru} r' u' + N'_\delta \delta' + N'_{\delta\delta\delta} \delta'^3 + N'_{u\delta} u' \delta' + N'_{uu\delta} u'^2 \delta' + N'_{rr\delta} r'^2 \delta' + N'_{rv\delta} r' v' \delta' \\
 &\quad + N'_{v\delta\delta} v' \delta'^2 + N'_{r\delta\delta} r' \delta'^2 + N'_{vv\delta} v'^2 \delta' + N_0 + N_{0u} u' + N_{0uu} u'^2
 \end{aligned} \tag{4.1}$$

where the hydrodynamic derivatives $X'_{(\cdot)}, Y'_{(\cdot)}, N'_{(\cdot)}$ are the parameters that need to be identified. u', v', r' are the non-dimensional velocities in surge, sway, and yaw directions.

The Abkowitz model is generally considered a nonlinear hydrodynamic model, whereas it can be viewed as a linear model concerning the hydrodynamic parameters. The motion equations are discretized by using Euler's stepping method, and the derived regression model is shown as Eq. (4.2).

$$\begin{aligned}
 u'(n+1) - u'(n) &= AX(n) \\
 v'(n+1) - v'(n) &= BY((n) \\
 r'(n+1) - r'(n) &= CN((n)
 \end{aligned} \tag{4.2}$$

where n and $n+1$ are the adjacent sampling time steps. A, B, C are parameter vectors formed by hydrodynamic derivatives to be identified. $X(n), Y(n), N(n)$ are the variables vectors expressed as:

$$\begin{aligned}
 X(n) &= \frac{U^2}{L} \times \frac{\Delta t}{m - X'_u} \times [u', u'^2, u'^3, v'^2, r'^2, r'v, \delta'^2, u' \delta'^2, v' \delta', u' v' \delta', u' v'^2, \\
 &\quad u' r'^2, u' v' r', r' \delta', u' r' \delta', 1]^T \\
 Y(n) &= \frac{U^2}{L} \times \frac{\Delta t}{S} \times [v', r', v'^3, v'^2 r', r'^3, v' r'^2, v' u'^2, r' u'^2, v' u', r' u', \delta', \delta'^3, \\
 &\quad u' \delta', u'^2 \delta', v' \delta'^2, v'^2 \delta', r' \delta'^2, r'^2 \delta', r' v' \delta', 1, u', u'^2]^T \\
 N(n) &= \frac{U^2}{L^2} \times \frac{\Delta t}{S} \times [v', r', v'^3, v'^2 r', r'^3, v' r'^2, v' u'^2, r' u'^2, v' u', r' u', \delta', \delta'^3, \\
 &\quad u' \delta', u'^2 \delta', v' \delta'^2, v'^2 \delta', r' \delta'^2, r'^2 \delta', r' v' \delta', 1, u', u'^2]^T
 \end{aligned} \tag{4.3}$$

where $S = (m' - Y'_v)(I'_{zz} - N'_r) - (m' x'_g - Y'_r)(m' x'_g - N'_v)$. The rudder angle is represented by δ and $\delta' = \dot{\delta}$. It should be mentioned that the five zeros frequency added mass

derivatives $X'_u, Y'_v, Y'_r, N'_v,$ and N'_r usually have enough preciseness, which can be found in semi-empirical formulas or calculated through strip theory. They can always be estimated beforehand. Only the parameter sets $A, B,$ and C are unknown and they will be identified by the SVM algorithm. Mention that the hydrodynamic derivatives $X'_{(\cdot)}$ in surge equation are simply obtained by (4.4) once the vector A is determined. While b_i and $c_i, (i = 1, 2, \dots, 22)$ are not direct hydrodynamic coefficients in sway and yaw motion equation, they need further treatment by (4.5).

$$X'_{(\cdot)} = \frac{L(m' - X'_u)}{\Delta t} A \quad (4.4)$$

$$\begin{bmatrix} Y'_{(\cdot)} \\ N'_{(\cdot)} \end{bmatrix} = \begin{bmatrix} \frac{(I'_{zz} - N'_r)\Delta t}{SL} & -\frac{(m'x'_g - Y'_r)\Delta t}{SL} \\ -\frac{(m'x'_g - N'_v)\Delta t}{SL^2} & \frac{(m' - Y'_v)\Delta t}{SL^2} \end{bmatrix}^{-1} \begin{bmatrix} B \\ C \end{bmatrix} \quad (4.5)$$

In general, the identification process is conducted as the following steps:

- (1) Collect the sample experiment data $\{(t_i, u_i, v_i, r_i, \delta_i), i = 1, \dots, l\}$ based on full-scale sea trials or simulation.
- (2) Construct the input and output vectors for each SVM regressor according to (4.2).
- (3) Train the SVM regressor and optimize the hydrodynamic coefficients.
- (4) Substitute the identified results back into model (4.1) to get identified ship model.
- (5) Verify the generalization performance of the obtained model.

4.2 Experimental results

In this section, the effectiveness of the SVM-based identification algorithm will be investigated in a standard vessel model with and without disturbance.

4.2.1 Identification without disturbance

The experiments are performed in the Marine Systems Simulator [46] developed by the Norwegian University of Science and Technology and cooperating groups. The Mariner class vessel [47] is selected as a benchmark for verification in this study. It should be noted that in the hydrodynamic model of the Mariner class vessel, only 10 hydrodynamic coefficients in the surge motion equation, 15 in the sway equation, and 15 in the yaw equation are considered, and the others are zeros. The SVM regressor is implemented by using Scikit-learn [53] in Python. Following the procedure, as shown in Fig. 4.1, the parameters are identified and verified against the planar motion mechanism (PMM) experimental values, as shown in Table. 4.1. It can be seen that most of the numerical coefficients agree well with the benchmark values.

4.2.2 Identification under disturbance

When preparing the disturbed maneuver data, the bias $w_1 \in \mathbb{R}^{3 \times 1}$ and process noise $w_2 \in \mathbb{R}^{3 \times 1}$ are defined according to the rule proposed by Sutulo et al. [54]:

$$w_i = \max(\varphi_i) k_{0i} k_{i\zeta} \quad (4.6)$$

Table 4.1: Identified non-dimensional hydrodynamic coefficients ($\times 10^{-5}$).

X-Coef	SVM	PMM	Y-coef	SVM	PMM	N-coef	SVM	PMM
X'_u	-182.5	184.0	Y'_v	-1158.2	-1159.9	N'_v	-262.4	-264.0
X'_{uu}	-116.6	-110.0	Y'_r	-498.1	-498.8	N'_r	-165.4	-166.0
X'_{uuu}	-220.0	-215.0	Y'_{vvv}	-8150.4	-8078.5	N'_{vvv}	1667.5	1636.0
X'_{vv}	-923.0	-899.0	Y'_{vvr}	15312.0	15358.0	N'_{vvr}	-5484.0	-5483.0
X'_{rr}	13.8	18.0	Y'_{vu}	-1156.2	-1160.0	N'_{vu}	-250.6	-264.0
X'_{rv}	779.3	798.0	Y'_{ru}	-497.3	-498.9	N'_{ru}	-162.2	-166.0
$X'_{\delta\delta}$	-94.6	-95.0	Y'_δ	277.6	278.0	N'_δ	-139.0	-139.0
$X'_{u\delta\delta}$	-190.2	-190.0	$Y'_{\delta\delta\delta}$	-89.6	-90.0	$N'_{\delta\delta\delta}$	42.3	45.0
$X'_{v\delta}$	92.3	93.0	$Y'_{u\delta}$	554.3	556.1	$N'_{u\delta}$	-270.0	-278.0
$X'_{uv\delta}$	86.1	93.0	$Y'_{uu\delta}$	271.7	278.0	$N'_{uu\delta}$	-87.8	-139.0
			$Y'_{v\delta\delta}$	-3.6	-4.0	$N'_{v\delta\delta}$	17.5	13.0
			$Y'_{vv\delta}$	1213.1	1190.1	$N'_{vv\delta}$	-476.2	-489.0
			Y'_0	-8.6	-8.0	N'_{0u}	8.0	6.0
			Y'_{0uu}	-2.7	-4.0	N'_{0uu}	-0.4	3.0

where ζ is the discrete zero-mean Gaussian white noise process. φ is the primary clean reference response. $\max(\varphi_i)$ refers to the maximum absolute value of the clean response and it scales the noise signal to the origin response. k is a response specific reduction factor, which is set to be 0.05 for rudder angle response, 0.2 for the surge velocity, and 1.0 for other remaining responses. k_0 is the general reduction factor used to label the noisy extent, which is assumed to be 5%, 10%, and 20% as listed in Table. 4.2.

To investigate the effect of disturbance level on the identification results, experiments are designed according to Table. 4.3. To eliminate the outliers in the random process, every case is executed in one hundred trials. The Savitzky-Golay filter is applied to preprocess and smooth the training data. The identified parameters are found to be normally distributed, and thus the average is chosen as the general solution. The identified models at different disturbance levels are obtained by substituting those results. Typically, the extensively trained SVM results are able to reproduce the training trajectory. Therefore, a more critical evaluation of the model fidelity is that it should be capable of predicting other maneuvers that the SVM has not been trained on. An 18° turning circle operation is then undertaken to examine its generalization performance. The comparisons between the SVM predictions and origin model reference in 3DOF velocities, heading angle, and ship trajectory are shown in Fig. 4.2. It can be seen that the model identified under disturbance and process noise could basically capture the ship's dynamic properties and generate a relatively accurate response. The prediction errors at NL1 and NL2 are considered allowable. Generally, the deviation gets more extensive when the disturbance level is higher. Note that at the same disturbance level NL1, the variation of surge speed is more evident than that of sway and yaw speed.

To quantitatively measure the prediction errors, the maneuvering characteristics for turning circles are calculated and listed in Table. 4.4. The table shows that the predicted maneuver properties at different disturbance levels have various deviations from the model reference. More concretely, at NL1 and NL2, the discrepancies are almost lower than 10%, while at NL3, the errors are around 20%. It reveals that when the ship is

Table 4.2: Disturbance/noise level set up.

Noise Level (NL)	k_0
NL0	0%
NL1	5%
NL2	10%
NL3	20%

Table 4.3: Experiment case set up.

Case	Disturbance bias	Process noise
1	NL1	NL1
2	NL2	NL1
3	NL3	NL1

Table 4.4: Maneuvering characteristics comparison between SVM predictions and model reference.

Maneuvering characteristics	Model reference	SVM-NL1		SVM-NL2		SVM-NL3	
	Value (m)	Value (m)	Deviation (%)	Value (m)	Deviation (%)	Value (m)	Deviation (%)
Steady turning radius	667	644	3.5	595	10.8	707	6.0
Maximum transfer	1279	1306	2.1	1242	2.9	1594	24.6
Maximum advance	746	801	7.4	796	6.7	905	21.3
Transfer at 90 (deg) heading	546	578	5.9	557	2.0	694	27.1
Advance at 90 (deg) heading	742	796	7.3	791	6.6	895	20.6
Tactical diameter at 180 (deg) heading	1275	1302	2.1	1237	3.0	1586	24.4

exposed to gentle and moderate environments, the identified model is able to keep its key characteristics, and its predictive capability could be considered acceptable. Although relatively obvious dispersions in NL3 scenario are observed, it could still indicate a potential path in the short future. These results reveal that the SVM-based approach could realize parameter identification in the disturbed environment to a certain accuracy, which practically extends the applicable scope in scenarios.

4.3 Chapter summary

This chapter presents a case study on interpolation kind of physics-data cooperation by estimating the model parameters through data-driven tools. An SVM-based system identification procedure is produced for the scenario where the ship maneuvers in stochastic environments. By taking the 3DOF Abkowitz model plant as known, maneuver data is utilized to optimize the uncertain hydrodynamic derivatives subjected to unavoidable environmental influence. The estimated ship model matches the reality better, proving the positive effects of data engagement.

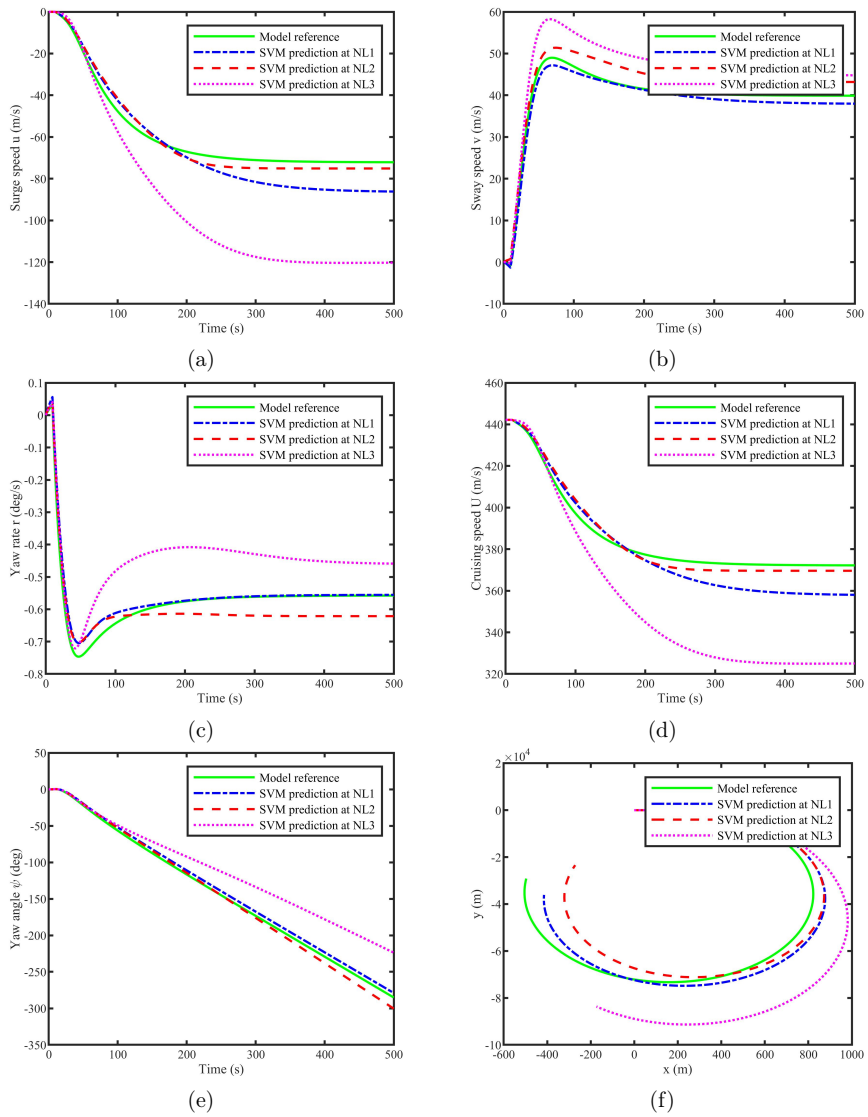


Figure 4.2: The SVM predictions at different disturbance levels compared with model reference of 18° turning circle.

Case study: Knowledge transfer

High-fidelity models capable of accurately predicting ship motion are critical for promoting innovation and efficiency in the maritime industry. Creating an advanced model that comprehensively represents the system and its interaction with dynamic environments has always been challenging. Many models cover partial, not complete, domain knowledge about the underlying system. Benefiting from the collected process data, the physics-data cooperative model is promising to enhance the model quality and offer accurate predictors. How to implement the cooperation is of interest and has been investigated in this chapter. This chapter is based on the research results from papers III, V, and VI.

5.1 Incorporating approximate dynamics into data-driven calibrator

This section proposes a physics-data cooperative model to develop the representative model for the elongated R/V Gunnerus, based on the best available approximate dynamics offered by the short version Gunnerus. The proposed approach is validated in both simulator and real-world full-scale sea trials.

5.1.1 Methodology

The hybrid model contains two complementary parts originating from two separate domains: model-based and data-driven. The way they collaborate is expressed as:

$$\begin{aligned}\dot{X} &= f(X, u) \\ y &= g(X, u, f(X, u))\end{aligned}\tag{5.1}$$

where X is the state of the approximate system. u and y are registered as representative system control and output, respectively. f represents the preliminary model based on physical disciplines, and the output of the reference model is integrated as an additional input to the neural network model g , which functions to map the prior model to the representative model of the new system.

The complete flowchart of the proposed model is shown in Fig. 5.1. The model groundwork (top yellow box) is built on a hydrodynamic model of a similar vessel. It serves to provide approximate ship states $\hat{X} = [\hat{\eta}_m, \hat{\nu}_m]^T$ reacting to the control command and environment configuration. $[RPM(t_0), \delta(t_0)]^T$ is the propulsion system feedback, and $[\beta_w(t_0), V_w(t_0)]^T$ refers to the wind conditions. Similar hydrodynamic properties characterize the reference model, and therefore, acceptable model dispersion is within expectation. Upon the preliminary model, the data-driven NN calibrator (bottom green box) is built to map the rough dynamics to a surrogate model that is able to accurately

predict ship behaviors. It is believed that the preliminaries of the ship dynamics are carried forward into the data-driven model by means of informative input.

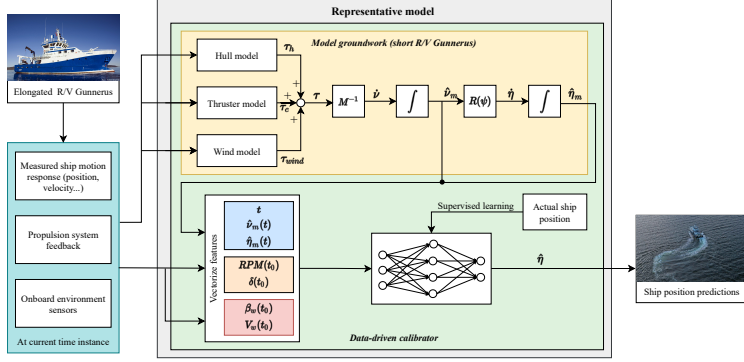


Figure 5.1: A complete flowchart showing the incorporating of approximate dynamics into the data-driven calibrator.

A fully connected feed-forward NN model is applied as a calibrator. Three hidden layers are specified in the network architecture, and each hidden layer contains ten neurons. The input features include prediction time ahead of the current instance, model predicted vessel velocities and positions in the horizontal plane, propulsion feedback, and external environmental factors. Supposing prediction starts at t_0 , the corresponding input vector and desired output will be expressed as:

- Input: $[t_i, \hat{v}_m(t_0 + t_i | t_0), \hat{\eta}_m(t_0 + t_i | t_0), RPM(t_0), \delta(t_0), \beta_w(t_0), V_w(t_0)]$
- Output: $\hat{\eta}(t_0 + t_i | t_0)$

where $t_i \in [t_0, t_0 + t_h]$ is the forward time interval, $\hat{\eta}_m(t_0 + t_i | t_0)$ represents the reference model predicted positions starting from t_0 . $RPM(t_0)$, $\delta(t_0)$, $\beta_w(t_0)$, and $V_w(t_0)$ are sensor data recorded at t_0 .

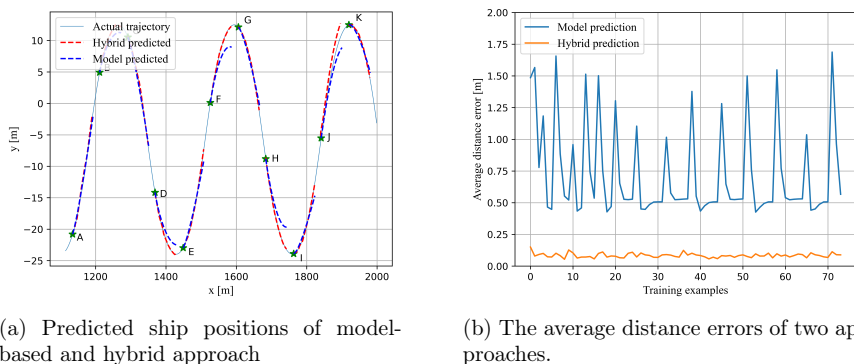
5.1.2 Experimental results

Simulation studies

The zigzag simulation experiments are conducted in Vico, the co-simulation platform developed by our team. To evaluate the predictive model performance, the following metrics are applied:

- Mean absolute error (MAE) (5.2) for evaluating errors in north and east directions.
- Average distance error (5.3) for evaluating mean variation from actual location.

$$MAE = \frac{1}{N} \sum_{i=1}^N |\hat{x}_i - x_i| \quad (5.2)$$



(a) Predicted ship positions of model-based and hybrid approach

(b) The average distance errors of two approaches.

Figure 5.2: The predictive performance of hybrid approach in simulation studies.

$$e_{ave} = \frac{1}{N} \sum_1^N \sqrt{(\hat{x}_i - x_i)^2 + (\hat{y}_i - y_i)^2} \quad (5.3)$$

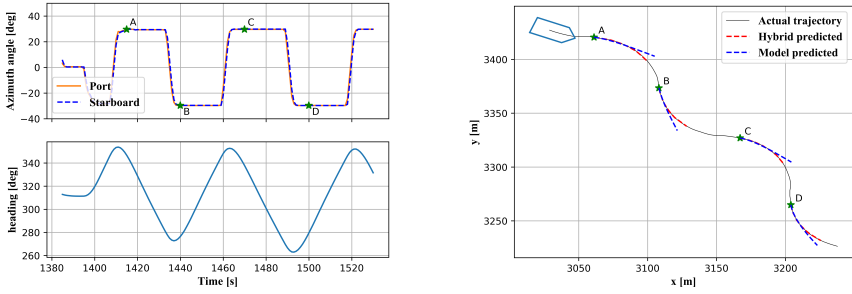
where N refers to the sample number.

By performing both reference model prediction and hybrid method, we obtain the forecasting performance of 30 seconds in the future during the zigzag maneuver in calm water, as shown in Fig. 5.2a. The green star marks the start position of each prediction. This figure shows that the hybrid approach calibrates the turning maneuverability of the reference model as the prediction horizon grows. The slight discrepancies observed at trace J are caused by the control command transiting when prediction starts, and such sequences are initially not covered in the training data. In that case, the calibration performance might be somewhat degraded. Fig. 5.2b shows the variation of average error of both approaches with respect to each training example. It indicates that the hybrid method works well in decreasing errors and improving prediction accuracy.

Full-scale trials

The maneuvering experiment of elongated R/V Gunnerus was conducted in November 2019 in Trondheim, Norway. During this process, thirteen sensor channels related to the ship motion of the vessel were sampled, including positions, velocities, environments, as well as commands.

During maneuvering, the thruster turning angle and ship heading are changing, as shown in Fig. 5.3a. In this process, the tunnel thruster is turned off. By integrating the sampled signals in the current instance as well as the preliminary mathematical model outputs into the neural network, the desired positions at the next instance are obtained. The prediction interval is 15 seconds, and the calibration results are verified as shown in Fig. 5.3b. It is viewed that the hybrid predictions have a satisfactory agreement with the actual ship trajectory compared with those propagated by the reference mathematical model. The hybrid predictive model is proven effective and can be applied in realistic ocean scenarios.



(a) Azimuth turning angle and ship heading during maneuvering.

(b) Hybrid predictions in comparison with model predictions in real life.

Figure 5.3: The predictive performance of hybrid approach in real-life experiment.

5.2 Knowledge transferring across ships

Incorporating the prior domain knowledge into the data-driven models gives an insight into the grey-box modeling. As found in the last section, when the approximate ship dynamics are carried on and fed into the neural network, the predictive performance of the research vessel is greatly enhanced. However, concerns must be taken when applying this method on other ships other than the vessel used in the previous study. The reason lies in the fact that the knowledge to be transferred is provided by exactly the same vessel as the research object but with a shorter length. The strong resemblance in geometry and configuration manifested by the two vessels leads to no doubt about the feasibility of the preliminary acquisitions. Nonetheless, there is not always such a proper reference model readily accessible since physical conversions are not as usual on the other ships.

To generalize the grey-box modeling methodology to a more realistic context, we propose a framework by transferring and adapting the ship domain knowledge leveraged by the existing benchmark ship to enhance the prediction of the target research vessel. The benchmark ship, which preserves and reveals preliminary knowledge on operation, is also called the source ship.

5.2.1 Methodology

Enabling the knowledge transfer process, the source ship S is required to bear a certain resemblance in the feature space with the target ship T , that is,

$$S \cap T \neq \emptyset \quad (5.4)$$

Yet due to the physical constraints and other mismatched factors, the states \mathbf{x} will distribute differently $P(\mathbf{x}_s) \neq P(\mathbf{x}_t)$. The domain adaptation has to be executed. As shown in Fig. 5.4, the knowledge flows between the source and target ship space. The upper layer is the source domain, where the source ship dynamics are constructed and numerically solved. The lower layer reflects the target space where the ship data is sampled and the nonlinear transfer functions.

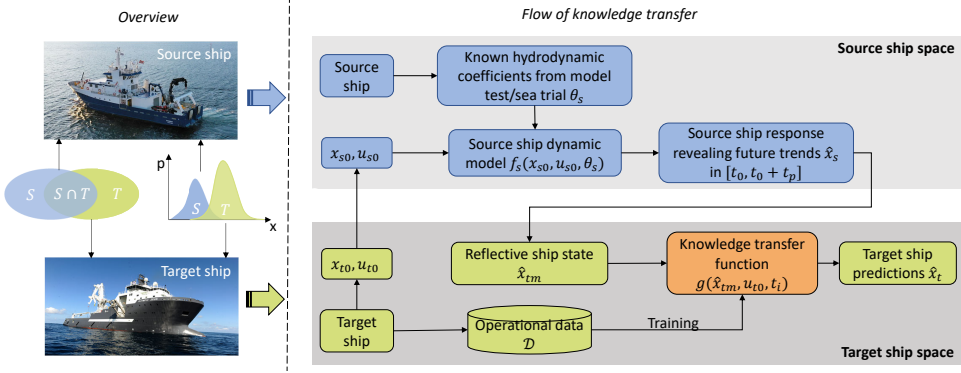


Figure 5.4: The structure overview of knowledge transfer across ships.

Knowledge transfer flow

Consider a target ship whose nonlinear representation $\dot{\mathbf{x}}_t = f_t(\mathbf{x}_t, \mathbf{u}_t)$ is explicitly absent. \mathbf{u} is the control input which is assumed to be constant over the sampling interval, and \mathbf{x} is the ship state containing position and velocity variables. An operational data set $D = \{(\mathbf{x}_t^i, \mathbf{y}_t^i)\}_{i=1}^N$ of target ship is sampled. There is also a source ship with a high-fidelity representative model $\dot{\mathbf{x}}_s = f_s(\mathbf{x}_s, \mathbf{u}_s)$. Assume that the target ship forecasting is triggered at time t_0 , the ship status and control signals are recorded as \mathbf{x}_{t_0} and \mathbf{u}_{t_0} , respectively. To ensuring the initiation state and control signal are within the source ship physical range, a linear transfer function $l(\cdot)$ is introduced as Eq. (5.5).

$$\begin{aligned} \mathbf{x}_{s0} &= l_x(\mathbf{x}_{t0}) = \frac{\mathbf{x}_{t0}}{\Gamma_t} \Gamma_s \\ \mathbf{u}_{s0} &= l_u(\mathbf{u}_{t0}) = \frac{\mathbf{u}_{t0}}{\mathbf{u}_{t_{max}}} \mathbf{u}_{s_{max}} \end{aligned} \quad (5.5)$$

where $\Gamma_t = [L_t, L_t, 1, U_t, U_t, U_t/L_t]$, $\Gamma_s = [L_s, L_s, 1, U_s, U_s, U_s/L_s]$. U and L are the ship design speed and ship length. The subscripts s and t indicate source ship and target ship. In order to ensure the domain knowledge to be readily transferable, the source ship is required to meet the prerequisites that it functions analogously to the target ship, and meanwhile, the model plant f_s and hydrodynamic parameters θ_s are known beforehand. The source model is generally estimated and validated through model tests or sea trial experiments. Once the source model is properly prepared, the transmitted variables \mathbf{x}_{s0} , \mathbf{u}_{s0} are fed into it. By numerically iterating the source model Eq. (5.6) forward, the ship response $\hat{\mathbf{x}}_s$ over the prediction horizon t_p is foreseed.

$$\dot{\hat{\mathbf{x}}}_s = f_s(\mathbf{x}_{s0}, \mathbf{u}_{s0}, \theta_s) \quad (5.6)$$

Then the source model predictions over prediction intervals are transversed back to the target ship domain by:

$$\hat{\mathbf{x}}_{tm} = l_x^{-1}(\hat{\mathbf{x}}_s) \quad (5.7)$$

With the linear transformations across the source and target domain successfully performed, the instructive trends $\hat{\mathbf{x}}_{tm}$ are leveraged by the source ship. Nonetheless, con-

siderable discrepancies between the predictions and their true state still exist since the nonlinear hydrodynamic effects, which are not to be ignored in the ship maneuver model, have not been accounted for in this process. Upon the reflective ship states $\hat{\mathbf{x}}_{tm}$, the nonlinear knowledge transfer function g acts to adapt the bias by the neural network, as shown in Eq. (5.8). In this way, the knowledge leveraged by the source ship is aggregated and adapted to the target ship domain with the model-based linear transfer function and data-driven nonlinear calibration function. Consequently, the motion prediction of the target ship is enhanced with the accompany of referenced ship dynamics.

$$\begin{aligned}\hat{\mathbf{x}}_t &= g(\hat{\mathbf{x}}_{tm}, \mathbf{u}_{t0}, t_i) \\ &= g(l_x^{-1}(f_s(l_x(\mathbf{x}_{t0}), l_u(\mathbf{u}_{t0}), \theta_s)))\end{aligned}\quad (5.8)$$

Feature resemblance

When concretizing the knowledge transfer concept, the target ship and the source ship are assigned by two actual vessels in practice. The main geometric and propulsive characteristics of the two vessels are listed in Section 2.4.1 and Section 2.4.3. The maneuverability of a ship is usually impacted by several key parameters, such as the length-beam ratio, beam-draft ratio, block coefficient, etc. Therefore, in order to use the leveraged information with reasonable confidence, the source ship is required to, as a minimum, have similar characteristic vectors with the target ship. The characteristic vector is introduced as Eq. (5.9) to evaluate the similarity among ships. Δ in the vector is the ship's volume.

$$\ell = [C_b, L/B, B/T, L/\Delta^{1/3}, Ar/L_{pp}T, D_p/T]'\quad (5.9)$$

To measure the correlation between ships' characteristic vectors, the similarity coefficient κ is employed.

$$\kappa(X, Y) = \frac{N \sum x_i y_i - \sum x_i \sum y_i}{\sqrt{N \sum x_i^2 - (\sum x_i)^2} \sqrt{N \sum y_i^2 - (\sum y_i)^2}}\quad (5.10)$$

where $x_i \in X$ and $y_i \in Y$ are the elements in each vector, and N refers to the sample size. The κ value ranges between -1 and 1, and the larger κ is, the stronger association between the two vectors will be. $\kappa(\ell_t, \ell_s)$ is calculated to be 0.95, indicating that the two vessels' characteristics are pretty similar. ℓ_t and ℓ_s are the characteristic vectors of target and source ships, respectively.

Aside from the feature consistency, the control modes of the two vessels are also required to be as close as possible. The thruster configurations of the source ship and target ship are clarified in the two subsections mentioned above. The target ship is controlled by the propellers (6,7) and rudders (8,9) in parallel mode. The revolution speed and blade pitch angles of propellers are controllable. Two sets of individually operated tunnel thrusters at the bow and stern of the vessel (1,2,4,5) are operated by RPM commands and produce the lateral force. On the source ship, the two main propellers and rudders controlled by RPM and turning angles serve the propulsion, and the single tunnel thruster works in the same way as the target ship. If the tunnel thrusters and the forward thruster are excluded from the control mode of the target

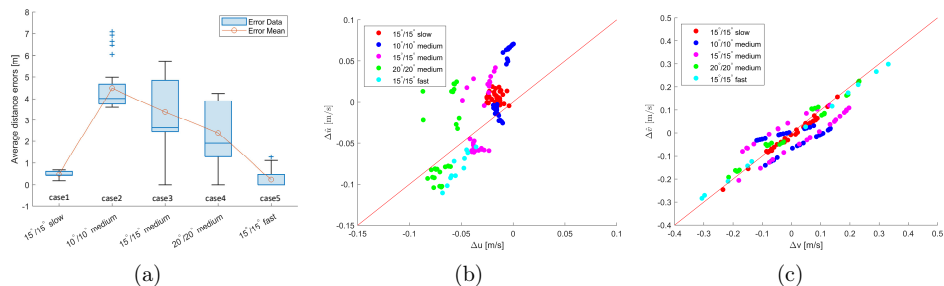


Figure 5.5: Target ship predictions: (a) Average distance error, (b) Relative surge velocity, and (c) Relative sway velocity.

ship, the two vessels are manipulated in a similar way. In the following experiments, they both are operated by the RPM and rudder angle commands, and the blade angle on the target ship is kept constant at the maximum value. From the analysis of physical principles and control model, it is suggested that the source ship and target ship have a specific knowledge shared in common. Meanwhile, dissimilarities in features exist.

5.2.2 Experimental results

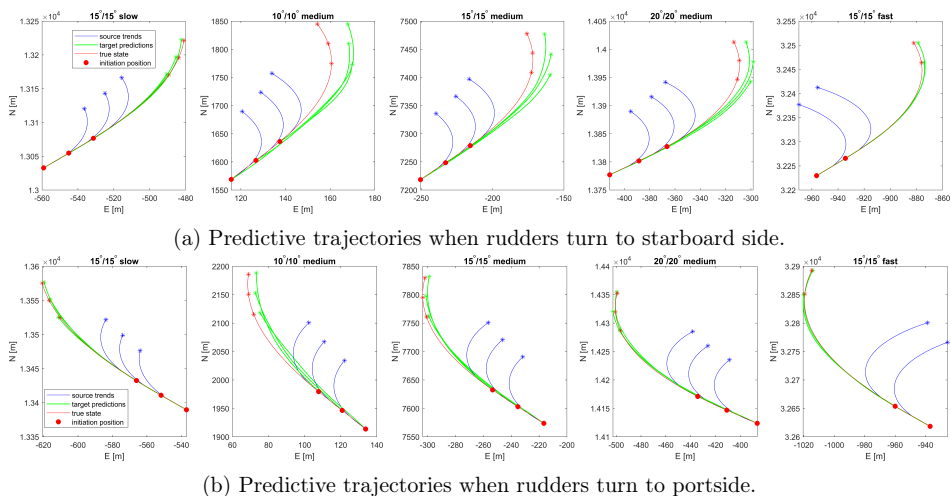


Figure 5.6: The predictive trajectories of target ship and the trends leveraged by source ship at test scenarios.

Five zigzag scenarios are tested under different speeds and execution angles, and the average distance error is presented as Fig. 5.5a, where slow, medium, and fast correspond to the three different revolutions percentages. The predictive performance of 15°/15° slow scenario is observed to be the best. Comparing the mean errors of cases 1,2,4, and 5, although these four scenarios all have at least one execution variable covered by the

training data, the divergence of cases 1 and 5 is much lower than that of cases 2 and 4. It leads to the conviction that the ship's approach speed contributes more when predicting. Fig. 5.5b and Fig. 5.5c exhibit the predicted relative surge and sway velocities against the target true states. The velocities shown in the figure are the relative values with respect to the initiation states. From the two figures, it is evident that, in general, the sway velocities are forecasted with higher accuracy.

An illustration of the target ship's predictive performance is presented in Fig. 5.6. The red dot indicates the initiation position where the prediction is triggered, and the blue lines refer to the trends 30 seconds ahead leveraged by the source ship model. The target ship's true states are reflected by the red line, and the green line presents the target ship's predictions. The ultimate positions of each projection are marked with star signs. Comparing the test cases when the rudder is positioned at different sides, generally, the discrepancies from the portside are not as visible as those of the starboard side. These satisfactory test results demonstrate the effectiveness of the knowledge transfer framework.

5.3 Physics and data competition

The above two sections aim to investigate the representative modeling of a new vessel benefiting from a best available/benchmark ship. Results have shown that the physics-data cooperative approach enhances the model quality and suits well to the target domain. These two cases originate from realistic challenges and basis, attempting to work out a solution to deal with the limited physical and data information. While if the three models (physics-based, data-driven, and physics-data hybrid) are all accessible at the same time, they will work in a competitive way. In such a context, this section aims to construct three models simultaneously and assess the model performance in ship docking prediction.

5.3.1 Methodology

The methodology of integrating the prior dynamic knowledge and neural network-based black-box model is proposed to improve the ship's predictive performance. As shown in Fig. 5.7, there are three ways to establish ship models—physics-based model, physics-data hybrid model, and purely data-driven model.

The singly physics-based model is developed on the marine structure properties and the parameters specified through model tests. Without the prior model information, a data-driven model is derived depending on the ship docking operation data set D . At last, a physics-data cooperative model is constructed relying on both knowledge and data. The prior information is given by a simplified numerical model of the target ship without considering the waves and current effects. A comparison of the hybrid model and the data-based model on the accuracy and efficiency is performed to validate the cooperative methodology's benefit.

5.3.2 Experimental results

The research vessel Gunnerus serves as the testbed in this work. The experimental data were sampled from the history data acquired through log files created by a data acquisition system onboard the R/V Gunnerus. A docking operation dataset of a one-year time period starting from August 2016 to June 2017 was selected. Information regarding

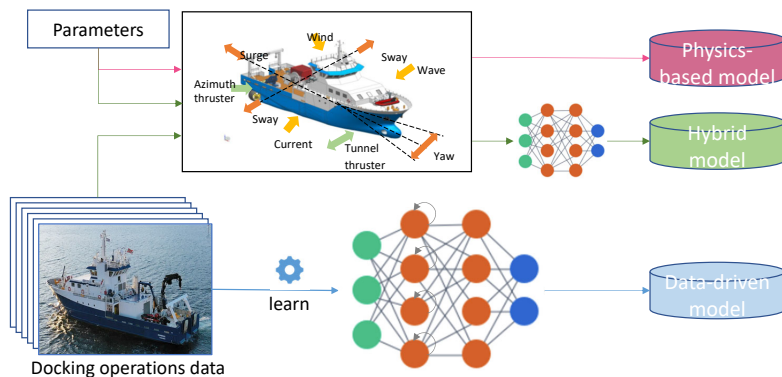


Figure 5.7: Overview of the three model constructions.

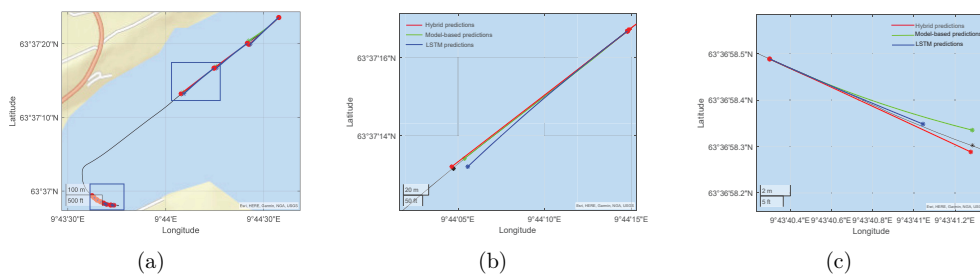


Figure 5.8: Predicted trajectories of three models.

the procedures of isolating dockings from daily cruise data and the measurement range of each sensor channel can be found in [36]. In this dataset, the sampling rate of all variables is 1Hz, and 70 complete docking operations, which were each 1000 seconds in length, were recorded. For the solely data-driven model without the assistance of a priori model, a recursive neural network structure LSTM was trained on 50 docking operations to learn the ship states one step ahead. The purely physics-based model, the hybrid model, as well as the purely data-driven model are verified on the same test data set.

In the test docking scenario, the predictions made by three different models are performed. The predicted trajectories of three models are visualized in Fig. 5.8. According to the surge speed and thruster orientation distribution, the docking process has two stages: before and after the portside thruster turns around 320s. Thus two detailed predictions are exhibited in Fig. 5.8b-5.8c. From these figures, the red circle represents the ship's position where the forecasting is initiated. The star signs mark the final predictive position at 30 seconds ahead. Three colors display the foreseen trajectories made by different models—red: hybrid, green: physics model, and blue: data-driven model. And the black line is the ship's real trajectory. It is observed that the hybrid model predicts the most accurately in both command profiles. When the ship speed is relatively higher, the hydrodynamic model performs slightly better than the data-driven model, but in

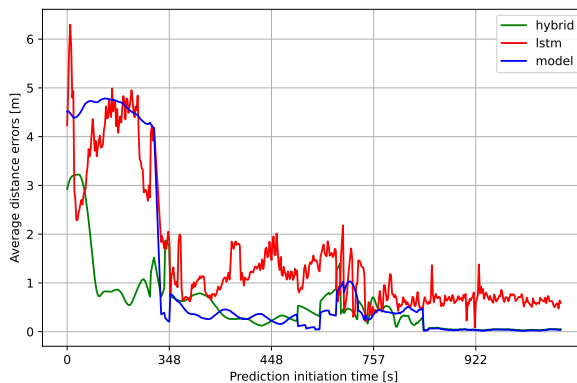


Figure 5.9: The predictive average distance errors of three various models.

the low-speed maneuver, the LSTM model generates more visible errors.

A detailed prediction error comparison is shown in Fig. 5.9. At the higher speed before decreasing, the hybrid model considerably reduces the dispersion. When the ship is decelerating, the hydrodynamic model matches more suitably with the actual system, so as well the hybrid model. The data-driven model also exhibits a remarkable decrease in average distance error but is still slightly more extensive than the physical and hybrid models. It reveals that the domain knowledge-based model represents the system better at low-speed maneuvers. In this operation phase, either the physics or hybrid models are qualified to offer credible predictions. However, when the ship is cruising at high speed, the hybrid model would be the best choice among these three candidates. The data-driven model performance is believed to be improved if more operation data is supplied. However, the data poverty limits the further optimization of the network, even though almost ten times the operations of the hybrid model used have been utilized for training the LSTM. On the contrary, the hybrid model can achieve excellent accuracy with limited data and a more straightforward network structure, which spares more effort and computational consumption than building everything from scratch.

5.4 Chapter summary

This chapter exploits physics-data cooperative modeling approaches to improve the model quality and supply high-fidelity short-term ship motion predictions. Applying a purely dynamic-based predictor calls for accurate model parameters, requiring extensive procedures and efforts. In the cases presented in this chapter, the model is enhanced from three levels, depending on how much information could be learned and adapted from the physical understanding:

- The ship dynamic model is mostly established. Still, some impacting factors are missing, such as the measurements and models of the ocean waves and currents. Upon that, only limited data is utilized to calibrate the model and get predictions.
- The exact simulation model of the researched vessel is absent. Still, there is one best available ship that is highly similar to the objective (the shorter ship in the

case study). The representative model of the elongated vessel is constructed on this approximate model and a certain amount of real operation data.

- Neither the numerical model nor a best approximate model are accessible. The target ship migrates and adapts the domain knowledge from a benchmark ship that shares certain common properties to develop itself.

The physics-data cooperation proposed in this chapter works well not only in promoting predictive accuracy but also in releasing data requirements.

Conclusion and further work

This thesis revolves around ship motion predictions by exploiting the physics-data cooperative modeling approaches. The majority of the research work is allocated to exploring the disciplines and relationships between the physics-based and data-driven models and how they can be integrated to benefit each other. Current ship motion predictions are mainly made by either the kinetic/model-based approach or direct data-based approach. Driven by the desire to bridge the gap and leverage the cooperative features of the two participants, this thesis has proposed a physics-data cooperation mechanism aiming to promote the ship's predictive models and offer perceptive insights into the essential modeling activities.

6.1 Summary of contributions

Exploring the physics-data cooperation modeling technology and providing predictive insights into the facilities, enabling solid decision-support onboard, as stated in RO1, is the primary goal of this dissertation. In seeking to obtain it, the pure kinetic derived model-based research is first conducted to leverage the cooperation features as clarified in RO2. Case studies on thruster failure and conversions in Chapter 3 reveal that the simulation model, even not so accurate, is capable of offering instructive solutions to assist operational and maintenance decisions. The finding supports the argument that the model derived on the basis of a deep understanding of the underlying process is rational and consists of the physical properties, despite some unavoidable errors such as simplifications. Two other pieces of research are implemented based on this conclusion. One is to optimize the physics-based simulation model on the parameter level by employing process data. The other is to develop a surrogate model upon the available numerical model assisted by limited operation data, calibrating and adapting the model in principle. As claimed by the physics-data hybrid model proposed in Chapter 2, the two case studies each focus on one category. One presents an analysis on identifying the hydrodynamic parameters in the ship maneuvering model in line with RO4. One proposes a knowledge transfer concept between the target ship and a relevant similar ship to achieve RO5. Results confirm the increased model fidelity and prediction accuracy observed for the hybrid approach relative to either participant.

The main contributions of this dissertation are as follows:

- Propose a physics-data cooperation concept for complex system modeling from both functionality and implementation architecture aspects.
- Present model optimizations by estimating uncertain parameters in ship maneuvering model subjected to environmental disturbances.

- Propose a hybrid predictor that can merge knowledge from a pre-determined, physics-based ship motion model and data sampled from the ship. Predictions are considered for zigzag maneuvering and docking scenarios.
- Propose a knowledge transfer approach to construct the representative model for the target ship benefiting from the well-established domain knowledge of a benchmark vessel.
- Offer three models, including pure kinetics, pure data-based, and physics-data unified, for ship motion prediction.

6.2 Summary of publications

The summary of publications is as follow:

Paper I presents a simulation model-based thruster failure detection and isolation method for dynamically positioned offshore surface vessels. Based on the prior knowledge of the mathematical model of a DP ship subjected to wind disturbances, estimated ship states can be obtained as a reference. The thruster failures are detected if the residual exceeds the safety threshold. A sliding window together with a probability analysis is applied to locate the failed thruster. The method is validated in a simulated environment and can effectively detect and isolate the failure.

Paper II presents a data-driven approach for identifying the uncertain hydrodynamic coefficients under environmental disturbance for a 3 degree of freedom nonlinear maneuvering model. The identification is performed on multiple maneuvers datasets. The model fidelity is found to be affected by the sea states, while predictions of different maneuvers convince the generalization capability of the estimated model.

Paper III proposes a hybrid modeling methodology in which prior knowledge describing the ship's dynamic effects is incorporated into a data-driven calibrator, yielding a representative model with high predictive capability. Enabled by integrating model estimated ship states into the calibrator, the informative information could be interpreted and carried forward. Simulation and full-scale experiments are conducted on the research vessel Gunnerus to exemplify the concept. A best available numerical model and a neural network are prepared to be the foundation and calibrator, respectively. Experiment results show that the cooperative model dramatically improves the predictive capability of the research vessel.

Paper IV presents research related to the ship propulsion retrofit process based on the co-simulation technique. The ship maneuverability before and after refitting propulsion units is simulated and analyzed. Through the experiments, propulsion performance improvements are observed. Technically, the study supports that co-simulation as an enabling tool in the maritime field appears promising, benefiting from its modularity and re-usability, which lays a solid foundation for later work.

Paper V builds on the approach presented in paper III. A knowledge transfer strategy is proposed to migrate and adapt the domain knowledge from the existing benchmark ship to the target ship. The benchmark, or source ship, is explicitly different from the target ship but carries somewhat resemblance in the feature space. Therefore it is employed to leverage domain knowledge to enhance the target model. While in paper III, the prior domain knowledge is supplied by a shorter version research ship, which main-

tains most properties unchanged. To clarify the resemblance between source and target ships, a characteristic vector is introduced to evaluate the geometric and configuration similarities. The derived target model is verified to be capable of accurately predicting maneuver trajectories in various scenarios.

Paper VI is a continuation of the works presented in paper III and V. The predictors of paper III and V output the trajectory of the vessel on the entire prediction interval at once, while this predictor output single-step prediction and is re-iterated to provide the complete trajectory prediction. This way, the performance of hydrodynamic-based, data-driven without physics informed, and hybrid predictors are comparable. The proposed approach is validated in the real docking operation of a research vessel. The results convinced that the physics-data hybrid way yields a more accurate model with relaxed data requirements and less learning consumption.

6.3 Future work

This thesis has focused on ship motion prediction by exploiting physics-data cooperation approaches. A recurring theme has been the synthesis of ship dynamic model and machine learning methods to model the functional relationship presented in each research item. The below bullet points provide suggestions for how the presented research may be extended.

- Model optimization with tunable parameters using machine learning approaches is found to be affected by the training data distribution. For a cruise ship in service, it experiences departure, acceleration, autopilot, and deceleration until it docks in the harbor. Different sailing stages should render different features, which inspires us to optimize the vessel model locally after recognizing the operation pattern and ocean situations.
- Currently, the predictors, either hybrid or data-driven, are trained offline with sufficient data supplied. It is not always the case in reality that the training data are all experienced and well prepared. Unseen scenarios and anomalies are not rare during a ship's commissioning. In seeking to continuously offer high-fidelity forecasts to support crew onboard or autonomous control systems, online or incremental learning plays an essential role. Considering the stochastic disturbance the ship exposed to, predictions with uncertainty analysis will be preferred in future work.
- Aside from the research items investigated in the thesis, there should be other means of physics-data cooperation to be exploited. Actually, the terminology "physics-data cooperation" used in this dissertation is loosely defined, and it could be achieved in various manners. There is yet no widely accepted definition given regarding the synthesis of knowledge and data. Distributed work is found conducted for a specific problem in the literature. A comprehensive survey of the hybrid modeling philosophy, including implementation approaches, model assessment, challenges in the marine domain, etc., is in demand.

References

- [1] S. Weyer, T. Meyer, M. Ohmer, D. Gorecky, and D. Zühlke, “Future modeling and simulation of cps-based factories: an example from the automotive industry,” *IFAC-PapersOnLine*, vol. 49, pp. 97–102, 1 2016.
- [2] M. Kitada, M. Baldauf, A. Mannov, P. A. Svendsen, R. Baumler, J. U. Schröder-Hinrichs, D. Dalaklis, T. Fonseca, X. Shi, and K. Lagdami, “Command of vessels in the era of digitalization,” *Advances in Intelligent Systems and Computing*, vol. 783, pp. 339–350, 7 2018.
- [3] K. Nomoto, T. Tauguchi, K. Honda, and S. Hirano, “On the steering qualities of ships,” technical report, international shipbuilding progress, vol 4,” 1957.
- [4] M. A. Abkowitz, “Lectures on ship hydrodynamics—steering and manoeuvrability,” tech. rep., 1964.
- [5] A. Ogawa, T. Koyama, and K. Kijima, “Mmg report-i, on the mathematical model of ship manoeuvring,” *Bull Soc Naval Archit Jpn*, vol. 575, no. 22-28, 1977.
- [6] M. Haranen, P. Pakkanen, R. Kariranta, and J. Salo, “White, grey and black-box modelling in ship performance evaluation,” in *1st Hull performance & insight conference (HullPIC)*, pp. 115–127, 2016.
- [7] N. R. Kristensen, H. Madsen, and S. B. Jørgensen, “Parameter estimation in stochastic grey-box models,” *Automatica*, vol. 40, no. 2, pp. 225–237, 2004.
- [8] K. J. Åström and C. G. Källström, “Identification of ship steering dynamics,” *Automatica*, vol. 12, no. 1, pp. 9–22, 1976.
- [9] B. Mei, L. Sun, G. Shi, and X. Liu, “Ship maneuvering prediction using grey box framework via adaptive rm-svm with minor rudder,” *Polish Maritime Research*, vol. 26, no. 3, pp. 115–127, 2019.
- [10] M. Committee *et al.*, “Final report and recommendations to the 24th ittc,” *Proceedings of the 24th ITTC*, vol. 1, pp. 137–198, 2005.
- [11] D. P. Solomatine and A. Ostfeld, “Data-driven modelling: some past experiences and new approaches,” *Journal of Hydroinformatics*, vol. 10, pp. 3–22, 1 2008.
- [12] M. I. Jordan and T. M. Mitchell, “Machine learning: Trends, perspectives, and prospects,” *Science*, vol. 349, no. 6245, pp. 255–260, 2015.
- [13] H. J. Tulleken, “Grey-box modelling and identification using physical knowledge and bayesian techniques,” *Automatica*, vol. 29, no. 2, pp. 285–308, 1993.

- [14] T. I. Fossen, *Handbook of marine craft hydrodynamics and motion control*. John Wiley & Sons, 2011.
- [15] O. Bousquet, S. Boucheron, and G. Lugosi, "Introduction to statistical learning theory," in *Summer school on machine learning*, pp. 169–207, Springer, 2003.
- [16] V. Gavrishchaka, O. Senyukova, and M. Koepke, "Synergy of physics-based reasoning and machine learning in biomedical applications: towards unlimited deep learning with limited data," *Advances in Physics: X*, vol. 4, no. 1, p. 1582361, 2019.
- [17] L. Ljung, "Black-box models from input-output measurements," in *Imtc 2001. proceedings of the 18th ieee instrumentation and measurement technology conference. rediscovering measurement in the age of informatics (cat. no. 01ch 37188)*, vol. 1, pp. 138–146, IEEE, 2001.
- [18] J. Sjöberg, Q. Zhang, L. Ljung, A. Benveniste, B. Delyon, P.-Y. Glorennec, H. Hjalmarsson, and A. Juditsky, "Nonlinear black-box modeling in system identification: a unified overview," *Automatica*, vol. 31, no. 12, pp. 1691–1724, 1995.
- [19] M. Hotvedt, B. Grimstad, and L. Imsland, "Identifiability and physical interpretability of hybrid, gray-box models - a case study," *IFAC-PapersOnLine*, vol. 54, pp. 389–394, 1 2021.
- [20] L. Yang, G. Chen, N. G. M. Rytter, J. Zhao, and D. Yang, "A genetic algorithm-based grey-box model for ship fuel consumption prediction towards sustainable shipping," *Annals of Operations Research*, pp. 1–27, 2019.
- [21] K. Tan and Y. Li, "Grey-box model identification via evolutionary computing," *Control Engineering Practice*, vol. 10, no. 7, pp. 673–684, 2002.
- [22] W. Luo and Z. Zou, "Parametric identification of ship maneuvering models by using support vector machines," *Journal of ship research*, vol. 53, no. 01, pp. 19–30, 2009.
- [23] X.-g. Zhang and Z.-j. Zou, "Identification of abkowitz model for ship manoeuvring motion using ε -support vector regression," *Journal of hydrodynamics*, vol. 23, no. 3, pp. 353–360, 2011.
- [24] M. Blanke and M. Knudsen, "Efficient parameterization for grey-box model identification of complex physical systems," *IFAC Proceedings Volumes*, vol. 39, no. 1, pp. 338–343, 2006.
- [25] Z. Wang, C. G. Soares, and Z. Zou, "Optimal design of excitation signal for identification of nonlinear ship manoeuvring model," *Ocean Engineering*, vol. 196, p. 106778, 2020.
- [26] W. Luo and X. Li, "Measures to diminish the parameter drift in the modeling of ship manoeuvring using system identification," *Applied Ocean Research*, vol. 67, pp. 9–20, 2017.
- [27] R. R. Sheno, P. Krishnankutty, and R. P. Selvam, "Sensitivity study of hydrodynamic derivative variations on the maneuverability prediction of a container ship," in

-
- International Conference on Offshore Mechanics and Arctic Engineering*, vol. 56550, p. V007T06A008, American Society of Mechanical Engineers, 2015.
- [28] X. Yu, L. Georges, and L. Imsland, “Data pre-processing and optimization techniques for stochastic and deterministic low-order grey-box models of residential buildings,” *Energy and Buildings*, vol. 236, p. 110775, 2021.
- [29] M. Aliramezani, A. Norouzi, and C. R. Koch, “A grey-box machine learning based model of an electrochemical gas sensor,” *Sensors and Actuators B: Chemical*, vol. 321, p. 128414, 2020.
- [30] I. Lagaris, A. Likas, and D. Fotiadis, “Artificial neural networks for solving ordinary and partial differential equations,” *IEEE Transactions on Neural Networks*, vol. 9, no. 5, pp. 987–1000, 1998.
- [31] S. A. Niaki, E. Haghghat, X. Li, T. Campbell, and R. Vaziri, “Physics-informed neural network for modelling the thermochemical curing process of composite-tool systems during manufacture,” *arXiv preprint arXiv:2011.13511*, 2020.
- [32] Z. Zhang, R. Rai, S. Chowdhury, and D. Doermann, “Midphynet: Memorized infusion of decomposed physics in neural networks to model dynamic systems,” *Neurocomputing*, vol. 428, pp. 116–129, 2021.
- [33] M. Lutter, C. Ritter, and J. Peters, “Deep lagrangian networks: Using physics as model prior for deep learning,” *arXiv preprint arXiv:1907.04490*, 2019.
- [34] X.-G. Wang, Z.-J. Zou, F. Xu, and R.-Y. Ren, “Sensitivity analysis and parametric identification for ship manoeuvring in 4 degrees of freedom,” *Journal of Marine Science and Technology*, vol. 19, no. 4, pp. 394–405, 2014.
- [35] S. Estrada-Flores, I. Merts, B. De Ketelaere, and J. Lammertyn, “Development and validation of “grey-box” models for refrigeration applications: A review of key concepts,” *International Journal of Refrigeration*, vol. 29, no. 6, pp. 931–946, 2006.
- [36] R. Skulstad, G. Li, T. I. Fossen, B. Vik, and H. Zhang, “A hybrid approach to motion prediction for ship docking—integration of a neural network model into the ship dynamic model,” *IEEE Transactions on Instrumentation and Measurement*, vol. 70, pp. 1–11, 2021.
- [37] F. M. Gray and M. Schmidt, “A hybrid approach to thermal building modelling using a combination of gaussian processes and grey-box models,” *Energy and Buildings*, vol. 165, pp. 56–63, 2018.
- [38] Ø. N. Smogeli, “Control of marine propellers: from normal to extreme conditions,” 2006.
- [39] B. E. Boser, I. M. Guyon, and V. N. Vapnik, “A training algorithm for optimal margin classifiers,” in *Proceedings of the Fifth Annual Workshop on Computational Learning Theory*, COLT '92, (New York, NY, USA), pp. 144–152, Association for Computing Machinery, 1992.

- [40] <https://ulstein.com/references/olympic-zeus>.
- [41] C. Gomes, C. Thule, D. Broman, P. G. Larsen, and H. Vangheluwe, “Co-simulation: a survey,” *ACM Computing Surveys (CSUR)*, vol. 51, no. 3, pp. 1–33, 2018.
- [42] D. Broman, C. Brooks, L. Greenberg, E. A. Lee, M. Masin, S. Tripakis, and M. Wetter, “Determinate composition of fimus for co-simulation,” in *2013 Proceedings of the International Conference on Embedded Software (EMSOFT)*, pp. 1–12, IEEE, 2013.
- [43] L. I. Hatledal, Y. Chu, A. Styve, and H. Zhang, “Vico: An entity-component-system based co-simulation framework,” *Simulation Modelling Practice and Theory*, vol. 108, p. 102243, 2021.
- [44] L. I. Hatledal, R. Skulstad, G. Li, A. Styve, and H. Zhang, “Co-simulation as a fundamental technology for twin ships,” 2020.
- [45] <https://www.ntnu.edu/gunnerus>.
- [46] T. Perez, O. Smogeli, T. Fossen, and A. Sorensen, “An overview of the marine systems simulator (mss): A simulink toolbox for marine control systems,” *Modeling, identification and Control*, vol. 27, no. 4, pp. 259–275, 2006.
- [47] M. Chislett and J. Strom-Tejsen, “Planar motion mechanism tests and full-scale steering and manoeuvring predictions for a mariner class vessel,” *International Shipbuilding Progress*, vol. 12, no. 129, pp. 201–224, 1965.
- [48] L. Liu, D. Y. Yang, and D. M. Frangopol, “Ship service life extension considering ship condition and remaining design life,” *Marine Structures*, vol. 78, p. 102940, 2021.
- [49] R. Skjetne, Ø. Smogeli, and T. I. Fossen, “Modeling, identification, and adaptive maneuvering of CyberShip II: A complete design with experiments,” pp. 65–70, 2004.
- [50] L. I. Hatledal, F. Collonval, and H. Zhang, “Enabling python driven co-simulation models with pythonfmu,” in *Proceedings of the 34th International ECMS-Conference on Modelling and Simulation-ECMS 2020*, ECMS European Council for Modelling and Simulation, 2020.
- [51] V. Hassani, A. Ross, Ø. Selvik, D. Fathi, F. Sprenger, and T. E. Berg, “Time domain simulation model for research vessel gunnerus,” in *International Conference on Off-shore Mechanics and Arctic Engineering*, vol. 56550, p. V007T06A013, American Society of Mechanical Engineers, 2015.
- [52] H. Yasukawa and R. Sakuno, “Application of the mmg method for the prediction of steady sailing condition and course stability of a ship under external disturbances,” *Journal of Marine Science and Technology*, vol. 25, no. 1, pp. 196–220, 2020.
- [53] F. Pedregosa, G. Varoquaux, A. Gramfort, V. Michel, B. Thirion, O. Grisel, M. Blondel, P. Prettenhofer, R. Weiss, V. Dubourg, J. Vanderplas, A. Passos, D. Cournapeau, M. Brucher, M. Perrot, and E. Duchesnay, “Scikit-learn: Machine

learning in Python,” *Journal of Machine Learning Research*, vol. 12, pp. 2825–2830, 2011.

- [54] S. Sutulo and C. G. Soares, “An algorithm for offline identification of ship manoeuvring mathematical models from free-running tests,” *Ocean engineering*, vol. 79, pp. 10–25, 2014.

Appendix

A large, stylized, grey letter 'A' logo is positioned in the top right corner of the page. It is partially overlapped by a grey rectangular bar that extends from the left edge of the page towards the right.

Paper I

This paper is not included due to copyright restrictions
Available in 2020 IEEE International Conference on Mechatronics and Automation. IEEE
conference proceedings 2020 s. 898-904
<https://doi.org/10.1109/CMA49215.2020.9233745>
and institutionsarkiv: <https://hdl.handle.net/11250/2686009>

B

Paper II

Parameter identification of ship manoeuvring model under disturbance using support vector machine method

Tongtong Wang , Guoyuan Li , Baiheng Wu , Vilmar Æsøy and Houxiang Zhang 

Department of Ocean Operations and Civil Engineering, Norwegian University of Science and Technology, Aalesund, Norway

ABSTRACT

Demanding marine operations increase the complexity of manoeuvring. A highly accurate ship model promotes predicting ship motions and advancing control safety. It is crucial to identify the unknown hydrodynamic coefficients under environmental disturbance to establish accurate mathematical models. In this paper, the identification procedure for a 3 degree of freedom hydrodynamic model under disturbance is completed based on the support vector machine with multiple manoeuvres datasets. The algorithm is validated on the clean ship model and the results present good fitness with the reference. Experiments in different sea states are conducted to investigate the effects of the turbulence on the identification performance. Generalisation results show that the models identified in the gentle and moderate environments have less than 10% deviations and are considered allowable. The higher perturbations, the lower fidelity the identified model has. Models identified under disturbance could provide different levels of reliable support for the operation decision system.

ARTICLE HISTORY

Received 10 November 2020
Accepted 21 April 2021

KEYWORDS

Parameter identification;
manoeuvring model;
support vector machine;
disturbance; nonlinear

1. Introduction

Obtaining a model that can accurately describe the ship dynamics and its interaction with the environment has always been of considerable interest to academic researchers and marine industries. The model is expected to be high fidelity so that can be used for designing high-performance model-based control strategies (Zheng et al. 2018), as well as developing computer-based simulators for virtual testing (Li et al. 2016).



However, the modelling process is found complex due to the nonlinear properties of ship dynamics. The models obtained from experiments are thought to be the most accurate and reliable, yet they can also be the most economically costly to develop. Only a limited number of hull ships have had any parameters determined experimentally. Although lots of empirical methods associated with various model series have been developed, they can only provide reliable estimates when the hull form fits some tested series well enough, so that they are suggested to be used with great care. An alternative of theoretical calculations appears to recourse to computer fluid dynamics (CFD). The CFD techniques are already matured enough to provide estimates that, in general, can be viewed even more credible than empirical methods (Martelli et al. 2021). However, building proper finite element models necessitates expert experience, and in addition, it often is computationally intensive for on-line use. System identification theory comes up for its efficiency and economy. When addressing the ship manoeuvring model configuration issue, in general, it has to deal with complicated hydrodynamic effects associated with nonlinear and coupled coefficients, which challenge the researchers a lot (Åström and Källström 1976; Skjetne et al. 2004).

To address the challenges in ship dynamics identification, researchers offer various methods, for example, least-square method (Ding 2014), Bayesian approach (Xue et al. 2020), the maximum likelihood method (Chen et al. 2018, july), extended Kalman filter

method (Perera et al. 2015), and so on. These methods are demonstrated valid for a more or less wide range of hull forms and environment configurations. However, the conventional approaches are found sensitive to noise and initial estimations would influence the converging performance. Regarding the circumstances outlined it would be practically difficult to identify the model plant in a realistic environment. Given the technological and computational advances in instrumenting process, a branch of identification method by machine learning has been established.

The techniques in the form of neural networks (NNs) have been applied as a regression process to model the nonlinear ship dynamics and predict future trajectories. In the work of Rajesh and Bhattacharyya (2008), NN was employed to estimate the unknown time equation clubbed by all nonlinear hydrodynamic derivatives of large tankers. This experience shows that NNs work well on approaching nonlinearities, yet meanwhile, the exploration to parameters associated with the ship is kept out of reach. Similarly, in the work of Cheng et al. (2019), the NN was used to generate a surrogate model based on the ship motion data. Again, it is a black-box model, and the parameters are not correlated to specific physical properties of the ship.

In the cases where the hydrodynamic derivatives are preferred to be presented in detail, another machine learning technique – support vector machine (SVM) can help. This approach proposed by Vapnik (1999) features a kernel-based learning process and facilitates the possibility of acquiring regression coefficients. It is increasingly applied to estimate ship dynamics, for instance, in the work of Luo and Zou (2009), as well as Zhang and Zou (2011), the authors implemented the Abkowitz model identification of a benchmark ship. It is shown that the SVM approach works well when there is no disturbance accounted for in the system.

CONTACT Guoyuan Li  guoyuan.li@ntnu.no  Department of Ocean Operations and Civil Engineering, Norwegian University of Science and Technology, Postboks 1517, N-6025 Aalesund, Norway

© 2021 The Author(s). Published by Informa UK Limited, trading as Taylor & Francis Group

This is an Open Access article distributed under the terms of the Creative Commons Attribution-NonCommercial-NoDerivatives License (<http://creativecommons.org/licenses/by-nc-nd/4.0/>), which permits non-commercial re-use, distribution, and reproduction in any medium, provided the original work is properly cited, and is not altered, transformed, or built upon in any way.

However, the ship dynamics have always changing due to the interaction with environmental disturbance and load conditions. Developing a reliable model to a considerable extent under such interference to provide onboard decision support for autonomous vessels where no human expertise could dominate, is practically pivotal. Inspired by the pragmatic challenge, increasing attention has been drawn to the system identification problem in random environments. The SVM-based identification is found to be insensitive to instrumental noise and capable of achieving high generalisation performance (Sutulo and Soares 2014; Wang et al. 2019). Examples of identifying ship model in waves are reported in the work by Hou and Zou (2016) and Selvam and Bhattacharyya (2010). In their work, the excitation forces and moments of waves are estimated first by numerical calculation or experiment measurements. Whereas the instant signals of waves or ocean currents are always not available onboard, which consequently limits the assessment of environmental loads. An alternative solution is modelling the slow-varying environmental forces as a stochastic process to compensate for the lack of realistic ship manoeuvring data. Achieving reliable estimation under such disturbance is the target of this study. The extent of perturbations varies to simulate different sea states. Within this context, the authors intend to address the impact of external disturbance on the parameter identification performance and seek estimations to a considerable accuracy by using the SVM-based identification approach so that they can be used in different operating scenarios according to their fidelities.

The structure of this paper is organised as follows. Section 2 formulates the parameter identification problem and procedure. This is followed by a review of the ship manoeuvring model and the concept of SVM algorithms. In Section 3, the identification algorithm is implemented for a clean system, aiming to verify the fidelity of the numerical model. Section 4 focuses on the disturbance experiment design and results discussion. The marine ship is assumed to expose to different levels of environmental perturbations, and the fidelity of the identified model is of particular concern. Conclusions and future work are presented in the final section.

2. Parameter identification

The parameter identification of the ship manoeuvring model is complex due to the respective hydrodynamic effects. Normally, the ship dynamics are described by a group of derivative equations, associated with linear and nonlinear terms. Specifically, the identification process is described in Figure 1. The regression model, derived from the ship manoeuvring model, determines the input and output features of the SVM. After preparing the data containing ship motion and propulsion commands, the SVM is extensively trained and optimal coefficients are then generated. By substituting the identified results back into the ship manoeuvring model, the estimated model is obtained and could be further examined. Particularly, the generalisation capability of the identified model should be stressed properly.

The training datasets include the vessel's multiple different manoeuvres. Note that the ship motion data should be taken extra cleaning treatment to eliminate the measurement noise if it is collected from the onboard sensors.

Models to describe ship dynamics can take many forms. To highlight the ship hydrodynamic properties, the Abkowitz model expressed in form of Taylor series is selected. A benchmark ship – a Mariner class vessel acts as research platform. The major steps concerning identification as shown in the dash box are expanded in the following subsections.

2.1. Ship manoeuvring model

For an offshore surface vessel performing manoeuvring tasks, its horizontal 3 degree of freedom (DOF) behaviour in non-dimensional form can be expressed as

$$\begin{bmatrix} m' - X_{\dot{u}}' & 0 & 0 \\ 0 & m' - Y_{\dot{v}}' & m'x'_g - Y_{\dot{r}}' \\ 0 & m'x'_g - N_{\dot{v}}' & I_{zz}' - N_{\dot{r}}' \end{bmatrix} \begin{bmatrix} \dot{u}' \\ \dot{v}' \\ \dot{r}' \end{bmatrix} = \begin{bmatrix} X' \\ Y' \\ N' \end{bmatrix} \quad (1)$$

where the superscript represents dimensionless variables. m' is the ship mass, x'_g is the position of gravity centre in the longitudinal direction of the body-fixed coordinate system. \dot{u}' , \dot{v}' , \dot{r}' are the accelerations in surge, sway, and yaw directions. X' , Y' and N' represent forces along the ship longitudinal and lateral directions, as well as the moments about the vertical axis, respectively. $X_{\dot{u}}'$, $Y_{\dot{v}}'$, $Y_{\dot{r}}'$, $N_{\dot{v}}'$, $N_{\dot{r}}'$ are non-dimensional added mass coefficients. I_{zz}' is the inertia moment about the vertical axis.

The non-dimensional variables are defined as

$$\begin{aligned} \dot{u}' &= \frac{\dot{u}L}{U^2}, \dot{v}' = \frac{\dot{v}L}{U^2}, \dot{r}' = \frac{\dot{r}L^2}{U^2}, u' = \frac{u}{U}, v' = \frac{v}{U}, r' = \frac{rL}{U}, U \\ &= \sqrt{(U_0 + u)^2 + v^2} \\ X' &= \frac{X}{0.5\rho L^2 U^2}, Y' = \frac{Y}{0.5\rho L^2 U^2}, N' = \frac{N}{0.5\rho L^2 U^2} \end{aligned}$$

where ρ is the density of water, L is the ship length, U is registered as the instantaneous ship speed, u refers to perturbed surge velocity about nominal speed U_0 .

The non-dimensional forms of hydrodynamic forces/moments in the Abkowitz model are represented as Equation (2).

$$\begin{aligned} X' &= X'_{\dot{u}}u' + X'_{uu}u'^2 + X'_{uuu}u'^3 + X'_{vv}v'^2 + X'_{rr}r'^2 + X'_{rv}r'v' \\ &+ X'_{\dot{u}}\delta'^2 + X'_{\dot{u}\delta}u'\delta' + X'_{\dot{u}v}v'\delta' + X'_{\dot{u}v\delta}u'v'\delta' + X'_{\dot{u}vv}u'v'^2 \\ &+ X'_{\dot{u}rr}u'r'^2 + X'_{\dot{u}vr}u'v'r' + X'_{\dot{r}}\delta'r' + X'_{\dot{u}r\delta}u'r'\delta' + X'_{\dot{r}\delta} \end{aligned} \quad (2-a)$$

$$\begin{aligned} Y' &= Y'_{\dot{v}}v' + Y'_{\dot{r}}r' + Y'_{vvv}v'^3 + Y'_{vvr}v'^2r' + Y'_{rrr}r'^3 \\ &+ Y'_{vrr}v'r'^2 + Y'_{vu}v'u'^2 + Y'_{ruu}r'u'^2 \\ &+ Y'_{vu}v'u' + Y'_{ru}r'u' + Y'_{\dot{v}}\delta' + Y'_{\dot{v}\delta}v'\delta' + Y'_{\dot{v}u}u'\delta' \\ &+ Y'_{\dot{u}u}u'^2\delta' + Y'_{\dot{v}\delta}v'\delta'^2 + Y'_{\dot{v}v}v'^2\delta' + Y'_{\dot{r}\delta}r'\delta'^2 \\ &+ Y'_{\dot{r}\delta}r'^2\delta' + Y'_{\dot{r}\delta}r'v'\delta' + (Y'_0 + Y'_{0u}u' + Y'_{0uu}u'^2) \end{aligned} \quad (2-b)$$

$$\begin{aligned} N' &= N'_{\dot{v}}v' + N'_{\dot{r}}r' + N'_{vvv}v'^3 + N'_{vvr}v'^2r' + N'_{rrr}r'^3 \\ &+ N'_{vrr}v'r'^2 + N'_{vu}v'u'^2 + N'_{ruu}r'u'^2 + N'_{vu}v'u' \\ &+ N'_{ru}r'u' + N'_{\dot{v}}\delta' + N'_{\dot{v}\delta}v'\delta'^3 + N'_{\dot{v}\delta}v'\delta' + N'_{\dot{v}u}u'\delta' \\ &+ N'_{\dot{r}\delta}r'^2\delta' + N'_{\dot{r}\delta}r'v'\delta' + N'_{\dot{v}\delta}v'\delta'^2 + N'_{\dot{r}\delta}r'\delta'^2 \\ &+ N'_{\dot{v}\delta}v'^2\delta' + (N_0 + N'_{0u}u' + N'_{0uu}u'^2) \end{aligned} \quad (2-c)$$

The hydrodynamic derivatives $\{X'_{(\cdot)}, Y'_{(\cdot)}, N'_{(\cdot)}\}$ are the parameters that need to be identified.

2.2. Regression model

The Abkowitz model is generally considered as a nonlinear hydrodynamic model, whereas it can be viewed as a linear model with respect to the hydrodynamic parameters. The motion equations are discretised by using Euler's stepping method and the derived

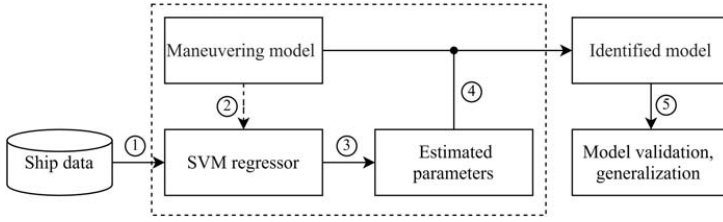


Figure 1. Scheme of parameter identification for ship manoeuvring model.

regression model is

$$\begin{aligned} w'(n+1) - w'(n) &= AX(n) \\ v'(n+1) - v'(n) &= BY(n) \\ r'(n+1) - r'(n) &= CN(n) \end{aligned} \quad (3)$$

where A, B, C are parameter vectors formed by hydrodynamic derivatives to be identified, given as

$$A = [a_1, a_2, \dots, a_{16}]_{1 \times 16}$$

$$B = [b_1, b_2, \dots, b_{22}]_{1 \times 22}$$

$$C = [c_1, c_2, \dots, c_{22}]_{1 \times 22}$$

where $X(n), Y(n), N(n)$ are the variables vectors, n and $n+1$ are the adjacent sampling time steps. By solving the governing model Equation (1), one can get the variable vectors given as Equation (4), compounding by ship velocities and rudder angle.

$$\begin{aligned} X(n) &= [u', u'^2, u'^3, v'^2, r'^2, r'v', \delta^2, u'\delta^2, v'\delta', u'v'\delta', u'v'^2, u'r'^2, \\ &u'v'r', r'\delta', u'r'\delta', 1]^T \times \frac{U^2}{L} \times \frac{\Delta t}{m' - X'_u} \end{aligned} \quad (4-a)$$

$$\begin{aligned} Y(n) &= [v', r', v'^3, v'^2r', r'^3, v'r'^2, v'u'^2, r'u'^2, v'u', r'u', \delta', \delta^3, u'\delta', \\ &u'^2\delta', v'\delta^2, v'^2\delta', r'\delta^2, r'2\delta', r'v'\delta', 1, u', u'^2]^T \\ &\times \frac{U^2}{L} \times \frac{\Delta t}{S} \end{aligned} \quad (4-b)$$

$$\begin{aligned} N(n) &= [v', r', v'^3, v'^2r', r'^3, v'r'^2, v'u'^2, r'u'^2, v'u', r'u', \delta', \delta^3, u'\delta', \\ &u'^2\delta', v'\delta^2, v'^2\delta', r'\delta^2, r'2\delta', r'v'\delta', 1, u', u'^2]^T \\ &\times \frac{U^2}{L^2} \times \frac{\Delta t}{S} \end{aligned} \quad (4-c)$$

where $S = (m' - Y'_v)(I'_{zz} - N'_r) - (m'x'_g - Y'_r)(m'x'_g - N'_r)$. The rudder angle is represented by δ and $\delta' = \dot{\delta}$. It should be mentioned that the five zeros frequency added mass derivatives X'_u, Y'_v, Y'_r, N'_r and N'_r usually have enough preciseness, which can be found in semi-empirical formulas or calculated through strip theory. They can always be estimated beforehand. Only the parameter sets A, B , and C are unknown and they will be identified by the SVM algorithm. Mention that the hydrodynamic derivatives $X'_{(\cdot)}$ in surge equation are simply obtained by Equation (5) once the vector A is determined. While b_i and c_i ($i = 1, 2, \dots, 22$) are not direct hydrodynamic coefficients in sway and yaw motion equation, they

need further treatment by Equation (6).

$$X'_{(\cdot)} = \frac{L(m' - X'_u)}{\Delta t} A \quad (5)$$

$$\begin{bmatrix} Y'_{(\cdot)} \\ N'_{(\cdot)} \end{bmatrix} = \begin{bmatrix} \frac{(I'_{zz} - N'_r)\Delta t}{SL} & -\frac{(m'x'_g - Y'_r)\Delta t}{SL} \\ -\frac{(m'x'_g - N'_r)\Delta t}{SL^2} & \frac{(m' - Y'_v)\Delta t}{SL^2} \end{bmatrix}^{-1} \begin{bmatrix} B \\ C \end{bmatrix} \quad (6)$$

2.3. Support vector machine algorithm

Support vector machine (SVM) learning strategy was formally proposed in the 1990s by Vapnik (1999). As mentioned before, this approach is widely used in system engineering and is considered to be a powerful tool in system identification. As a batch technique, it does not require any initial estimation values and avoids lengthy iterations. It also has a better global optimal extremum, compared with traditional neural networks.

Generally, SVM used for regression is also called SVR. Given the training dataset $\{(x_i, y_i), x_i \in \mathbb{R}^n, y_i \in \mathbb{R}\}$, x_i is the input vector and y_i is the output. For regression purposes, the general approximation function of SVM is shown as

$$f(x) = W^T \Phi(x) + b \quad (7)$$

where W is the weight matrix and b is the bias term. $\Phi(\cdot)$ is the nonlinear function, which is mapping the input data to a high dimensional feature space. The goal is to find the optimal weights and threshold that best fit the data. It is proposed to do so by defining the criteria Equation (8) that simultaneously measures structure risk and empirical risk. It differs from conventional neural networks, which rely on only the empirical risk minimisation so that the SVM features a sparse solution.

$$\min_{w,b,\epsilon} \left(\frac{1}{2} W^2 + \gamma \sum_{i=1}^l (\xi_i + \hat{\xi}_i) \right) \quad (8)$$

Subject to:

$$\begin{aligned} f(x_i) - y_i &\leq \epsilon + \xi_i, \\ y_i - f(x_i) &\leq \epsilon + \hat{\xi}_i, \\ \xi_i &\geq 0, \hat{\xi}_i &\geq 0 \end{aligned}$$

where $i = 1 \dots l$, l is the number of samples, and γ is the penalty factor with positive values. ξ_i and $\hat{\xi}_i$ are non-negative slack variables. ϵ is the tube size referring to the precision by which the function is to be approximated. Errors are to be accepted when the samples are located in the tube. The introduction of tube and slack variables in the SVM algorithm promotes its robustness to noise and generalisation performance. Solving for the optimal weights and bias is a process of convex optimisation, which is

made simpler by using Lagrange multipliers and formulating the dual optimisation problem given as

$$\max_{\alpha, \alpha^*} \sum_{i=1}^l y_i(\alpha - \alpha^*) - \sum_{i=1}^l \epsilon(\alpha - \alpha^*) - \frac{1}{2} \sum_{i,j=1}^l (\alpha_i - \alpha_i^*)(\alpha_j - \alpha_j^*)x_i, x_j \quad (9)$$

Subject to:

$$\sum_{i=1}^l (\alpha_i - \alpha_i^*) = 0, \quad \alpha, \alpha^* \in [0, \gamma]$$

where α, α^* are the Lagrangian multipliers. x_i, x_j refers to the kernel function. The solution for the weights is based on the Karsh-Kuhn-Tucker conditions. Finally, the approximation of the function $f(x)$ is given as

$$f(x) = \sum_{i=1}^l (\alpha_i - \alpha_i^*)x_i, x_i + b \quad (10)$$

The support vectors are those data on or outside the tube with non-zero Lagrange multipliers. To carry out parameter identification using SVM, the linear kernel function is then adopted, representing an inner product between its operands. So, the identified parameter θ can be regressed as

$$\theta = \sum_{i=1}^l (\alpha_i - \alpha_i^*)x_i \quad (11)$$

In general, the identification process is conducted as the following steps:

1. Collect the sample experiment data $\{(t_i, u_i, v_i, r_i, \delta_i), i = 1, \dots, l\}$ based on full-scale sea trials or simulation.
2. Construct the input and output vectors for each SVM regressor according to Equations (3) and (4).
3. Train the SVM regressor and optimise the hydrodynamic coefficients.
4. Substitute the identified results back into model Equation (2) to get identified ship model.
5. Verify the generalisation performance of the obtained model.

3. Model validation

In this section, the effectiveness of the SVM-based identification algorithm will be investigated in a clean vessel model without disturbance.

The experiments are performed in the Marine Systems Simulator (MSS) (Perez et al. 2006) developed by the Norwegian University of Science and Technology and cooperating groups. It handles different simulation scenarios and provides enough resources for the implementation of mathematical models of marine systems. The Mariner class vessel (Chislett and Strom-Tejsen 1965) is selected as a benchmark for verification in this study. It should be noted that in the hydrodynamic model of the Mariner class vessel, only 10 hydrodynamic coefficients in surge motion equation, 15 in sway equation, and 15 in yaw equation are considered, and the others are zeros. The SVM regressor is implemented by using Scikit-learn in Python. Following the procedure as shown in Figure 1, the parameters are identified and verified against the experimental values.

3.1. Training data preparation

To cover as much as dynamic features, multiple manoeuvres are conducted in the simulator at 15 knots (7.717 m/s). The multiple manoeuvring datasets, including 20°/20°, 15°/15°, and 10°/10° zigzag tests, are sequentially generated, and equally sampled at 2 Hz in 900 s. 1800 samples are collected in total as the training data.

3.2. Identification results

Once the samples are extracted, the SVM is trained to fit the approximation function. The hyperparameters γ and ϵ in the SVM regression model with linear kernel are determined by grid search and cross validation. In this regression model, the regularisation factor γ is obtained as 10^3 , and ϵ is 0. The unknown non-dimensional hydrodynamic coefficients in Equation (2) are identified and the results are listed in Table 1, in comparison with the planar motion mechanism (PMM) experimental values. It can be seen that most of the numerical coefficients agree well with the real experimental values. Although some of them, for instance the coefficients N_0, N'_{ou}, N'_{ouu} in yaw direction, have relatively obvious discrepancies, they have a limited effect on the accuracy of the numerical model as their values are quite small.

3.3. Identified model validation

To verify the obtained hydrodynamic models, the prediction of the same multiple zigzag maneuver tests – 20°/20°, 15°/15°, and 10°/10°, is performed by the numerical model. Figure 2 shows that the model predicted velocities in three directions, as well as the angular displacement, achieve a satisfactory agreement with the references. The consistency in parameter value and prediction

Table 1. Identified non-dimensional hydrodynamic coefficients ($\times 10^{-5}$).

X-Coef	SVM	PMM	Y-Coef	SVM	PMM	N-Coef	SVM	PMM
X'_i	-185.2	-184.0	Y'_i	-1158.2	-1159.9	N'_i	-262.4	-264.0
X'_{uu}	-116.6	-110.0	Y'_r	-498.1	-498.9	N'_i	-165.4	-166.0
X'_{uuu}	-220.0	-215.0	Y'_{vvv}	-8150.4	-8078.5	N'_{vvv}	1667.5	1636.0
X'_{vv}	-923.0	-899.0	Y'_{vvr}	15312.0	15358.0	N'_{vvr}	-5484.0	-5483.0
X'_{rv}	13.8	18.0	Y'_{vu}	-1156.2	-1160.0	N'_{vu}	-250.6	-264.0
X'_{rv}	779.3	798.0	Y'_{ru}	-497.3	-498.9	N'_{ru}	-162.2	-166.0
X'_{gd}	-94.6	-95.0	Y'_g	277.6	278.0	N'_d	-139.0	-139.0
X'_{udd}	-190.2	-190.0	Y'_{ddd}	-89.6	-90.0	N'_{ddd}	42.3	45.0
X'_{ud}	92.3	93.0	Y'_{ud}	554.3	556.1	N'_{ud}	-270.0	-278.0
X'_{uvd}	86.1	93.0	Y'_{uud}	271.7	278.0	N'_{uud}	-87.8	-139.0
			Y'_{udd}	-3.6	-4.0	N'_{udd}	17.5	13.0
			Y'_{vvd}	1213.1	1190.1	N'_{vvd}	-476.2	-489.0
			Y_0	-3.6	-4.0	N_0	1.6	3.0
			Y'_{ou}	-8.6	-8.0	N'_{ou}	8.0	6.0
			Y'_{ouu}	-2.7	-4.0	N'_{ouu}	-0.4	3.0

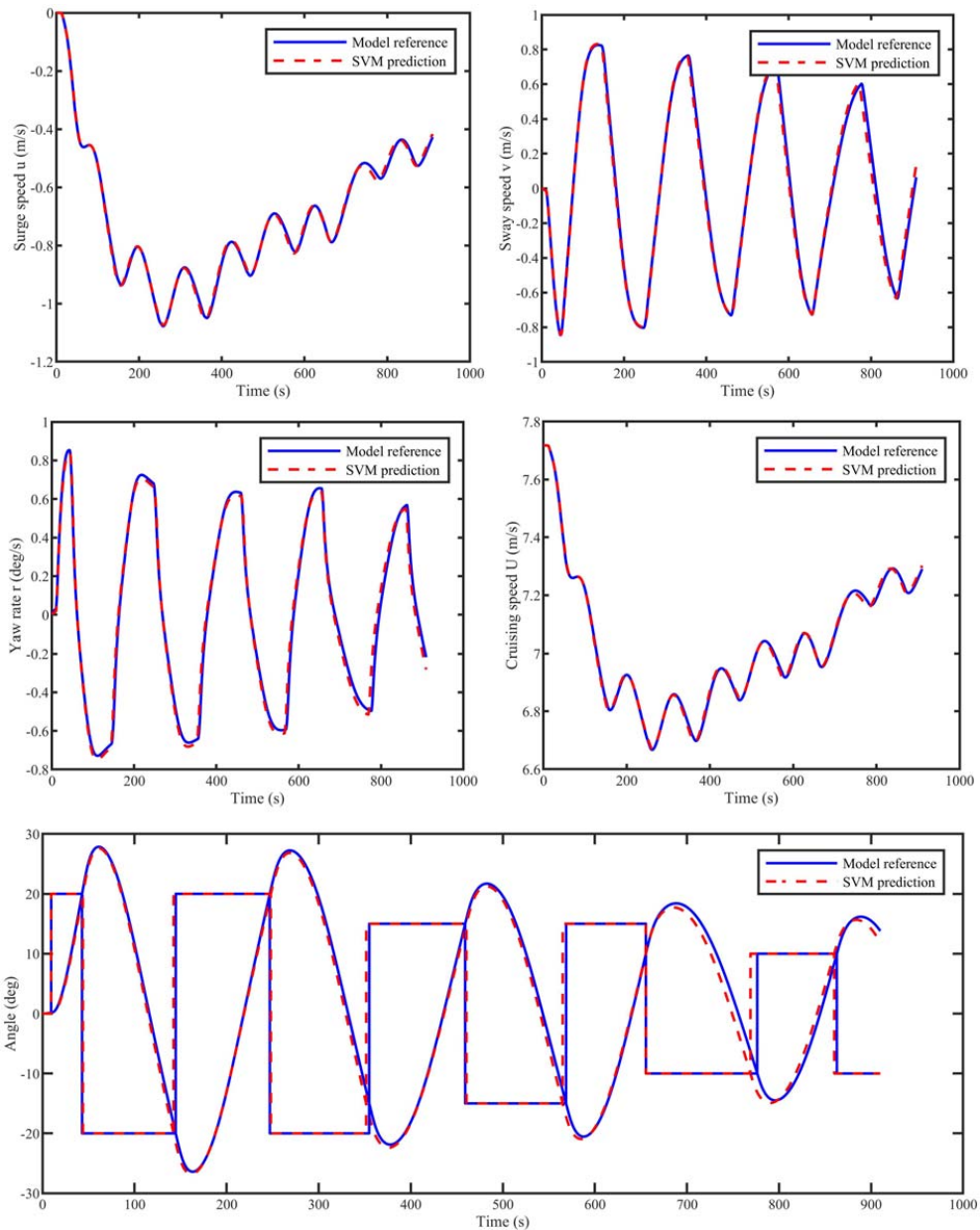


Figure 2. The validation between the SVM predictions and the model reference zigzag tests. (This figure is available in colour online.)

performance demonstrates the effectiveness and reproducibility of the SVM-based identification method.

4. Disturbance experiment

To estimate the hydrodynamic parameters under environmental disturbance, and investigate the influence on the model fidelity, disturbance experiments are conducted, and identification results are discussed in this section.

4.1. Disturbed manoeuvring models

The ship motion is always influenced by variations of wind, waves, and ocean currents in real world. These forces are not accounted for in the Abkowitz model presented in Section 2. A reasonable way to describe the environmental effects is modelling them as a stochastic process (Fossen 2011). Such a process can represent the slow-varying environmental forces and moments due to wind loads, second-order wave drift forces, and current forces. These effects are lumped

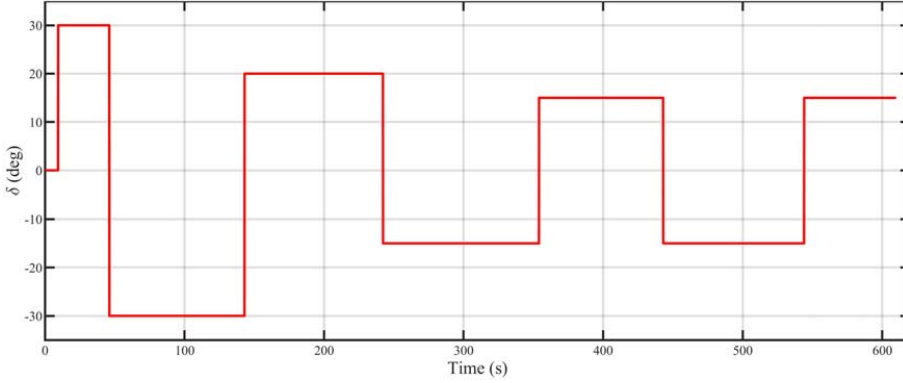


Figure 3. The excitation signal of multiple zigzag tests. (This figure is available in colour online.)

into a bias term $\mathbf{b} \in \mathbb{R}^3$ acting on the ship. The disturbed model is given as

$$\begin{bmatrix} m' - X'_u & 0 & 0 \\ 0 & m' - Y'_v & m'x'_g - Y'_f \\ 0 & m'x'_g - N'_v & I_{zz} - N'_f \end{bmatrix} \begin{bmatrix} \dot{u}' \\ \dot{v}' \\ \dot{r}' \end{bmatrix} = \begin{bmatrix} X' \\ Y' \\ N' \end{bmatrix} + \mathbf{R}^T(\psi)\mathbf{b} + \mathbf{w}_2 \quad (12)$$

where $\dot{\mathbf{b}} = \mathbf{w}_1$ represents the stochastic disturbances, and it is usually modelled as a Wiener process. The variables $w_i (i=1, 2)$ are zero-mean Gaussian noise vectors, referring to bias, and process noise respectively. \mathbf{R} is the rotation matrix shown as follows, transforming the ship motion from the body-fixed frame to the earth-fixed frame. ψ is to the ship heading.

$$\mathbf{R} = \begin{bmatrix} \cos \psi & -\sin \psi & 0 \\ \sin \psi & \cos \psi & 0 \\ 0 & 0 & 1 \end{bmatrix}$$

Note the measurement noise is not accounted for in this model, for the reason that we mainly focus on the effects of environmental effects and progress noise on the performance, which are practically meaningful and have not been closely studied. From Equation (12), the regression function is derived in a form as

$$\begin{bmatrix} \dot{v} \\ \dot{b} \end{bmatrix} = \begin{bmatrix} \mathbf{M}^{-1}\boldsymbol{\tau} \\ 0 \end{bmatrix} + \begin{bmatrix} 0 & \mathbf{M}^{-1}\mathbf{R}^T(\psi) \\ 0 & 0 \end{bmatrix} \begin{bmatrix} \mathbf{v} \\ \mathbf{b} \end{bmatrix} + \begin{bmatrix} \mathbf{M}^{-1}\mathbf{w}_2 \\ \mathbf{w}_1 \end{bmatrix} \quad (13)$$

where $\mathbf{M} \in \mathbb{R}^{3 \times 3}$ is the vessel mass matrix including added mass. $\mathbf{v} = [u, v, r]^T$ is the ship velocity vector, and $\boldsymbol{\tau} = [X, Y, N]^T$ represents hydrodynamic forces and moment, as described in Equation (2). The parameters inside the expression are the ones that need to be identified.

By applying the SVM method validated in Section 3, hydrodynamic coefficients in three directions are estimated, and the corresponding model fidelity is examined in detail.

4.2. Disturbance set up

When preparing the training data, more rudder commands are added to cover ship dynamic characteristics. Figure 3 shows the excitation signal distribution in the simulation period.

The bias $\mathbf{w}_1 \in \mathbb{R}^{3 \times 1}$ and process noise $\mathbf{w}_2 \in \mathbb{R}^{3 \times 1}$ are defined according to the rule proposed by Sutulo and Soares (2014):

$$w_i = \max(\varphi_i)k_0k_i\zeta \quad (14)$$

Table 2. Disturbance/noise level set up.

Noise level (NL)	k_0
NL0	0%
NL1	5%
NL2	10%
NL3	20%

where ζ is the discrete zero-mean Gaussian white noise process. φ is the primary clean reference. $\max(\varphi_i)$ refers to the maximum absolute value of the clean response and it scales the noise signal to the origin response. k is a response specific reduction factor, which is set to be 0.05 for rudder angle response, 0.2 for the surge velocity, and 1.0 for other remaining responses. k_0 is the general reduction factor used to label the noisy extent, which is assumed to be 5%, 10%, and 20% as listed in Table 2.

4.3. Identification results under disturbance

To investigate the effect of disturbance level on the identification results, a group of experiments is designed as listed in Table 3. The disturbance bias level is set varying from NL1 to NL3, while the process noise level is set constant at NL1. To eliminate the outliers in the random process, each experiment case is executed one hundred trials. The Savitzky–Golay filter is applied to preprocess and smooth the training data.

One trial of the disturbed accelerations in surge, sway, and yaw directions are presented in Figure 4. This example shows that the disturbance level in general has a more obvious consequence on the surge acceleration than on the sway and yaw directions. It is not unreasonable that the coupling between sway and yaw direction decreases the perturbation effects to some extent.

After the training datasets are prepared after hundreds of trials, the SVM algorithm is applied to train the regressor for the 3-DOF dynamic model. The identified parameters are found normally distributed and thus the average is chosen as the general solution. By

Table 3. Experiment case set up.

Case	Disturbance bias	Process noise
1	NL1	NL1
2	NL2	NL1
3	NL3	NL1

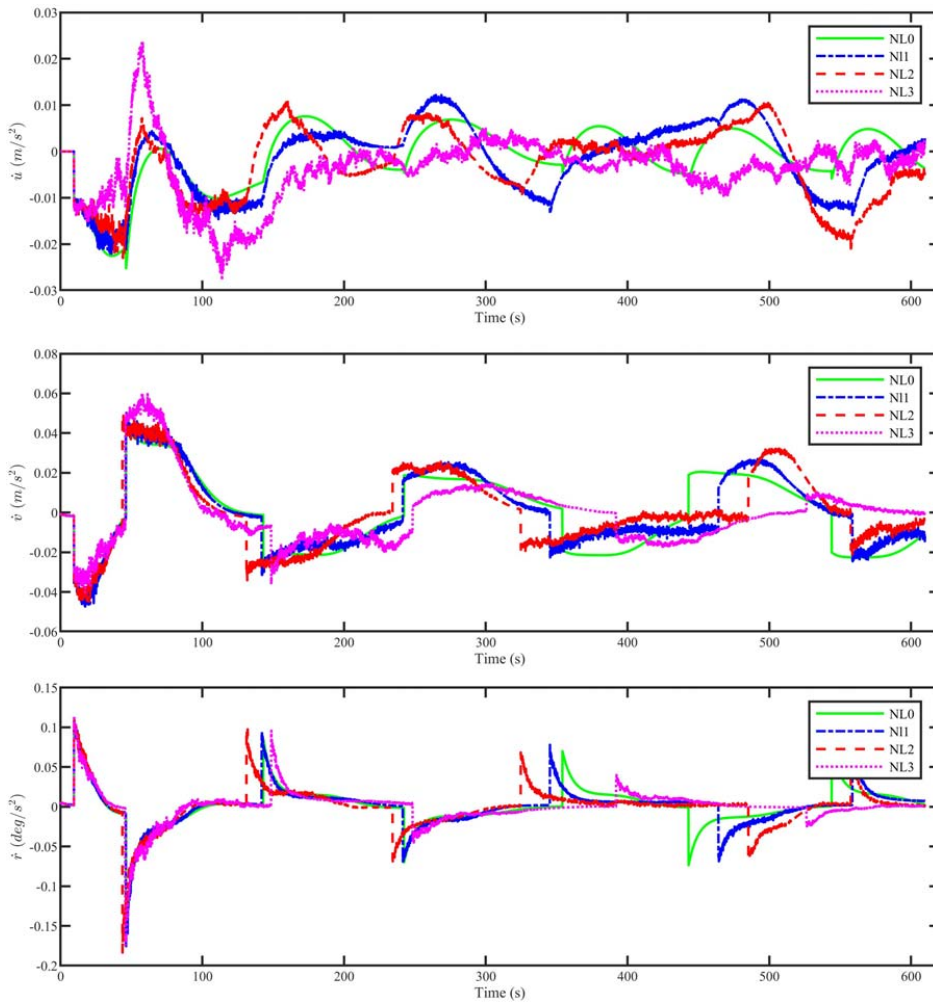


Figure 4. The disturbed accelerations in surge, sway, and yaw directions at different disturbance levels. (This figure is available in colour online.)

substituting those results into Equation (2), the identified models at different disturbance levels are then obtained.

Normally, the extensively trained SVM results are able to reproduce the training trajectory, therefore, a more critical evaluation of the model fidelity is that it should be capable of predicting other manoeuvres that the SVM has not been trained on. An 18° turning circle operation is then undertaken to examine its generalisation performance. The comparison between the SVM predictions and origin model reference in 3-DOF velocities, heading angle, and ship trajectory are shown in Figure 5. It can be seen that the model identified under disturbance and process noise could basically capture the ship's dynamic properties and generate a relative accurate response. The prediction errors at NL1 and NL2 are considered allowable. Generally, the deviation gets larger when the disturbance level is higher. Note that at the same disturbance level NL1, the deviation of surge speed is more obvious than that of sway and yaw speed, which is implied by the results from Figure 4.

To quantitatively measure the prediction errors, the manoeuvring characteristics for turning circles are calculated and listed in Table 4. The table shows that the predicted maneuver properties at different disturbance levels have various deviations from the model reference. More concretely, at NL1 and NL2, the discrepancies are almost lower than 10%, while at NL3, the errors are around 20%. It reveals that when the ship is exposed to gentle and moderate environments, the identified model is able to keep its key characteristics and its predictive capability could be considered acceptable. Although relatively obvious dispersions at NL3 scenario is observed, it could still indicate a potential path in the short future. These results reveal that the SVM-based approach could realise parameter identification in disturbed environment to a certain accuracy, which practically extends the applicable scope in kinds of scenarios.

Due to the correlation between the SVM input features, the parameter estimations may show a large dispersion from their experimental values. However, the model, as a whole, can still be able

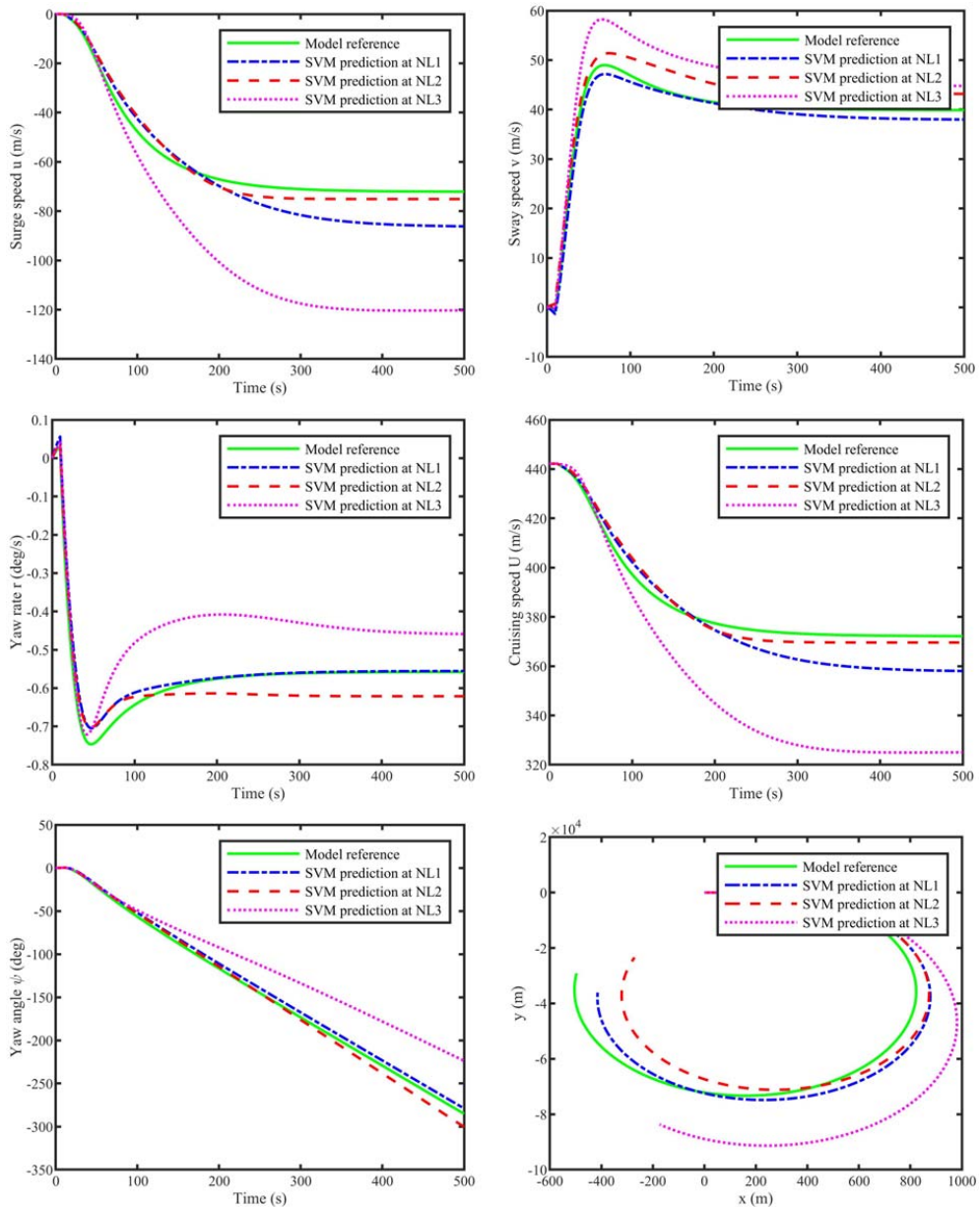


Figure 5. The SVM predictions at different disturbance levels compared with model reference of 18° turning circle. (This figure is available in colour online.)

Table 4. Manoeuvring characteristics comparison between SVM predictions and model reference.

Manoeuvring characteristics	Model reference	SVM_NL1		SVM_NL2		SVM_NL3	
	Value (m)	Value (m)	Deviation (%)	Value (m)	Deviation (%)	Value (m)	Deviation (%)
Steady turning radius	667	644	3.5	595	10.8	707	6.0
Maximum transfer	1279	1306	2.1	1242	2.9	1594	24.6
Maximum advance	746	801	7.4	796	6.7	905	21.3
Transfer at 90 (deg) heading	546	578	5.9	557	2.0	694	27.1
Advance at 90 (deg) heading	742	796	7.3	791	6.6	895	20.6
Tactical diameter at 180 (deg) heading	1275	1302	2.1	1237	3.0	1586	24.4

to predict new maneuver behaviour with different fidelities, even if the parameters cannot be assigned a physical interpretation. The generalisation capability of the identified model presented above is found evidence for this argument.

5. Conclusions

In this paper, an SVM-based parameter identification procedure is presented, which is applied to the scenario where ship manoeuvres in stochastic environments. The work focuses on the investigation of identification performance, as well as the model fidelity under different levels of perturbations. By taking multiple zigzag manoeuvres data in the MSS simulator, the SVM is well trained to get all hydrodynamic coefficients, linear and nonlinear, in a 3-DOF Abkowitz model. Satisfactory estimation results are achieved in the clean system, showing its approachability in marine domain. The method is then extended to incorporate stochastic process to the model plant to simulate real environment effects. Estimation results show that the fidelity is decreasing with respect to the interference levels. Models with prediction errors of the magnitude could be considered usable in 5% and 10% disturbance. Although the model dispersion is obvious under 20% perturbation, the intuitive predictions is still encouraging in which we could bring support to the operation decision system.

The main advantages of using the SVM identification method are the possible robustness to noise by tuning the penalty factor and width of the insensitive tube, so that being able to achieve better generalisation compared to traditional neural networks. Meanwhile, it offers an inspection of specific parameters associated with the vessel other than a grouped black-box model. Even if its strengths are obvious, its performance on a heavily polluted system is still limited. In addition, this approach is now validated on constant parameters, and it cannot be applied to time-varying coefficients. This drawback limits the on-line identifications that are always encountered in real life. For instance, for the operations that cause a large angular displacement of a vessel, such as takeoff and landing of autonomous aerial vehicles and helicopters, crane operations, and so on, the ship responses are changing associated with the operation status. Such cases push further research on time-varying parameter identification, which will be included in the future study. Furthermore, the presented identification procedure will be implemented in real-life sea trials to verify its adaptability in realistic scenarios. Efforts will also be paid to refine the SVM approach to improve the identification accuracy in strong environments.

Disclosure statement

No potential conflict of interest was reported by the author(s).

Funding

This work is in part supported by the MAROFF KPN project 'Digital Twins for Vessel Life Cycle Service' (Project no.: 280703), and in part support by the

IKTPLUS project 'Remote Control Centre for Autonomous Ship Support' (Project no. 309323) from Research Council of Norway.

ORCID

Tongtong Wang  <http://orcid.org/0000-0002-7774-1363>

Guoyuan Li  <http://orcid.org/0000-0001-7553-0899>

Baiheng Wu  <http://orcid.org/0000-0002-1824-6784>

Houxiang Zhang  <http://orcid.org/0000-0003-0122-0964>

References

- Åström KJ, Källström CG. 1976. Identification of ship steering dynamics. *Automatica (Oxf)*. 12(1):9–22.
- Chen H, Li Q, Wang Z. 2018, July. Improved maximum likelihood method for ship parameter identification. In 2018 37th Chinese Control Conference (CCC), Wuhan, China. 1614–1621. IEEE.
- Cheng X, Li G, Skulstad R, Major P, Chen S, Hildre HP, Zhang H. 2019. Data-driven uncertainty and sensitivity analysis for ship motion modeling in offshore operations. *Ocean Eng*. 179:261–272.
- Chislett MS, Strom-Tejsten J. 1965. Planar motion mechanism tests and full-scale steering and manoeuvring predictions for a mariner class vessel. *Int Shipbuilding Progress*. 12(129):201–224.
- Ding F. 2014. Combined state and least squares parameter estimation algorithms for dynamic systems. *Appl Math Model*. 38(1):403–412.
- Fossen TI. 2011. Handbook of marine craft hydrodynamics and motion control. Wiley. <https://onlinelibrary.wiley.com/doi/book/10.1002/9781119994138>
- Hou XR, Zou ZJ. 2016. Parameter identification of nonlinear roll motion equation for floating structures in irregular waves. *Appl Ocean Res*. 55:66–75.
- Li G, Skogeng PB, Deng Y, Hatledal LI, Zhang H. 2016, April. Towards a virtual prototyping framework for ship maneuvering in offshore operations. In OCEANS 2016-Shanghai. 1–6. IEEE.
- Luo WL, Zou ZJ. 2009. Parametric identification of ship maneuvering models by using support vector machines. *J Ship Res*. 53(1):19–30.
- Martelli M, Villa D, Viviani M, Donnarumma S, Figari M. 2021. The use of computational fluid dynamic technique in ship control design. *Ships Offsh Struct*. 16(1):31–45.
- Perera LP, Oliveira P, Guedes Soares C. 2015. System identification of nonlinear vessel steering. *J Offshore Mech Arct Eng*. 137(3):031302-1–031302-7.
- Perez T, Smogeli ØN, Fossen TI, Sørensen AJ. 2006. An overview of the marine systems simulator (MSS): a simulink toolbox for marine control systems. *Model Identif Control: Norwegian Res Bull*. 27(4):259–275.
- Rajesh G, Bhattacharyya SK. 2008. System identification for nonlinear maneuvering of large tankers using artificial neural network. *Appl Ocean Res*. 30(4):256–263.
- Selvam RP, Bhattacharyya SK. 2010. System identification of coupled heave-pitch motion of ships with forward speed in random ocean waves. *Ships Offsh Struct*. 5(1):33–49.
- Skjetne R, Smogeli ØN, Fossen TI. 2004. A nonlinear ship manoeuvring model: identification and adaptive control with experiments for a model ship. *Model Identif Control: Norwegian Res Bull*. 25(1):3–27.
- Sutulo S, Soares CG. 2014. An algorithm for offline identification of ship manoeuvring mathematical models from free-running tests. *Ocean Eng*. 79:10–25.
- Vapnik VN. 1999. An overview of statistical learning theory. *IEEE Trans Neural Netw*. 10(5):988–999.
- Wang Z, Zou Z, Soares CG. 2019. Identification of ship manoeuvring motion based on nu-support vector machine. *Ocean Eng*. 183:270–281.
- Xue Y, Liu Y, Ji C, Xue G. 2020. Hydrodynamic parameter identification for ship manoeuvring mathematical models using a Bayesian approach. *Ocean Eng*. 195:106612.
- Zhang XG, Zou ZJ. 2011. Identification of Abkowitz model for ship manoeuvring motion using ϵ -support vector regression. *J Hydrodyn*. 23(3):353–360.
- Zheng J, Meng F, Li Y. 2018. Design and experimental testing of a free-running ship motion control platform. *IEEE Access*. 6:4690–4696.



Paper III

This paper is not included due to copyright restrictions
available in IEEE Transactions on Industrial Informatics 2021 ;Volum 18.(3) s.
1781-1789 <https://doi.org/10.1109/Tii.2021.3088404>
and institusjonsarkiv: <https://hdl.handle.net/11250/2825522>

D

Paper IV

Effect of Ship Propulsion Retrofit on Maneuverability Research Based on Co-simulation ^{*}

Tongtong Wang¹[0000-0002-7774-1363], Lars Ivar Hatledal²[0000-0001-6436-7213],
Motoyasu Kanazawa¹[0000-0002-9405-2076], Guoyuan Li¹[0000-0001-7553-0899],
and Houxiang Zhang¹[0000-0003-0122-0964]

¹ Department of Ocean Operations and Civil Engineering,
Faculty of Engineering,

{[tongtong.wang](mailto:tongtong.wang@ntnu.no), [motoyasu.kanazawa](mailto:motoyasu.kanazawa@ntnu.no), [guoyuan.li](mailto:guoyuan.li@ntnu.no), [honzhang](mailto:honzhang@ntnu.no)}@ntnu.no

² Department of ICT and Natural Sciences,

Faculty of Information Technology and Electrical Engineering,

laht@ntnu.no

Norwegian University of Science and Technology (NTNU), Aalesund, Norway.

Abstract. Shipping has been dominating the transportation industry in worldwide trade. During the service life of a vessel, conversions in mid-life often occur for economic or technical purposes. By replacing expired components or updating the outdated technology to the latest operational standards, the service life could be greatly prolonged, and meanwhile the capability will be enhanced. Bringing ships-in-service to the latest technology creates the need for advanced methods and tools to simulate the ship main and auxiliary systems. Co-simulation is emerging as a promising technique in complex marine system modeling. The Functional Mock-up Interface (FMI) standard enables sub-models representing part of the vessel to be executed individually or as an integrated part of the overall system. The modularity and re-usability of the sub-models speed up the simulation cycle and ensure time-cost effectiveness, which benefits the ship conversion. This paper presents a research related to the ship propulsion retrofit process based on the co-simulation technique. The ship maneuverability before and after refitting propulsion units is simulated and analyzed. Through the experiments, propulsion performance improvements are observed. Eventually, the study supports that the co-simulation technique to be applied in the maritime field has an encouraging future.

Keywords: Propulsion retrofit · Ship maneuverability · Co-simulation.

^{*} This work was supported by a grant from the Research Council of Norway through the Knowledge-Building Project for industry "Digital Twins for Vessel Life Cycle Service" (Project no: 270803), and a grant from the IKTPLUSS Project "Remote Control Centre for Autonomous Ship Support" (Project no. 309323).

1 Introduction

Shipping, as a relatively energy-efficient, environmental-friendly, and sustainable model of mass transport, is the dominant transportation method for world-wide trade. Normally, the life cycle of a ship is estimated to be around 25 years, but the actual age of the short sea fleet, for example, is higher, reaching more than 30 - 35 years of age for perhaps as much as 40% of the fleet [9]. However, the life cycle of ship systems and major components is much shorter because of the ever faster technological developments. In general, 10-15 years after launching a ship, its main systems are outdated. Upgrading outdated technology in ships to the latest operational standards enhances the capability and prolongs the service life [13]. Furthermore, the international policies fostering the reduction of energy consumption and emissions are always issuing new regulations on energy efficiency and emission reduction [3]. For example, the International Maritime Organization (IMO) has implemented a stricter sulfur content limit—called the IMO 2020 sulfur cap—aiming at improve air quality and protect the environment. Further, IMO has initiated an extensive strategy of the energy efficiency existing ship index for existing ships, which indicate that the energy efficiency of ships should be satisfied during the operation phase. To comply with the new regulations, green technologies are implemented on-board ships [10]. Retrofitting the ships during the operation phase has become a popular choice for the transportation industry [15]. It is possible to upgrade the installed technology with new high-performance machines and significantly improve the system’s handling, economic efficiency, as well as emission reduction [8].

Given that modern ships are becoming more complex and integrated, retrofitting them is a complex and intricate engineering task. Optimal performance is relying on all subsystems to work optimally, both individually and aggregated [11][14]. Each subsystem is dedicated to a specific object of the vessel or equipment. Between distributed components, they exchange all relevant ship information, data, or analysis and make coordinated operational decisions. Considering the mutual and multi-disciplinary interaction between subsystems, co-simulation is emerging as a promising technique. Often, it is difficult to describe a truly complex system in a single tool. Instead, people are encouraged to develop models at the partial solution level, such as the dynamic properties check, control strategy design, or energy consumption optimization. It not only dramatically lessens the modeling pressure and promotes efficiency but enables the re-usability of different elements. Furthermore, a branch of components may be generated by different teams or suppliers, each in its own domain and each with its own tools. Using co-simulation, these models can be integrated as black-boxes without revealing the intellectual property of the owner [2]. In addition, considering now the demanding operation of an autonomous vessel, it is better to test ahead in a virtual environment for safety reasons. Co-simulation reduces efforts to conduct pre-training or perform tests by redirecting design attention and reusing the sub-system models. From an efficiency point of view, co-simulation greatly facilitates the ship retrofitting process. In a co-simulation, different subsystems are modeled separately and composed into a global simulation, where each model is



Fig. 1. Side view of the research vessel Gunnerus.

executed independently, sharing information at discrete time points. The Functional Mock-up Interface (FMI) standard is a commonly used standard for co-simulation, and model implementing the FMI is known as a Functional Mock-up Unit (FMU). The FMI enables an FMU exported by one tool to interoperate with a variety of host tools and for host tools to orchestrate interactions between FMUs exported by a variety of other tools [1]. A system can then be modelled as a collection of interconnected FMUs. Co-simulation thus enables retrofit decisions to be simulated ahead-of-time, cheaply and early in the process.

This study presents the propulsion retrofit process using the co-simulation technique, and the dynamic properties of the retrofitted devices are analyzed and discussed. The research vessel Gunnerus (see Fig. 1), owned and operated by the Norwegian University of Science and Technology (NTNU) serves as the test ship. The simulation fidelity was verified against real ship maneuver in [7] in terms of ship speed, course, and power consumption. Convinced by the high-fidelity resolution of the simulation, further research is conducted with more confidence. As reported in [16], The R/V Gunnrus went through a thruster refit in 2015. The original twin fixed-pitch ducted propellers and rudders were replaced with the Permanent Magnet (PM) rim-drive azimuthing thrusters. The original propellers were 5-bladed, high skew type with a diameter of 2.0 meters that rotated in a 19A type duct profile, and the new azimuthing thrusters incorporate a ring propeller in a tailor-made duct with a diameter of 1.9 meter with four blades having a forward skewed shape. Fig. 2 shows the propulsion configuration on Gunnerus before and after retrofit, where the left is the origin pitch propeller with ice-fins, and the right is the refitted azimuth thruster provided by Rolls-Royce. The same diesel-electric system supplied the propulsion and maneuvering power before and after the conversion. To document the effect of the change of propulsion



Fig. 2. The propulsion arrangement before and after retrofit.

system, a simulation test is carried out both before and after retrofiting the PM azimuthing thruster in this work. The ship maneuvering capabilities are then verified.

2 Problem Formulation

Thanks to the modularity and flexibility of co-simulation, the effort required to simulate the dynamic properties of the propulsion unit is greatly decreased. In this section, the ship maneuverability and the co-simulation diagram, as well as the FMUs used in this research will be explained.

2.1 Ship Maneuverability

Ship maneuverability is defined as the capability of the craft to carry out specific maneuvers. A maneuvering characteristic can be obtained by changing or keeping a predefined course and speed of the ship in a systematic manner by means of active controls. For most of the surface vessels, these controls are implemented by rudders, propellers and thrusters. The IMO approved standards for ship maneuverability, and the standards specify the type of standard maneuvers and associated criteria. It is always necessary for the vessels to apply these standards, and even some port and flag states adopted some of the IMO standards as their national requirements. To help the vessel prepare for implementation of the standards, prediction of the maneuverability performance in the design stage enables a designer to take appropriate measures in good time to achieve requirements. The prediction could be carried out by using existing data, scaled model test, or numerical simulation [12]. From the practical view, numerical simulation appears an effort-efficient way. Therefore, the ship maneuvering capabilities will be the main concern during simulation experiments.

To examine the course keeping capability of the ship, usually, the turning circle and Kempf's zigzag maneuver are selected. The maneuvers and their characteristics are described as Fig. 3 and Table. 1-2:

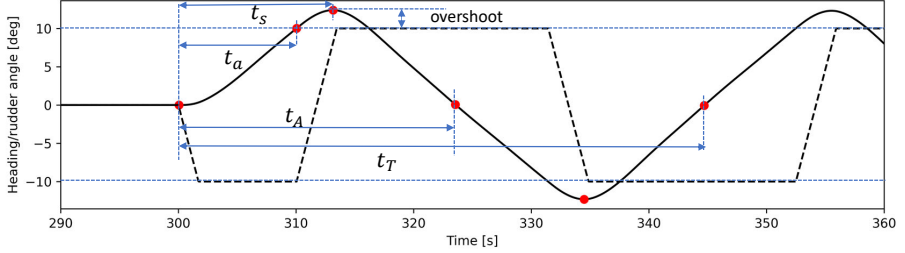


Fig. 3. Schematic of zigzag maneuver and its main characteristics.

Table 1. Zigzag maneuver characteristics.

Characteristic	Reference
Initial turning time t_a	The time from the rudder execution until the heading changes a desired degrees, 10° off the initial course in $10^\circ/10^\circ$ example.
Time to check yaw t_s	The time from the rudder execution until the maximum heading changes.
Reach time t_A	The time between the first rudder execution and the instance when the ship's heading is zero.
Complete time t_T	The time between the first rudder execution and the instance when the ship's heading is zero after third execution.
Overshoot angle	The angle through which the ship continues to turn in the original direction after execution of counter rudder.

2.2 Co-simulation Setup

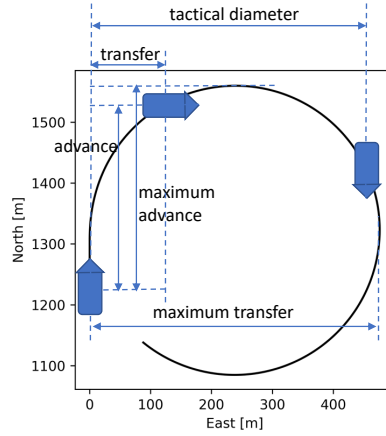
The ship maneuvering simulation is set up as Fig. 4 shows. Each block represents an FMU of which the input and output variables are declared. The experiment is performed in Vico, a generic co-simulation framework based on the Entity-Component-System software architecture that supports the FMI as well as the System Structure and Parameterization (SSP) standards [5]. The user may manipulate the wind, waves, and ocean currents to mimic environmental conditions. An overview of FMUs applied in the maneuvering simulation is presented. All the FMUs, except the *VesselModel* and *PMAzimuth*, are developed by the authors using PythonFMU [6].

1. VesselModel

The vessel model reflects the vessel's hydrodynamic properties, such as the

Table 2. Turning circle maneuver and its main characteristics.

Characteristic	Unit
Steady turning radius	m
Transfer at 90 deg heading	m
Advance at 90 deg heading	m
Maximum Transfer	m
Maximum Advance	m
Tactical diameter at 180 deg heading	m



mass, resistance, and cross-flow drag, as well as restoring forces. It is a 6 degree of freedom (DOF) time-domain simulation model developed by MAR-INTEK's vessel simulator (VeSim) [4]. Summing all the external forces acting on the ship, the dynamic equations of vessel motions are then solved. It can be implemented in sea-keeping and maneuvering problems for marine vessels subjected to waves, wind, and currents based on a unified nonlinear model Eq. 1.

$$(M_{RB} + M_A)\dot{\nu} + C(\nu)\nu + D(\nu) + g(\eta) + \int_0^t h(t - \tau)\nu(\tau) d\tau = q \quad (1)$$

where the 6DOF ship velocity state is expressed as the vector $\nu = [u, v, w, p, q, r]'$ referred to the coordinate shown in Fig. 5. The $[u, v, w]$ are the linear velocity along x_b, y_b, z_b directions, and $[p, q, r]$ are the angular velocities rotating around three directions. $M_{RB} \in \mathbb{R}^{6 \times 6}$ is the rigid body mass, and $M_A \in \mathbb{R}^{6 \times 6}$ is the added mass. $C(\nu) = C_{RB}(\nu) + C_A(\nu) \in \mathbb{R}^{6 \times 6} \times \mathbb{R}^6$ is describing the generalized coriolis-centripetal forces. $D(\nu) \in \mathbb{R}^{6 \times 6} \times \mathbb{R}^6$ is a vector of damping forces and moments. $g(\eta) \in \mathbb{R}^6$ is a vector of gravitational/buoyancy forces and moments. And $h(\tau)$ refers to impulse response functions calculated by SINTEF OCEAN's potential theory. $q \in \mathbb{R}^6$ is the external forces and moments acting on the ship. The model itself is fully coupled and it can be used for simulation and prediction of coupled vehicle motion.

2. PID controller

The PID controller is created to generate shaft speed and rudder angle commands according to Eq. 2. In the control law, the $k_{\{\cdot\}}$ is the parameter enabling tuning, and the predefined approach speed u_d as well as the ship heading ψ_d are issued by the *ZigzagController*.

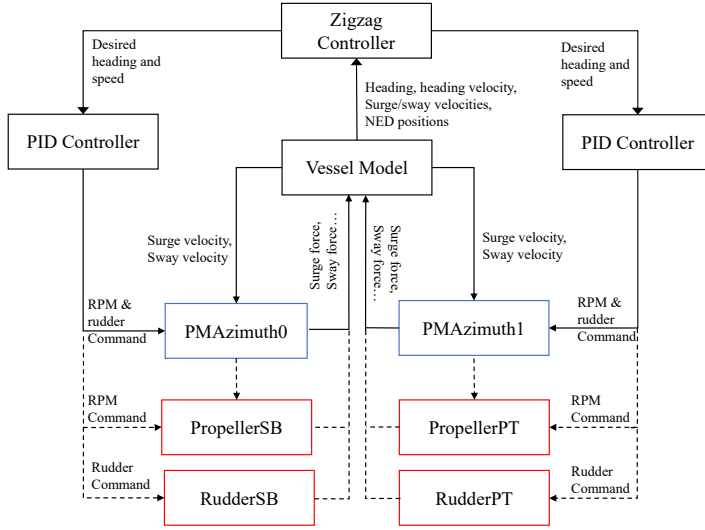


Fig. 4. Diagram showing the relationship of the engaged ship components.

$$\begin{aligned}
 RPM &= k_{pu}(u - u_d) + k_{iu} \int_0^t (u - u_d)dt + k_{du} \frac{d}{dt}(u - u_d) \\
 \delta &= k_{ppsi}(\psi - \psi_d) + k_{ipsi} \int_0^t (\psi - \psi_d)dt + k_{dpsi} \frac{d}{dt}(\psi - \psi_d)
 \end{aligned} \tag{2}$$

3. Zigzag controller

It is a logistic solver without numerical computation. Given the current ship speed and heading, it can tell to which side the rudder should turn and deliver the command saturation to the connected *PID controller*.

4. PMAzimuth

It is a hydrodynamic model of the azimuth thruster without actuator, implemented by the manufacturer Kongsberg Maritime using VeSim. Feeding a specific RPM and angle command, vessel speed, as well as the loss factor into the model, it produces a 3DOF force on heave, surge, and sway directions.

5. Propeller

Both the propeller and rudder are generic models parametrized to R/V Gunnerus. The surge force related to the propeller is calculated with:

$$\tau_p = f(n, u) \tag{3}$$

where n is the propeller shaft speed (r/min), and u is the vessel's surge velocity. Note that the sway force and yaw moment due to propeller are neglected as they have smaller magnitudes compared to those of hull and rudder components.

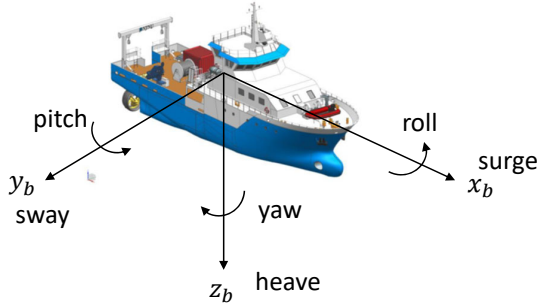


Fig. 5. The ship body coordinate and motion in 6DOF.

6. Rudder

The rudder is modelled according to [17]. It can be expressed as:

$$\tau_r = g(u, v, r, n, \delta, \theta) \quad (4)$$

where u, v, r are the velocities in surge, sway, and yaw directions respectively. And δ is the rudder angle. θ refers to the hull-rudder interaction coefficients.

3 Experiment Results

Experiments are implemented with the designed co-simulation diagram in Vico. The detailed experimental scenarios and the corresponding ship maneuverability, with either pitch propeller or PMAzimuth thruster installed, are presented in this section.

3.1 Simulation Scenarios

Ship maneuvering experiments with a different set of propulsion units are implemented. It is also worth noticing that the ship maneuverability could be affected by water depth, environmental forces, ship speed and hydrodynamic derivatives. To ensure the results comparable, identical settings except only the propulsion units are employed. The ship is assuming cruising on calm and deep water without external environmental disturbances. Eight maneuver test scenarios are defined as Table. 3 shows, aiming to investigate the propulsion performance under different execution angles and speeds.

A $10^\circ - 10^\circ$ zigzag test means that the rudder and azimuth angles are given a command of $\pm 10^\circ$, and when the ship heading change reaches 10° the rudder/azimuth reverse to the opposite side. The 10° in turning circle refers to the constant rudder/azimuth angle. As a key parameter, the ship surge speed is given as the steady velocity before the zig-zag/turning circle maneuvers are initiated. During the process, 300 seconds are saved first to warm up and drive the ship to the pre-defined speed, and 300 seconds are arranged for operations. The simulation time step is set to 0.05s.

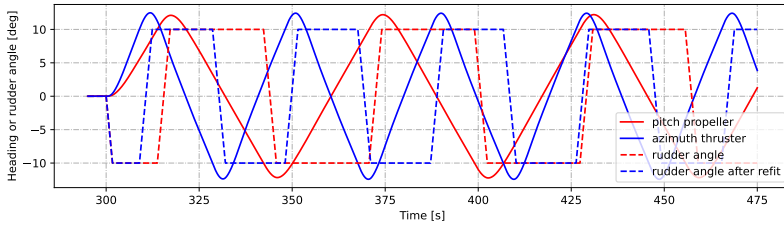
3.2 Results Analysis

In this section, the main maneuver characteristics of the ship before and after conversion will be observed and discussed.

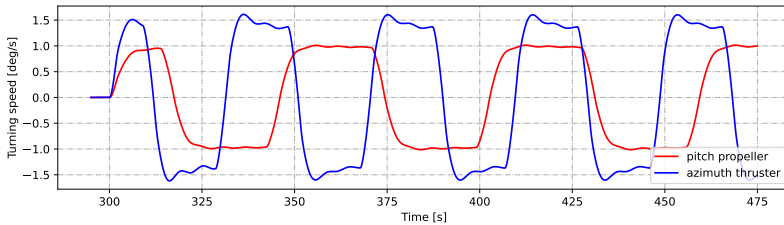
Zigzag Maneuver Zigzag trajectories for the ship using both the pitch propellers and azimuth thrusters are simulated. Three selected test results are presented and compared in Fig. 6-8. Naturally, differences in turning velocities are observed from these figures. A more noticeable yaw velocity distinction between the pitch propeller and azimuth arises during 10° turn command. The statistic results are summarized in Table. 4. It could be observed that the measured key time parameters in the azimuth group are effectively decreased. This conclusion

Table 3. Maneuver experiment cases implemented in Vico.

Maneuver	Execution	Speed
Zig-zag	10° – 10°	low
		high
	20° – 20°	low
		high
Turning circle	10°	low
		high
	20°	low
		high

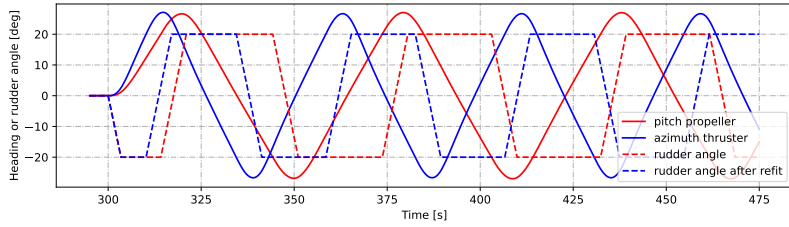


(a) 10°/10° zigzag ship heading and command angle at higher speed.

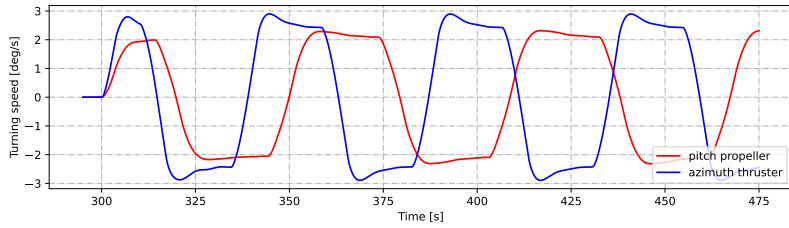


(b) Ship turning velocities under propeller or azimuth actuation.

Fig. 6. 10°/10° zigzag properties at higher speed.

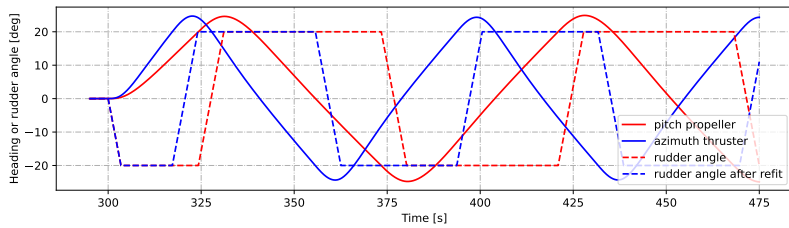


(a) $20^\circ/20^\circ$ zigzag ship heading and command angle at higher speed.

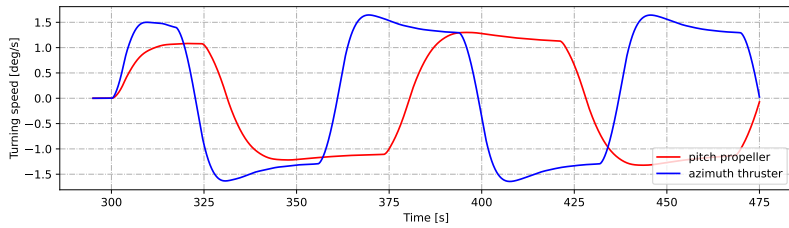


(b) Ship turning velocities under propeller or azimuth actuation.

Fig. 7. $20^\circ/20^\circ$ zigzag properties at higher speed.



(a) $20^\circ/20^\circ$ zigzag ship heading and command angle at lower speed.



(b) Ship turning velocities under propeller or azimuth actuation.

Fig. 8. $20^\circ/20^\circ$ zigzag properties at lower speed.

Table 4. The zigzag characteristics for the ship before and after propulsion unit retrofit.

Characteristics		10°/10°			10°/10°			20°/20°			20°/20°		
		pr	azi	gain[%]	pr	azi	gain[%]	pr	azi	gain[%]	pr	azi	gain[%]
Approach speed	[m/s]	4.7	4.78	-	2.4	2.5	-	4.7	4.73	-	2.45	2.47	-
t_a	[s]	13.7	8.9	35	24.25	15.6	35.7	8.95	6.45	27.9	14.9	10.4	30.2
t_s	[s]	3.6	2.9	19.4	5	3.6	28	10.8	8.25	23.6	16.3	12.2	25.2
t_A	[s]	31.9	21.3	33.2	54.4	35.25	35.2	34.5	26.25	23.9	55.6	40.7	26.8
t_T	[s]	60.3	40.75	32.4	103.2	67	35.1	64.15	50.3	21.6	103.8	78.75	24.1
First overshoot angle	[°]	2.17	2.37	-9.2	1.57	1.6	-1.9	6.64	6.7	-0.9	4.6	4.7	-2.1
Second overshoot angle	[°]	2.2	2.42	-10	1.58	1.61	-1.9	6.87	6.68	2.8	4.8	4.36	9.2
Average overshoot angle	[°]	2.2	2.42	-10	1.576	1.6	-1.5	7.01	6.7	4.4	4.92	4.35	11.6

reveals that the ship with azimuth installed reaches the desired course within a shorter time, and it responds more quickly to the given command.

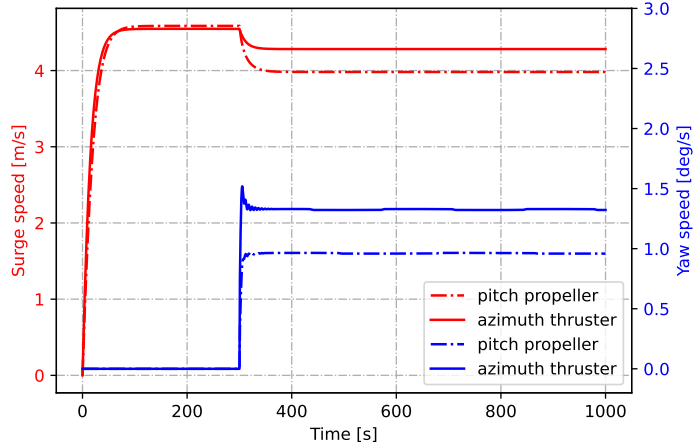
Meanwhile, it is observed in Fig. 6 that the rudder rate of both systems are similar, as they reverse from port-side to starboard in a similar amount of time. Although it takes longer time for the ship using conventional rudders to drive itself to the target course, it does not necessarily generate a larger overshoot angle. Instead, their average overshoot angles are related to the execution command and maneuver speed as indicated in Table. 4. If a smaller angle command is given to the azimuth, it would even lead to a slightly larger average overshoot angle compared to the conventional rudder, even with a lower or higher forward speed. With an increasing angle command, the azimuth thrusters are observed to perform outstandingly.

Turning Circle The turning circle maneuver experiments are conducted under the resembling co-simulation structure (Fig. 4) but replacing the *Zigzag controller* with *Turning controller*. The execution angle and speed are distinguished into two categories: 10° and 20°, higher and lower approach speed, respectively.

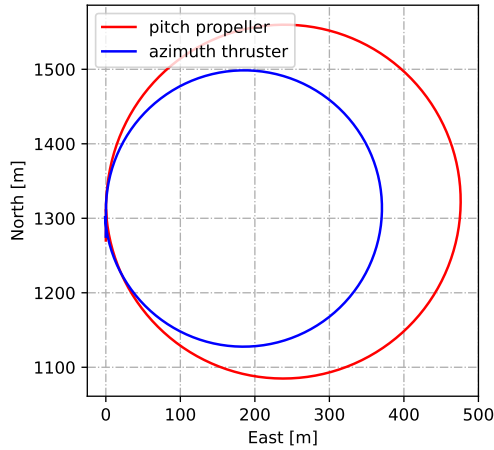
The statistical maneuver results are presented in Table. 5. Among the four cases, two of them are selected to visualize the differences (See Fig. 9-10). The ship equipped with either the conventional pitch propellers and rudders, or azimuths, are approaching at similar speeds before execution. From Fig. 9a, a drop of surge speed is observed when the rudder is instantiated, and the drop of pitch

Table 5. The turning characteristics for the ship before and after propulsion unit retrofit.

Characteristics		10°			10°			20°			20°		
		pr	azi	gain [%]	pr	azi	gain [%]	pr	azi	gain [%]	pr	azi	gain [%]
Approach speed	[m/s]	4.7	4.8	-	2.4	2.5	-	4.7	4.7	-	2.4	2.5	-
Steady turning radius	[m]	237.5	185.5	21.9	237.8	186.3	21.6	90.4	91.3	-1	93.2	92.9	0.32
Maximum transfer	[m]	476.2	370.6	22.2	476.4	371.9	21.9	190.7	184.8	3.1	195.1	187.7	3.8
Maximum advance	[m]	266.7	200.5	24.8	265.5	200.3	24.5	127.8	108.9	14.8	128.3	109.6	14.6
Transfer	[m]	227.5	173.7	23.6	227.2	173.9	23.4	88.1	82.2	6.7	88.8	82.5	7.1
Advance	[m]	266.4	200.1	24.9	265.2	199.9	24.6	127	108.1	14.9	127.4	108.7	14.7
Tactical diameter	[m]	475.9	370.2	22.2	476.1	371.5	22.0	189.96	184.1	3.1	194.2	186.9	3.8



(a) The ship's surge and yaw speed when circling at 10° with a fast speed.

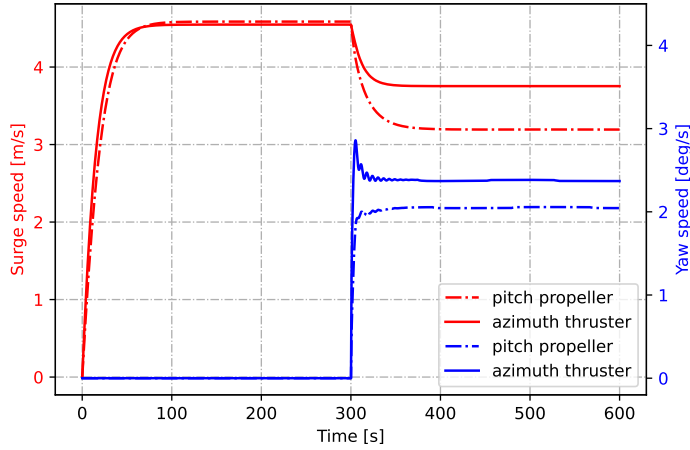


(b) Comparison of propeller and azimuth actuated ship trajectories.

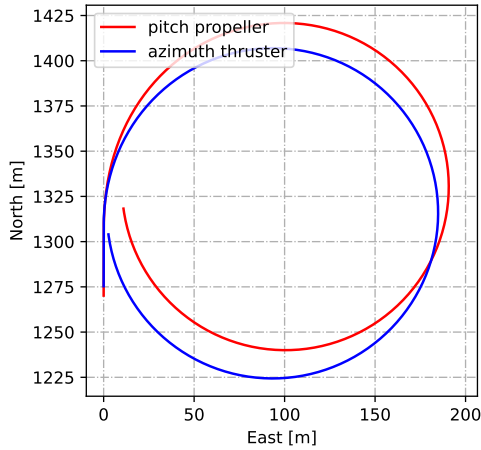
Fig. 9. 10° turning circle properties at higher speed.

propeller is more obvious compared to that of the azimuth. Meanwhile, a larger turning velocity is offered by the azimuth. The out-performance in response velocities is expected to lead to a narrowed turning radius which is verified in Fig. 9b.

Moreover, the statistical results show that the angle command affects the propulsion performance more than the approach speed. Comparing Fig. 9 and Fig. 10, the ship exhibits similar speeds before operation. However, the percent-



(a) The ship’s surge and yaw speed when circling at 20° with a fast speed.



(b) Comparison of propeller and azimuth actuated ship trajectories.

Fig. 10. 20° turning circle properties at higher speed.

age of decreased surge velocity with 20° rudder angle is higher than that with 10° counter angle. For the azimuth thruster, it drops about 6% in 10° and 19% in 20°. For the propeller, the values are 15% and 32%. When the rudder angle is given 20°, it not necessarily generates a large turning radius, as the propulsion moments could produce a higher yaw rate compared to 10°. This finding leads to a compromise in overall turning performance. Therefore, it is understandable

that the steady radius reduction at 20° command is smaller than that of the lower command.

4 Conclusion

The continuously improving knowledge and availability of high-performance machines and drives have created the need for advanced methods and tools to facilitate retrofitting existing ships. Usually, the retrofit is driven by environmental and/or technical reasons, such as to comply with new energy regulations or to upgrade outdated technology. Either way, it is beneficial to ensure fast refitting procedures by allowing easier integration of new components. Co-simulation reduces both the time and the costs of refitting procedures, extending the operative life of a vessel in service. In this research, the authors utilized the co-simulation techniques to model the ship maneuver process before and after propulsion conversion and evaluate the impact of new devices on the ship maneuverability, aiming to support decisions on measures to meet operational standards. By comparing the zigzag and turning circle maneuver characteristics in the present work, an improved course keeping capability is observed after refitting advanced permanent magnet driven azimuth thrusters on the ship. This practice supports that co-simulation enables time cost-effective redesign and fast virtual tests by taking advantage of its modularity and flexibility, and emerges as a promising technology in the maritime industry.

However, it should be clarified that the quality of the simulation model may vary, and the tests conducted in order to compare the maneuvering performance of the two systems, and are not necessarily a good measure of the daily maneuvering capabilities of the vessel. Agreeing with this situation, the experiments performed through co-simulation will be qualitatively informative so that the comparative conclusions drawn upon are credible.

In the present study, only the ship maneuvering performance investigation is within scope, but in many cases, energy consumption is the major concern. Therefore, further research on the energy cost of the ship with different propulsion sets installed will be implemented by taking advantage of co-simulation technology in the future.

References

1. Broman, D., Brooks, C., Greenberg, L., Lee, E.A., Masin, M., Tripakis, S., Wetter, M.: Determinate composition of fmus for co-simulation. In: 2013 Proceedings of the International Conference on Embedded Software (EMSOFT). pp. 1–12. IEEE (2013). <https://doi.org/10.1109/EMSOFT.2013.6658580>
2. Gomes, C., Thule, C., Broman, D., Larsen, P.G., Vangheluwe, H.: Co-simulation: a survey. *ACM Computing Surveys (CSUR)* **51**(3), 1–33 (2018). <https://doi.org/10.1145/3179993>
3. Half, A., Younes, L., Boersma, T.: The likely implications of the new imo standards on the shipping industry. *Energy policy* **126**, 277–286 (2019). <https://doi.org/10.1016/j.enpol.2018.11.033>

4. Hassani, V., Ross, A., Selvik, Ø., Fathi, D., Sprenger, F., Berg, T.E.: Time domain simulation model for research vessel gunnerus. In: International Conference on Offshore Mechanics and Arctic Engineering. vol. 56550, p. V007T06A013. American Society of Mechanical Engineers (2015). <https://doi.org/10.1115/OMAE2015-41786>
5. Hatledal, L.I., Chu, Y., Styve, A., Zhang, H.: Vico: An entity-component-system based co-simulation framework. *Simulation Modelling Practice and Theory* **108**, 102243 (2021). <https://doi.org/10.1016/j.simpat.2020.102243>
6. Hatledal, L.I., Collonval, F., Zhang, H.: Enabling python driven co-simulation models with pythonfmu. In: Proceedings of the 34th International ECMS-Conference on Modelling and Simulation-ECMS 2020. ECMS European Council for Modelling and Simulation (2020). <https://doi.org/10.7148/2020-0235>
7. Hatledal, L.I., Skulstad, R., Li, G., Styve, A., Zhang, H.: Co-simulation as a fundamental technology for twin ships (2020). <https://doi.org/10.4173/mic.2020.4.2>
8. Hou, H., Krajewski, M., Ilter, Y.K., Day, S., Atlar, M., Shi, W.: An experimental investigation of the impact of retrofitting an underwater stern foil on the resistance and motion. *Ocean Engineering* **205**, 107290 (2020). <https://doi.org/10.1016/j.oceaneng.2020.107290>
9. Koenig, P., Nalchajian, D., Hootman, J.: Ship service life and naval force structure. *Naval Engineers Journal* **121**(1), 69–77 (2009). <https://doi.org/10.1111/j.1559-3584.2009.01141.x>
10. Li, K., Wu, M., Gu, X., Yuen, K., Xiao, Y.: Determinants of ship operators' options for compliance with imo 2020. *Transportation Research Part D: Transport and Environment* **86**, 102459 (2020). <https://doi.org/10.1016/j.trd.2020.102459>
11. Ling-Chin, J., Roskilly, A.: Investigating a conventional and retrofit power plant on-board a roll-on/roll-off cargo ship from a sustainability perspective—a life cycle assessment case study. *Energy Conversion and Management* **117**, 305–318 (2016). <https://doi.org/10.1016/j.enconman.2016.03.032>
12. Liu, J., Hekkenberg, R., Rottevel, E., Hopman, H.: Literature review on evaluation and prediction methods of inland vessel manoeuvrability. *Ocean Engineering* **106**, 458–471 (2015). <https://doi.org/10.1016/j.oceaneng.2015.07.021>
13. Liu, L., Yang, D.Y., Frangopol, D.M.: Ship service life extension considering ship condition and remaining design life. *Marine Structures* **78**, 102940 (2021). <https://doi.org/10.1016/j.marstruc.2021.102940>
14. Mauro, F., La Monaca, U., la Monaca, S., Marinò, A., Bucci, V.: Hybrid-electric propulsion for the retrofit of a slow-tourism passenger ship. In: 2020 International Symposium on Power Electronics, Electrical Drives, Automation and Motion (SPEEDAM). pp. 419–424. IEEE (2020). <https://doi.org/10.1109/SPEEDAM48782.2020.9161920>
15. Peri, D.: Robust design optimization for the refit of a cargo ship using real seagoing data. *Ocean Engineering* **123**, 103–115 (2016). <https://doi.org/10.1016/j.oceaneng.2016.06.029>
16. Steen, S., Selvik, Ø., Hassani, V.: Experience with rim-driven azimuthing thrusters on the research ship gunnerus. In: Proc. of High-Performance Marine Vessels (2016)
17. Yasukawa, H., Sakuno, R.: Application of the mmg method for the prediction of steady sailing condition and course stability of a ship under external disturbances. *Journal of Marine Science and Technology* **25**(1), 196–220 (2020). <https://doi.org/10.1007/s00773-019-00641-4>



E

Paper V

This paper is awaiting publication and is not included in NTNU Open

F

Paper VI

Physics-informed Data-driven Approach for Ship Docking Prediction

Tongtong Wang, *Member, IEEE*, Robert Skulstad, Motoyasu Kanazawa,
Guoyuan Li, *Senior Member, IEEE*, Vilmar Æsøy, and Houxiang Zhang, *Senior Member, IEEE*
Department of Ocean Operations and Civil Engineering
Norwegian University of Science and Technology
Postboks 1517, N-6025, Aalesund, Norway
{*tongtong.wang, robert.skulstad, motoyasu.kanazawa, guoyuan.li, vilmar.aesoy, hozh*}@ntnu.no

Abstract—Accurate ship motion predictions play a vital role in supporting the decision-making process onboard. Generally, the ship dynamics are described by either a deterministic model derived from hydrodynamic principles or a black-box model learned from the observations. However, there are always cases in real life where the physics information is insufficient to develop a complete model, and the data quantity is also limited so that a data-driven model is away from expectation. For this obstacle, we propose a physics-data cooperative modeling approach based on a rough ship numerical model and a few operational data to enhance the model quality. The prior knowledge leveraged by the ship’s numerical model is integrated into the neural network as informative inputs, and the informed neural network calibrates the bias between model outcomes and actual states in principle. The proposed approach is validated in the real docking operation of a research vessel. Comparisons with both the purely hydrodynamic model and the data-driven model without physics informed are conducted. The results convinced that the physics-data hybrid way yields a more accurate model with relaxed data requirements and less learning consumption.

Index Terms—a priori knowledge, physics-informed, data-driven, docking, prediction.

I. INTRODUCTION

The maritime industry is undergoing a process of digital transformation with increasingly more data are collected from ship fleets. The development of advanced technologies, such as digital twins and cloud computing, greatly benefits shipping transportation on smart management. Undoubtedly, the continuous monitoring and assessment of ships and the construction of remote control centers advance the autonomous vessels towards a more flexible and intelligent manner of handling demanding ocean operations. As a fundamental technology for the digital twin of autonomous vessels, ship dynamic modeling has always been extensively investigated. Ship modeling is a broad concept that could be achieved by theory-induced hydrodynamic disciplines, system identification techniques, or data-driven algorithms such as machine learning, etc. Either way can provide credible support to the decision-making process onboard if it is capable of predicting ship motion with reasonable errors. While in reality, there are always obstacles to developing a comprehensive model of a ship because of

This work was supported by a grant from the Research Council of Norway through the Knowledge-Building Project for industry “Digital Twins for Vessel Life Cycle Service” (Project no: 270803).



Fig. 1: R/V Gunnerus when docking in Aalesund harbour, Norway.

the nonlinear time-varying dynamics properties of the system. The ship dynamics can vary with the sailing status, such as the trim or loading conditions. Moreover, the ship’s motion is greatly impacted by the ocean environments, which are difficult to accurately model. Therefore, the hydrodynamic-based models are always far from expectations because of their simplifications and deficiencies in precision. Contrary to physics’s discipline-based models, the data-driven ones rely only on observation data. They can reach state-of-the-art accuracy performance if sufficient data is given. However, the data-driven models are often argued for their non-transparency of the underlying process. The model uncertainties or errors are difficult to trace, and concerns may arise when applied in security-related domains. Besides, as the machine learning techniques evolve, the conventional neural networks are expected to go deeper to reach stringent requirements, putting more pressure on the computational cost.

For the cases where too limited data is available to construct a data-driven model, and certain prior knowledge is known but still not enough to get a complete physics-based model, we propose a model-data consolidation approach. The rough ship numerical model preserves and delivers the prior domain knowledge. When they are encoded to the data-driven neural network, improvements in model fidelity and learning efficiency are expected. The rough ship dynamic model, which is constructed on profiles, is credible to a certain extent. But because of the model simplifications and parameter

uncertainties, discrepancies between model estimations and reality always exist. In other words, the rough model partially reflects the existing system. By identifying and leveraging the prior knowledge into a neural network model trained on the ship maneuver data, a hybrid model is delivered. This way, the ship's dynamic quality is enhanced easily and quickly with only limited data. The model-data cooperation approach will be explained, and its effects on improving the ship motion prediction will be investigated in real ship docking operations. Fig. 1 shows the research vessel was approaching the dock in Aalesund harbor, Norway. The major contributions of the work are as follows:

- Proposing a model-data cooperation method based on a rough ship dynamic model and a limited amount of data to derive a representative model for the research vessel.
- The proposed hybrid approach is validated on the real ship docking operations.
- Comparing with the regular data-driven methods, the hybrid way requires fewer data and learning consumption.

The rest of the paper is organized as follows. Related works on ship motion prediction are discussed in Section II. The following Section III presents the proposed physics-data cooperation modeling framework. Detailed explanations of the modeling process are also presented here. The validation experiments on the docking operations of a real ship are conducted in Section IV to validate the efficiency of the proposed method. Meanwhile, the results in comparison with traditional approaches are shown. Conclusion and future work are shown in Section V.

II. RELATED WORK

The booming of artificial intelligence technologies promotes ship modeling into the digital era. Advanced data-driven algorithms are increasingly being applied to simulate autonomous vehicles. As a fundamental technology, the research on estimating ship states has lasted for decades, originating from hydrodynamic properties, classic Kalman filters, or the data analysis point of view. We reviewed recent works on ship motion estimating and predicting using data-driven related approaches.

Generally, the ship dynamic properties can be described in two ways, by deriving deterministic equations or by learning dependencies between input and output variables. The first branch is usually related to data-driven system identification paradigms. Examples where intelligent techniques are used to estimate the ship dynamic system are widely reported. For instance, the researchers employ the support vector machine algorithms to highlight the measurement noise [1] or the environmental disturbance [2] issues during the parameter identification process. Moreover, in terms of uncertainty analysis, the Bayesian approach [3] and Gaussian process [4] gain more popularity. It is natural to find that the data-driven estimation approaches are widely applied to stress the nonlinear phenomena of the dynamic system, and the results have shown their advantages.

Unlike the identified ship model, which is physically interpretable, the ship dynamics learned from the observations are wrapped as a black box. Usually, they are approximated by nonlinear regression functions with plenty of parameters like weights and bias in a neural network to be optimized. Li et al. [5] constructed a neural network (NN)-based model to predict the ship time series benefiting from the sensitivity analysis of the input space. Optimizing the network structure and the parameters could be crucial for the ultimate model fidelity. Numerous approaches are proposed to improve the model learning performance, such as using the particle swarm optimization (PSO) algorithm [6], [7] to tune the hyperparameters, or compacting the input vector space [8] to a reasonable dimension. Ideally, a nonlinear system can be reflected as accurately as possible if the network is well trained. However, in the real application, the results are not always going that way. Because the ship's motion is inevitably influenced by environmental factors such as winds, waves, and currents, its dynamics are even more complex by incorporating the elements of the draft, trim, thrust, etc. Meanwhile, the real ship operational data are measured with noise and uncertainties. Even worse, some sensor channels may go wrong to lose some data. There are more obstacles when applying the machine learning models in real life. Researchers have devoted efforts to fixing the practical issues. For instance, Hu et al. improved the regular Long-Short Term Memory (LSTM) network to deal with the random errors caused by the inertial navigation system [9]. In addition, some pre-processing techniques are utilized to improve the network capability, for instance, decomposing the original signals into sub-signals at different scales by using the wavelet analysis [10], [11], or the empirical mode decomposition techniques [12].

To achieve better performance, the network tends to go deeper and more complex and has higher requirements on the data quality and quantity. While in many scenarios where few conditions are experienced or limited data is measured, the purely data-driven methods are hard to meet the expectations. With the integration of prior domain knowledge, it is promising to improve the learning efficiency as well as the model performance.

III. METHODOLOGY

A. Overview of the method

The methodology of integrating the prior dynamic knowledge and neural network-based black-box model is proposed to improve the ship predictive performance. As shown in Fig. 2, there are three ways to establish ship models—solely physics-based model, physics-data hybrid model and a purely data-driven model.

In the proposed hybrid way, an approximate ship model (1) is developed to provide instructive information for the latent predictive model.

$$\dot{\mathbf{x}} = f_a(\mathbf{x}, \mathbf{u}, \theta) \quad (1)$$

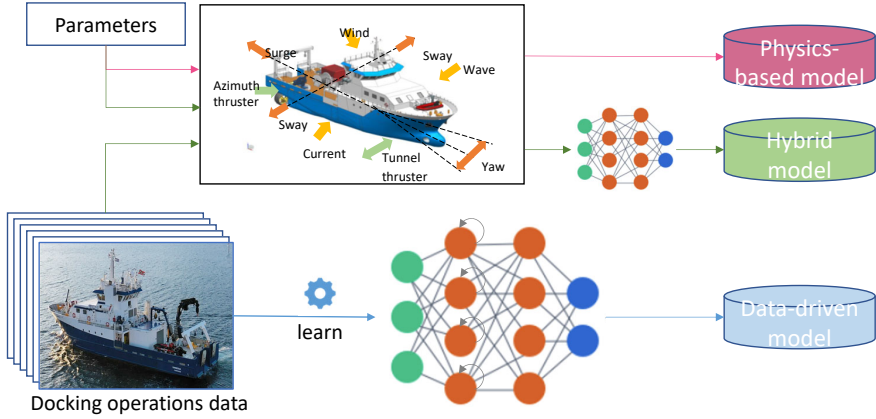


Fig. 2: Overview of the model-data cooperative modeling methodology.

where $\mathbf{x} = [x, y, \psi, u, v, r]'$ is the ship state vector, which contains the positions in North-East-Down (NED) coordinate, and velocities in the surge, sway, and yaw direction. For the research vessel we applied in this work, two main azimuth thrusters are installed at the stern and one tunnel thruster at the bow. Thus the control vector $\mathbf{u} = [RPM_p, \delta_p, RPM_s, \delta_s, RPM_t]'$ includes the shaft speeds in revolution-per-minute and the orientations of both stern thrusters, and the shaft speed of the tunnel thruster RPM_t . The subscripts p , and s refer to the portside and starboard side, respectively. Note that the control inputs are assumed to be constant over the sampling interval. Besides, there are plenty of parameters specified for the research vessel, such as those declaring the hydrodynamic effects, the thruster properties, as well as the ship geometry principles, etc. The vector θ consists of all these ship-related parameters. In this model, the parameter θ has been well prepared beforehand, and the values are either verified in model tests or supplied by the component manufacturer.

An operational data set of the research vessel $D = \{(\mathbf{x}_i^k, \mathbf{y}_i^k), k = 1, 2, \dots, n, i = 1, 2, \dots, m\}$ is sampled, where n docking operations are recorded, and each operation contains m samples. Suppose at time instance $t - 1$, the numerical model f_a receives the thruster commands, and will reveal the ship positions ahead of current time. The model prediction sequences $[\tilde{\mathbf{x}}_t, \tilde{\mathbf{x}}_{t+1}, \dots, \tilde{\mathbf{x}}_{t+\Delta}]$ are induced from the approximate model by (2).

$$\tilde{\mathbf{x}}_t = f_a(\mathbf{x}_{t-1}^k, \mathbf{u}_{t-1}, \theta) \quad (2)$$

Δ is the prediction horizon. Despite the much efforts went into the development of the numerical model, not all phenomena could be captured by one single model. Assumptions must be taken to simplify the expressions and describe the dominate properties. As a result, the leveraged model information $\tilde{\mathbf{x}}_t$ must have a certain discrepancies against the exact ship states \mathbf{x}_t .

By integrating the prior model predictions as the informative inputs into the neural network, the prior knowledge is carried forward and calibrated by the real operation data. This way, the prediction accuracy compared to the solely hydrodynamic model-based will be improved, and the learning efficiency compared to the purely data-driven model will also be promoted.

$$\begin{aligned} \hat{\mathbf{x}}_t &= g(\tilde{\mathbf{x}}_t, \mathbf{u}_{t-1}, t) \\ &= g(f_a(\mathbf{x}_{t-1}^k, \mathbf{u}_{t-1}, \theta), \mathbf{u}_{t-1}, t) \end{aligned} \quad (3)$$

Depending on the ship docking operation data set D , a data-driven model without the prior model information is also derived. A comparison of the hybrid model with the physics-based and data-driven models on the accuracy and efficiency will be performed to validate the cooperative methodology.

B. Approximate ship model

For the horizontal motion of a fully actuated offshore surface vessel under the wind disturbance, considering the surge, sway, and yaw motion components, the mathematical motion model of a ship in docking operation is expressed as [13]:

$$\begin{aligned} \dot{\eta} &= R(\psi)\nu \\ M\dot{\nu} + C_{RB}(\nu)\nu + C_A(\nu_r)\nu_r + D(\nu_r) &= \tau_c + \tau_{wi} + \tau_{wa} \end{aligned} \quad (4)$$

where $\eta = [x, y, \psi]$ contains the ship position and heading, $\nu = [u, v, r]$ is the speed vector, u, v, r refer to surge, sway, and yaw velocity, respectively. $R(\psi)$ is the horizontal plane rotation matrix due to the yaw angle. $M \in R^{3 \times 3}$ is the vessel inertia matrix including added mass; $C_{RB}(\nu) \in R^{3 \times 3}$ and $C_A(\nu_r) \in R^{3 \times 3}$ are the skew-symmetric Coriolis and centripetal matrices of the rigid body and the added mass; $D(\nu_r) \in R^3$ is the damping vector, including linear and nonlinear terms which are a function of the relative velocity ν_r between the vessel and the current. $\tau_c \in R^3$ is the control

vector consisting of forces and moments produced by the thruster system; τ_{wi} and τ_{wa} are the environmental load vectors of wind and waves, respectively. Given the measurement limitations of ocean currents and waves and the desire to reduce modeling efforts, the wave, and current effects are eliminated from the model. So the ν_r is reduced to ν instead.

The control force are contributed by the thruster units installed on the vessel. And the propeller thrust T and torque Q are generally formulated as a function of shaft speed n in revolution-per-minute, the thruster orientation δ , time-varying ship states x_p in interaction with thruster, and specific thruster parameters θ_p [14]. A numerical model of the forces produced by the two main azimuth thrusters was supplied by the thruster manufacturer. The actuator forces and moments are translated to the control forces and moments in horizontal plane by

$$\tau_c = T(\delta)F_T \quad (5)$$

$$T(\delta) = \begin{bmatrix} 0 & \cos(\delta_p) & \cos(\delta_s) \\ 1 & \sin(\delta_p) & \sin(\delta_s) \\ L_{tx} & L_{px} \sin(\delta_p) - L_{py} \cos(\delta_p) & L_{sx} \sin(\delta_s) - L_{sy} \cos(\delta_s) \end{bmatrix}$$

where δ is the thruster orientation, and $T(\delta)$ is the thrust configuration matrix, which describes the geometrical locations of the thrusters. $\tau_c = [\tau_x, \tau_y, \tau_n]^T$ refers to the control force vector acting on the vessel; $F_T = [T_t, T_p, T_s]^T$ represents forces vector produced by tunnel thruster, port main thruster and starboard main thruster, respectively.

The wind force is the only environmental disturbance that can be estimated based on the wind speed and velocity measured on board. The deterministic model to estimate wind forces is given in (6).

$$\tau_{wi} = \frac{1}{2} \rho_a V_{rw}^2 \begin{bmatrix} C_X(\gamma_{rw}) A_{FW} \\ C_Y(\gamma_{rw}) A_{LW} \\ C_N(\gamma_{rw}) A_{LW} L_{oa} \end{bmatrix} \quad (6)$$

The relative wind speed is defined as $V_{rw} = \sqrt{u_{rw}^2 + v_{rw}^2}$ and attack angle $\gamma_{rw} = -atan2(v_{rw}, u_{rw})$, where $u_{rw} = u - V_w \cos(\beta_w - \psi)$, and $v_{rw} = v - V_w \sin(\beta_w - \psi)$. V_w and β_w represent the wind speed and its direction, respectively. C_X, C_Y , and C_N are wind coefficients specific for the hull or superstructure shape. A_{FW} and A_{LW} are frontal and lateral projected areas and L_{oa} is the overall length of the ship.

The research vessel is numerically simulated by solving the dynamic model (4) with the Runge-Kutta fourth-order method.

C. Neural network calibrator

A feedforward neural network (FNN) structure is adopted to calibrate the bias and map the model predictions to the real ship states. Specifically, the input space was constructed by the forecasting time step, the corresponding model predicted ship velocities, and the wind measurement, as well as the thruster feedback when prediction is triggered. The output variables are the corresponding ship's real velocities in the surge, sway, and yaw direction.

One input layer, three hidden layers, and one output layer are specified in the network. The weights and biases of the FNN are updated by the Adam optimizer. The activation

TABLE I: Main dimensions of the research vessel.

Description	Parameter	Value
Length over all	$L_{oa}(m)$	31.25
Length between perpendiculars	$L_{pp}(m)$	28.9
Mass of vessel	$M(t)$	370
Dead weight	DWT	107
Breadth middle	$B_m(m)$	9.6
Draught	$d_m(m)$	2.6

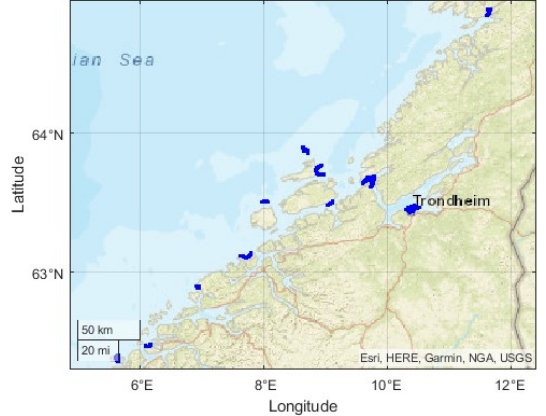


Fig. 3: R/V Gunnerus docking operations in 2016-2017, Norway.

function for the hidden layer is ReLU, and input measurements in the training set are normalized with a standard scalar. The training set evaluated the performance by minimizing the mean square error (MSE) metric between desired and regressed values. The proposed network is implemented by using Scikit-learn in Python.

D. Data-driven model

There are several choices existing when selecting a method for purely data-driven predictive modeling, such as the neural networks, either feedforward or recursive, the Gaussian Process, the Support vector machines, etc. Given the error accumulation effects when predicting multiple steps ahead, we prefer the recursive neural network (RNN) to recap the past states, as shown in (7).

$$\hat{\mathbf{x}}_t = G(\mathbf{x}_{t-1}, \mathbf{u}_{t-1}) \quad (7)$$

The Long-Short Term Memory (LSTM) networks, as a special kind of RNN, are particularly good at learning long-term dependencies and processing time-series forecasting because they work to retain useful information about previous data in the sequence instead of treating each data point independently. Thus, we applied the LSTM for nonlinear ship motions single-step prediction, and propagation will be performed to get 30 seconds predictions.

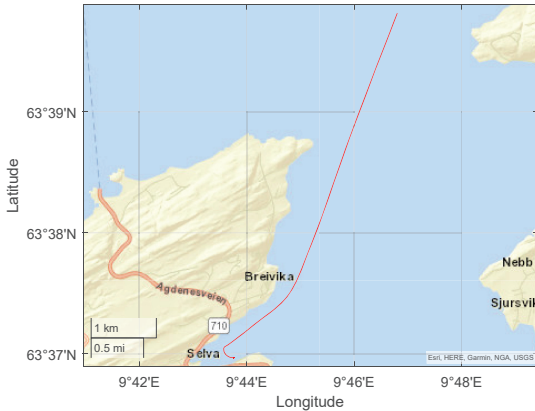


Fig. 4: Test docking scenario in Tromsø, Norway

The formulation of LSTM cells is as follows.

$$\begin{aligned}
 f_t &= \sigma(W^{f,h}h_{t-1} + W^{f,x}x_t) \\
 i_t &= \sigma(W^{i,h}h_{t-1} + W^{i,x}x_t) \\
 o_t &= \sigma(W^{o,h}h_{t-1} + W^{o,x}x_t) \\
 c_t &= f_t \odot c_{t-1} + i_t \odot \tanh(W^{c,h}h_{t-1} + W^{c,x}x_t) \\
 h_t &= o_t \odot \tanh(c_t)
 \end{aligned} \tag{8}$$

where the f , i , o and c represent the input gate, the forgetting gate, the output gate and the cell state, respectively. x_t is the input vector, W is the weight matrix, h_{t-1} and c_{t-1} are cell state and hidden state of the LSTM structure at the $t-1$ time step. σ refers the activation function sigmoid, \tanh is the hyperbolic tangent function, and \odot is the Hadamard product.

When constructing the nonlinear ship model, the input space contains the ship velocity states and controls at current time, and output the velocities one step ahead, i.e.,

- $I(t)=[u_t, v_t, r_t, n_{p_t}, \delta_{p_t}, n_{s_t}, \delta_{s_t}, n_{t_t}, V_{w_t}, \beta_{w_t}]$
- $O(t)=[u_{t+1}, v_{t+1}, r_{t+1}]$

Under the machine learning framework of Google TensorFlow, the LSTM was implemented in the Python language. The learning network structure contains one input layer, one hidden layer, one LSTM unit layer, and one output layer. Standardization is performed before data are fed into each layer network. The activation function of the output layer is a linear function. Adam is selected as the optimizer with a learning rate of 1×10^{-3} to update weights.

IV. EXPERIMENT

A. Data sets preparation

The research vessel (R/V) Gunnerus, owned and operated by the Norwegian University of Science and Technology, serves as the testbed in this work. The R/V Gunnerus was equipped with two permanent magnet-driven azimuth thrusters (PMAM) at the stern and one tunnel thruster at the bow. Its main dimensions are listed in Table. I.

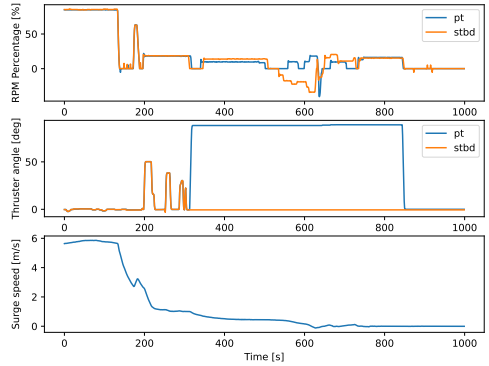


Fig. 5: The main thruster feedback during docking.

The experimental data were sampled from the history data acquired through log files created by a data acquisition system onboard the RV Gunnerus. The measurements contain the ship's GPS signal, six degrees of freedom (DoF) displacements and velocities, wind direction and speed measurement, as well as thruster feedbacks. A docking operation dataset of a one-year time period starting from August 2016 to June 2017 was selected, as shown in Fig. 3. A conversion from the position given as latitude and longitude in the earth-centered, earth-fixed (ECEF) frame to the local north–east–down (NED) frame in meters was performed on the data set. Information regarding the procedures of isolating dockings from daily cruise data and the measurement range of each sensor channel can be found in [15]. In this dataset, the sampling rate of all variables is 1Hz, and 70 complete docking operations, which were each 1000 seconds in length, were recorded.

For the model-data hybrid approach, six docking operations data were utilized for training the feedforward neural network, which maps the rough model predictions to the accurate ship states. For the solely data-driven model without the assistance of the prior model, a recursive neural network structure LSTM was trained on 50 docking operations to learn the ship states one step ahead.

The purely physics-based model, the hybrid model, as well as the purely data-driven model are verified on the same test data set.

B. Prediction performance

In the test docking scenario, as shown in Fig. 4, the predictions made by three different models are performed. The main thruster feedbacks and approach speed were recorded as Fig. 5. It is observed that the ship's forward speed decreases from around 6 m/s to zero at 850s, and the two main thrusters are controlled separately. The prediction accuracy is evaluated by the mean squared error (MSE) (9).

$$e = 1/l \sum_1^l (v - \hat{v})^2 \tag{9}$$

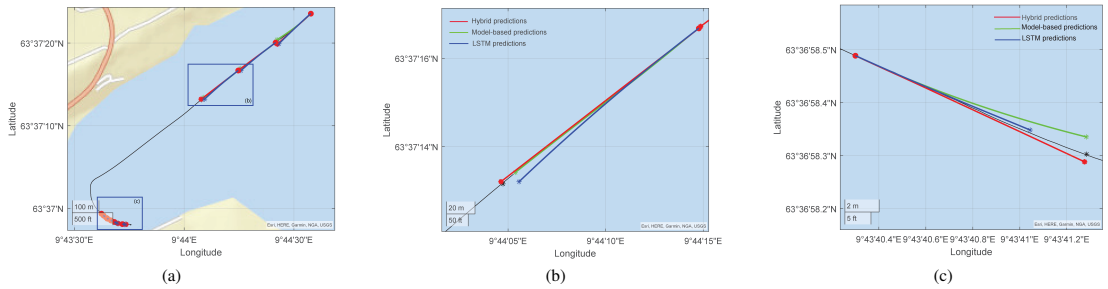


Fig. 6: Predicted trajectories of three models. (a) complete predictions during docking; (b) prediction details in the first period; (c) prediction details in the second period.

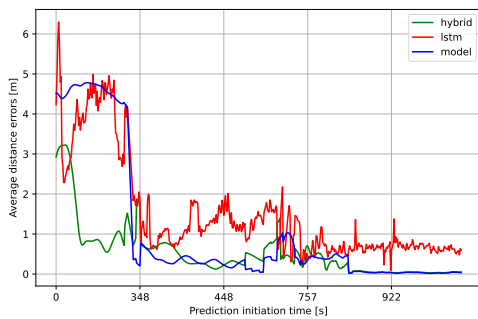


Fig. 7: The predictive average distance errors of three various models.

Given the predicted speed vector, the ship positions are updated by (10), where h is the time step.

$$\begin{aligned} \dot{\eta} &= R(\psi)\hat{v} \\ \eta_{t+1} &= \eta_t + \dot{\eta}h \end{aligned} \quad (10)$$

Another metric is introduced to evaluate the average Euclidean distance errors (11), where \hat{x}_i, \hat{y}_i represent the predicted NED positions, and x_i, y_i are corresponding ship true states. And l is the sample length.

$$d_e = 1/l \sum_1^l (\sqrt{(x_i - \hat{x}_i)^2 + (y_i - \hat{y}_i)^2}) \quad (11)$$

The predicted trajectories of three models are visualized in Fig. 6. According to the surge speed and thruster orientation distribution, there are two stages in the docking process, before and after the portside thruster turns around 320s. Thus two detailed predictions are exhibited in Fig. 6b-6c. From these figures, the red circle represents the ship's position where the forecasting is initiated. The star signs mark the final predictive position at 30 seconds ahead. Three colors display the foreseen trajectories made by different models—red: hybrid, green: physics model, and blue: data-driven model. And the black line

is the ship's real trajectory. It is observed that the hybrid model predicts the most accurately in both command profiles. When the ship speed is relatively higher at 190s, the hydrodynamic model performs slightly better than the data-driven model. Still, in the low-speed maneuver, the LSTM model generates more visible errors.

A more detailed prediction error comparison is shown in Fig. 7. It is more straightforward that the prediction errors are related to the ship's approach speed. At the higher speed before decreasing, the hybrid model considerably reduces the dispersion, and the hydrodynamic model and LSTM model behave worse, but generally, the latter works better than the former. When the ship is decelerating at a slow speed, the hydrodynamic model matches more suitably with the actual system, so well as the hybrid model. The data-driven model also exhibits a remarkable decrease in average distance error but is still slightly larger than the physical and hybrid models. It reveals that the domain knowledge-based model constructed on hydrodynamic properties captures the system better at low-speed maneuvers. In this operation phase, either the physics or hybrid models are qualified to offer credible predictions. However, when the ship is cruising at service speed, the hybrid model would be the best choice among these three candidates. The data-driven model performance is believed to be improved if more operation data is supplied. However, the reality limits the further optimization of the network even almost ten times operations of the hybrid model used are utilized for training the LSTM. On the contrary, the hybrid model can achieve excellent accuracy with limited data and a simpler network structure, which spares more effort and computational consumption than building everything from scratch.

V. CONCLUSION

In this paper, for the cases where partial but not complete information is known, the physics-based model is not qualified to comprehensively represent the system. Meanwhile, limited observation data is available. We propose a physics-data co-operation modeling approach to enhance the model quality. The prior knowledge leveraged by the rough ship numerical

model is carried forward into the neural network as informative inputs, and the informed neural network calibrates the bias between model outcomes and real states in principle. The proposed approach is validated in the real docking operation of a research vessel. Results have shown that compared to the solely hydrodynamic model, the hybrid model outperforms in accuracy. Compared to the purely data-driven model, the hybrid one could be achieved with fewer data and faster computation. Moreover, depending on the current operational phase, flexible choices can be made among the three kinds of model candidates, which brings vital support to the decision-support process onboard ships.

REFERENCES

- [1] H. Xu and C. G. Soares, "Hydrodynamic coefficient estimation for ship manoeuvring in shallow water using an optimal truncated ls-svm," *Ocean Engineering*, vol. 191, p. 106488, 2019.
- [2] T. Wang, G. Li, B. Wu, V. Aesøy, and H. Zhang, "Parameter identification of ship manoeuvring model under disturbance using support vector machine method," *Ships and Offshore Structures*, pp. 1–9, 2021.
- [3] Y. Xue, Y. Liu, C. Ji, and G. Xue, "Hydrodynamic parameter identification for ship manoeuvring mathematical models using a bayesian approach," *Ocean Engineering*, vol. 195, p. 106612, 2020.
- [4] W. A. Ramirez, Z. Q. Leong, H. Nguyen, and S. G. Jayasinghe, "Non-parametric dynamic system identification of ships using multi-output gaussian processes," *Ocean Engineering*, vol. 166, pp. 26–36, 2018.
- [5] G. Li, B. Kawan, H. Wang, and H. Zhang, "Neural-network-based modelling and analysis for time series prediction of ship motion," *Ship technology research*, vol. 64, no. 1, pp. 30–39, 2017.
- [6] G. Zhang, F. Tan, and Y. Wu, "Ship motion attitude prediction based on an adaptive dynamic particle swarm optimization algorithm and bidirectional lstm neural network," *IEEE Access*, vol. 8, pp. 90087–90098, 2020.
- [7] Y. Yao, L. Han, and J. Wang, "Lstm-pso: Long short-term memory ship motion prediction based on particle swarm optimization," in *2018 IEEE CSAA Guidance, Navigation and Control Conference (CGNCC)*, 2018, pp. 1–5.
- [8] Y. Liu, W. Duan, L. Huang, S. Duan, and X. Ma, "The input vector space optimization for lstm deep learning model in real-time prediction of ship motions," *Ocean Engineering*, vol. 213, p. 107681, 2020.
- [9] X. Hu, B. Zhang, and G. Tang, "Research on ship motion prediction algorithm based on dual-pass long short-term memory neural network," *IEEE Access*, vol. 9, pp. 28429–28438, 2021.
- [10] J.-C. Yin, A. N. Perakis, and N. Wang, "A real-time ship roll motion prediction using wavelet transform and variable rbf network," *Ocean Engineering*, vol. 160, pp. 10–19, 2018.
- [11] T. Zhang, X.-Q. Zheng, and M.-X. Liu, "Multiscale attention-based lstm for ship motion prediction," *Ocean Engineering*, vol. 230, p. 109066, 2021.
- [12] Z. Nie, F. Shen, D. Xu, and Q. Li, "An emd-svr model for short-term prediction of ship motion using mirror symmetry and svr algorithms to eliminate emd boundary effect," *Ocean Engineering*, vol. 217, p. 107927, 2020.
- [13] T. Fossen, *Handbook of Marine Craft Hydrodynamics and Motion Control*. John Wiley & Sons, 2011.
- [14] Ø. N. Smogeli, "Control of marine propellers: from normal to extreme conditions," 2006.
- [15] R. Skulstad, G. Li, T. I. Fossen, B. Vik, and H. Zhang, "A hybrid approach to motion prediction for ship docking—integration of a neural network model into the ship dynamic model," *IEEE Transactions on Instrumentation and Measurement*, vol. 70, pp. 1–11, 2021.

ISBN 978-82-326-5724-7 (printed ver.)
ISBN 978-82-326-5633-2 (electronic ver.)
ISSN 1503-8181 (printed ver.)
ISSN 2703-8084 (online ver.)



NTNU

Norwegian University of
Science and Technology